Evanescent Waves in the Near- and the Far Field

HENK F. ARNOLDUS

Department of Physics and Astronomy, Mississippi State University,
P.O. Drawer 5167, Mississippi State, Mississippi, 39762-5167, USA
arnoldus@ra.msstate.edu

Abstract. Radiation emitted by a localized source can be considered a combination of traveling and evanescent waves, when represented by an angular spectrum. We have studied both parts of the radiation field by means of the Green's tensor for the electric field and the "Green's vector" for the magnetic field. It is shown that evanescent waves can contribute to the far field, despite their exponential decay, in specific directions. We have studied this far-field behavior by means of an asymptotic expansion with the radial distance to the source as large parameter. As for the near field, we have shown explicitly how the singular behavior of radiation in the vicinity of the source is entirely due to the evanescent waves. In the process of studying the traveling and evanescent waves in both the near field and the far field, we have found a host of new representations for the functions that determine the Green's tensor and the Green's vector. We have obtained new series involving Bessel functions, Taylor series, asymptotic series up to all orders and new integral representations.

Advances in Imaging and Electron Physics ***132*** *(2004) 1-67*

Table of Contents

I. Introduction

Radiation emitted by a localized source of atomic dimensions is usually observed in the far field with a macroscopic detector like a photomultiplier tube. This far-field wave is a spherical wave and its modulation in phase and amplitude carries information on the characteristics of the source. The recent dramatic advances in nanotechnology (Ohtsu, 1998) and the increasing experimental feasibility of measuring electromagnetic fields on a length scale of an optical wavelength in the vicinity of the source with near-field microscopes (Pohl, 1991; Pohl and Courjon, 1993; Courjon and Bainier, 1994; Paesler and Moyer, 1996; Grattan and Meggitt, 2000; Courjon, 2003), has made it imperative to study in detail the optical properties of radiation fields with a resolution of a wavelength or less around the source.

It is well known that radiation emitted by a localized source has four typical components, when considering the dependence on the radial distance to the source. Let the source be located near the origin of coordinates, and let vector **r** represent a field point. We shall assume that the radiation is monochromatic with angular frequency ω with corresponding wave number $k_o = \omega / c$. The spherical wave in the far field mentioned above then has an overall factor of $\exp(ik_o r)/r$, and this is multiplied by a complex amplitude depending on the details of the source. The important property of this component of the field is that it falls off with distance as $1/r$. Since the intensity is determined by the square of the amplitude, the outward energy flow per unit area is proportional to $1/r^2$. When integrated over a sphere with radius r around the source, the emitted power becomes independent of the radius of the sphere, and therefore can be observed in “infinity”. Conversely, any component of the field that falls off faster than $1/r$ will not contribute to the power at macroscopic distances. The complete radiation field has three more components that become important when we want to consider optical phenomena on a length scale of a wavelength. The field has a component proportional to $1/r^2$, which is called the middle field, and a component that falls off as $1/r^3$, which is the near field contribution. In addition, there is a delta function in the field which only exists inside the source, and this part is therefore usually omitted. It has been realized for a long time that this delta function is necessary for mathematical consistency (Jackson, 1975), and more recently it appeared that for a proper account of the near field this contribution can not be ignored any longer (Keller, 1996, 1999a, 1999b). Especially when considering **k**-space descriptions of parts of the field, this delta function has to be included, since it spreads out over all of **k**-space (Arnoldus, 2001, 2003a).

In near-field optics, a representation of the radiation field in configuration (**r**) space is not always attractive, since all parts of the field (near, middle and far) contribute more or less equally, depending on the distance to the source. Moreover, the separate parts are not solutions of Maxwell’s equations individually, so the coupling between all has to be retained. A description in configuration (**k**) space has the advantage that the Fourier plane waves of the decomposition do not couple among each other, but the problem here is that the separate plane waves do not satisfy Maxwell’s equations. The reason is that at a given frequency ω, only plane waves with wave number $k_o = \omega / c$ can be a solution of Maxwell’s equations, whereas in **k**-space waves with any wave number k appear. The solution to this problem is to adopt what is called an “angular spectrum” representation. Here, we make a Fourier transform in x and y, but not in z, so this is a two-dimensional

Fourier transform in the xy-plane. The wave vector $\mathbf{k}_{||}$ in the xy-plane can have any magnitude and direction. The idea is then that we associate with this $\mathbf{k}_{||}$ a three-dimensional plane wave of the form $\exp(i\mathbf{K}\cdot\mathbf{r})$, with an appropriate complex amplitude, such that this wave is a solution of Maxwell's equations. In particular, the magnitude of **K** has to be $K = k_o = \omega / c$, which implies that, given $\mathbf{k}_{||}$, the z-component of **K** is fixed, apart from a possible minus sign. The wave vector **K** of a partial wave in this representation is given by

$$\mathbf{K} = \mathbf{k}_{||} + \beta\,\mathrm{sgn}(z)\,\mathbf{e}_z \tag{1}$$

with $\mathrm{sgn}(z)$ the sign of z, and with the parameter β defined as

$$\beta = \begin{cases} \sqrt{k_o^2 - k_{||}^2} & , \quad k_{||} < k_o \\ i\sqrt{k_{||}^2 - k_o^2} & , \quad k_{||} > k_o \end{cases} . \tag{2}$$

For $k_{||} < k_o$, this parameter is positive, and therefore the sign of K_z is the same as the sign of z. Hence, $\exp(i\mathbf{K}\cdot\mathbf{r})$ is a traveling plane wave, which travels in the direction away from the xy-plane. For $k_{||} > k_o$, β is positive imaginary, and this corresponds to a wave which decays in the z-direction. The sign of K_z is chosen such that for $z > 0$ the wave decays in the positive z-direction and for $z < 0$ it decays in the negative z-direction, a choice which is obviously dictated by causality. Waves of this type are called evanescent waves, and in an angular spectrum representation these waves have to be included. Since $\mathbf{k}_{||}$ is real, the evanescent waves travel along the xy-plane in the direction of $\mathbf{k}_{||}$. ***Figure 1*** schematically illustrates the two types of waves in the angular spectrum.

The advantage of the fact that each partial wave in the angular spectrum is a solution of the free-space Maxwell equations can not be overemphasized. For instance, when the source is located near an interface, each partial wave reflects and refracts in the usual way, and this can be accounted for by Fresnel reflection and transmission coefficients. The total reflected and refracted fields are then simply superpositions of these partial waves, and the result is again an angular spectrum representation. This yields an exact solution for the radiation field of a source near an interface (Sipe, 1981, 1987), and the result has been applied to calculate the radiation pattern of a dipole near a dielectric interface (Lukosz and Kunz, 1977a, 1977b; Arnoldus and Foley, 2003b, 2003d) and a nonlinear medium (Arnoldus and George, 1991), and to the computation of the lifetime of atomic states near a metal (Ford and Weber, 1981, 1984).

Evanescent waves have a long history, going back to Newton (de Fornel, 2001), and common wisdom tells us that evanescent waves dominate the near field whereas the traveling waves in the angular spectrum account for the far field. The latter statement derives from the fact that evanescent waves die out exponentially, away from the *xy*-plane, and can therefore not contribute to the far field. On the other hand, near the source each traveling and each evanescent wave in the angular spectrum is finite in amplitude, giving no obvious reason why evanescent waves are more prominent in the near field than traveling waves. In this paper we shall show explicitly that in particular the singularity of the field near the origin (as in $1/r^3$, etc.) results entirely from the contribution of the evanescent waves. On the other hand, we shall show that evanescent waves do end up in the far field, despite their exponential decay, defying common sense.

II. Solution of Maxwell's Equations

We shall consider a localized source of radiation in which the charge density $\rho(\mathbf{r},t)$ and the current density $\mathbf{j}(\mathbf{r},t)$ oscillate harmonically with angular frequency ω. We write

$$\mathbf{j}(\mathbf{r},t) = \mathrm{Re}[\mathbf{j}(\mathbf{r})e^{-i\omega t}] \tag{3}$$

with $\mathbf{j}(\mathbf{r})$ the complex amplitude, and similarly for $\rho(\mathbf{r},t)$. The electric field $\mathbf{E}(\mathbf{r},t)$ and the magnetic field $\mathbf{B}(\mathbf{r},t)$ will then have the same time dependence, and their complex amplitudes are $\mathbf{E}(\mathbf{r})$ and $\mathbf{B}(\mathbf{r})$, respectively. We assume the charge and current densities to be given (as is for instance the case for a molecule in a laser beam). The electric and magnetic fields are then the solution of Maxwell's equations:

$$\nabla \cdot \mathbf{E}(\mathbf{r}) = \rho(\mathbf{r})/\varepsilon_o \tag{4}$$

$$\nabla \times \mathbf{E}(\mathbf{r}) = i\omega\mathbf{B}(\mathbf{r}) \tag{5}$$

$$\nabla \cdot \mathbf{B}(\mathbf{r}) = 0 \tag{6}$$

$$\nabla \times \mathbf{B}(\mathbf{r}) = -\frac{i\omega}{c^2}\mathbf{E}(\mathbf{r}) + \mu_o\mathbf{j}(\mathbf{r}) \ . \tag{7}$$

If we take the divergence of Eq. (7) and use Eq. (4) we find

$$\nabla \cdot \mathbf{j}(\mathbf{r}) = i\omega\rho(\mathbf{r}) \tag{8}$$

which expresses conservation of charge.

In order to obtain a convenient form of the general solution we temporarily introduce the quantity

$$\mathbf{P}(\mathbf{r}) = \frac{i\omega\mu_o}{4\pi}\int d^3\mathbf{r}'\,\mathbf{j}(\mathbf{r}')\,g(\mathbf{r}-\mathbf{r}') \tag{9}$$

where $g(\mathbf{r})$ is the Green's function of the scalar Helmholz equation

$$g(\mathbf{r}) = \frac{e^{ik_o r}}{r} \quad . \tag{10}$$

It follows by differentiation that

$$\nabla^2 g(\mathbf{r}-\mathbf{r}') = -k_o^2 g(\mathbf{r}-\mathbf{r}') \, , \quad \mathbf{r}' \neq \mathbf{r} \quad . \tag{11}$$

If we then wish to evaluate $\nabla^2 \mathbf{P}(\mathbf{r})$, then it seems that the entire **r** dependence enters through $g(\mathbf{r}-\mathbf{r}')$ in the integrand, and with Eq. (11) this would give $\nabla^2 \mathbf{P}(\mathbf{r}) = -k_o^2 \mathbf{P}(\mathbf{r})$. However, it should be noted that $g(\mathbf{r})$ has a singularity at $r = 0$, and therefore the integrand of the integral in Eq. (9) is singular at $\mathbf{r}' = \mathbf{r}$. When the field point **r** is inside the source, it is understood that a small sphere around **r** is excluded from the range of integration. When we vary **r**, by applying the operator ∇^2 on $\mathbf{P}(\mathbf{r})$, then we also move the small sphere. It can then be shown (van Kranendonk and Sipe, 1977; Born and Wolf, 1980) that this leads to an extra term when moving ∇^2 under the integral. The result is

$$\nabla^2 \mathbf{P}(\mathbf{r}) = -\, k_o^2 \mathbf{P}(\mathbf{r}) - i\omega\mu_o \mathbf{j}(\mathbf{r}) \quad . \tag{12}$$

It can then be verified by inspection that the solution of Maxwell's equations is

$$\mathbf{E}(\mathbf{r}) = \mathbf{P}(\mathbf{r}) + \frac{1}{k_o^2} \nabla(\nabla \cdot \mathbf{P}(\mathbf{r})) \tag{13}$$

$$\mathbf{B}(\mathbf{r}) = \frac{-i}{\omega} \nabla \times \mathbf{P}(\mathbf{r}) \tag{14}$$

taking into consideration relation (8) between the charge and current densities.

In Eq. (13), the operator $\nabla(\nabla\cdot ...)$ acts on the integral in Eq. (9), and when we move this operator under the integral an additional term appears, similar to the second term on the right-hand side of Eq. (12). In this case we find

$$\mathbf{E}(\mathbf{r}) = -\frac{i}{3\varepsilon_o\,\omega}\mathbf{j}(\mathbf{r}) + \frac{i}{4\pi\,\varepsilon_o\,\omega}\int d^3\mathbf{r}'\Big(k_o^2\,\mathbf{j}(\mathbf{r}')\,g(\mathbf{r}-\mathbf{r}') \\ + \nabla\{\nabla\cdot[\mathbf{j}(\mathbf{r}')g(\mathbf{r}-\mathbf{r}')]\}\Big)\,. \qquad (15)$$

The $\nabla(\nabla\cdot ...)$ in the integrand only acts on the $\mathbf{r}$ dependence of $g(\mathbf{r}-\mathbf{r}')$, and therefore this can be written as

$$\nabla\{\nabla\cdot[\mathbf{j}(\mathbf{r}')g(\mathbf{r}-\mathbf{r}')]\} = [\mathbf{j}(\mathbf{r}')\cdot\nabla]\nabla g(\mathbf{r}-\mathbf{r}')\ . \qquad (16)$$

For the magnetic field we have to move $\nabla\times ...$ under the integral, but this does not lead to an additional term. We thus obtain

$$\mathbf{B}(\mathbf{r}) = \frac{-1}{4\pi\,\varepsilon_o\,c^2}\int d^3\mathbf{r}'\,\mathbf{j}(\mathbf{r}')\times\nabla g(\mathbf{r}-\mathbf{r}') \qquad (17)$$

where we have used $\nabla\times[\mathbf{j}(\mathbf{r}')g(\mathbf{r}-\mathbf{r}')] = -\mathbf{j}(\mathbf{r}')\times\nabla g(\mathbf{r}-\mathbf{r}')$.

III. Green's Tensor and Vector

The solutions for $\mathbf{E}(\mathbf{r})$ and $\mathbf{B}(\mathbf{r})$ from the previous section can be cast in a more transparent form by adopting tensor notation. To this end we notice that the right-hand side of Eq. (16) can be written as

$$[\mathbf{j}(\mathbf{r}')\cdot\nabla]\nabla g(\mathbf{r}-\mathbf{r}') = [\nabla\nabla g(\mathbf{r}-\mathbf{r}')]\cdot\mathbf{j}(\mathbf{r}')\ . \qquad (18)$$

Here, $\nabla\nabla g(\mathbf{r}-\mathbf{r}')$ is a tensor with a dyadic structure (given below), and the dot product between a dyadic form **ab** and a vector **c** is defined as $(\mathbf{ab})\cdot\mathbf{c}=\mathbf{a}(\mathbf{b}\cdot\mathbf{c})$ in terms of the regular dot product between the vectors **b** and **c**. The result is a vector proportional to **a**. The unit tensor $\overleftrightarrow{\mathrm{I}}$ has the effect of $\overleftrightarrow{\mathrm{I}}\cdot\mathbf{a}=\mathbf{a}$. The solution (15) for $\mathbf{E}(\mathbf{r})$ can then be written as

$$\mathbf{E}(\mathbf{r})=-\frac{i}{3\varepsilon_o\,\omega}\mathbf{j}(\mathbf{r})+\frac{i}{4\pi\,\varepsilon_o\,\omega}\int d^3\mathbf{r}'[k_o^2\,\overleftrightarrow{\mathrm{I}}\,g(\mathbf{r}-\mathbf{r}') \\ +\nabla\nabla g(\mathbf{r}-\mathbf{r}')]\cdot\mathbf{j}(\mathbf{r}')\ . \qquad (19)$$

In order to simplify this even more, we write the current density in the first term on the right-hand side as

$$\mathbf{j}(\mathbf{r})=\int d^3\mathbf{r}'[\overleftrightarrow{\mathrm{I}}\,\delta(\mathbf{r}-\mathbf{r}')]\cdot\mathbf{j}(\mathbf{r}') \qquad (20)$$

and then we combine the two integrals. The solution then takes the compact form

$$\mathbf{E}(\mathbf{r})=\frac{ik_o^2}{4\pi\,\varepsilon_o\,\omega}\int d^3\mathbf{r}'\overleftrightarrow{\mathrm{g}}(\mathbf{r}-\mathbf{r}')\cdot\mathbf{j}(\mathbf{r}')\ . \qquad (21)$$

Here, $\overleftrightarrow{\mathrm{g}}(\mathbf{r})$ is the Green's tensor, defined as

$$\overleftrightarrow{\mathrm{g}}(\mathbf{r})=-\frac{4\pi}{3k_o^2}\delta(\mathbf{r})\overleftrightarrow{\mathrm{I}}+\left(\overleftrightarrow{\mathrm{I}}+\frac{1}{k_o^2}\nabla\nabla\right)g(\mathbf{r})\ . \qquad (22)$$

This tensor has been studied extensively, and a book (Tai, 1971) is devoted to its use, although, oddly enough, the delta function on the right-hand side was not included.

In order to find $\overleftrightarrow{\mathrm{g}}(\mathbf{r})$ explicitly, we only need to work out the derivatives $\nabla\nabla g(\mathbf{r})$. At this point it is convenient to adopt dimensionless variables for coordinates with $1/k_o$ as unit of measurement. The dimensionless vector representing the field point will be denoted by $\mathbf{q} = k_o\mathbf{r}$. The magnitude of this vector, $q = k_o r$, is then the dimensionless distance of the field point from the origin, and such that $q = 2\pi$ corresponds to a distance of one optical wavelength. We shall also introduce the dimensionless Green's tensor by

$$\overleftrightarrow{\chi}(\mathbf{q}) = \frac{1}{k_o}\overleftrightarrow{\mathrm{g}}(\mathbf{r}) \ . \tag{23}$$

This Green's tensor is then found to be

$$\overleftrightarrow{\chi}(\mathbf{q}) = -\frac{4\pi}{3}\delta(\mathbf{q})\overleftrightarrow{\mathrm{I}} + (\overleftrightarrow{\mathrm{I}} - 3\hat{\mathbf{q}}\hat{\mathbf{q}})(i - \frac{1}{q})\frac{e^{iq}}{q^2} + (\overleftrightarrow{\mathrm{I}} - \hat{\mathbf{q}}\hat{\mathbf{q}})\frac{e^{iq}}{q} \tag{24}$$

from Eq. (22). The radial unit vector $\hat{\mathbf{q}}$ is the same as $\hat{\mathbf{r}}$, and $\delta(\mathbf{q}) = \delta(\mathbf{r})/k_o^3$ is the dimensionless delta function. The final expression for the electric field of a localized source then becomes

$$\mathbf{E}(\mathbf{r}) = \frac{ik_o^3}{4\pi\,\varepsilon_o\,\omega}\int d^3\mathbf{r}'\overleftrightarrow{\chi}(k_o(\mathbf{r} - \mathbf{r}'))\cdot\mathbf{j}(\mathbf{r}') \ . \tag{25}$$

The result for the magnetic field can be rewritten in a similar way, but this is a lot simpler. We define the dimensionless vector quantity

$$\boldsymbol{\eta}(\mathbf{q}) = -\frac{1}{k_o^2}\nabla g(\mathbf{r}) \tag{26}$$

in terms of which the magnetic field becomes

$$\mathbf{B}(\mathbf{r}) = -\frac{k_o^3}{4\pi\,\varepsilon_o\,\omega c}\int d^3\mathbf{r}'\,\boldsymbol{\eta}(k_o(\mathbf{r}-\mathbf{r}'))\times\mathbf{j}(\mathbf{r}') \tag{27}$$

greatly resembling Eq. (25) for the electric field. Apparently, the vector $\boldsymbol{\eta}(\mathbf{q})$ plays the same role for the magnetic field as the Green's tensor for the electric field, although it should be noted that this vector is not a Green's function in the usual sense. This Green's vector has the explicit form

$$\boldsymbol{\eta}(\mathbf{q}) = \left(\frac{1}{q} - i\right)\hat{\mathbf{q}}\,\frac{e^{iq}}{q} \ . \tag{28}$$

IV. Electric Dipole

We now consider a localized charge and current distribution of the most important form: the electric dipole. Its importance comes from the fact that most atomic and molecular radiation is electric dipole radiation. To see how this limit arises, we first consider a general distribution. Let the material be made up of particles, numbered with the subscript α. Each particle has a position vector $\mathbf{r}_\alpha(t)$, velocity

$$\mathbf{v}_\alpha(t) = \frac{d}{dt}\mathbf{r}_\alpha(t) \tag{29}$$

and electric charge q_α. The dipole electric dipole moment $\mathbf{d}(t)$ of the distribution is defined as

$$\mathbf{d}(t) = \sum_\alpha q_\alpha \mathbf{r}_\alpha(t) \ . \tag{30}$$

The time dependent current density can be expressed as (Cohen-Tannoudji *et.al.*, 1989)

$$\mathbf{j}(\mathbf{r},t) = \sum_{\alpha} q_{\alpha} \mathbf{v}_{\alpha}(t) \delta(\mathbf{r} - \mathbf{r}_{\alpha}(t)) \ . \tag{31}$$

We now assume that the linear dimensions of the distribution are very small, and centered around a given point $\mathbf{r}_o$. We then have $\mathbf{r}_{\alpha}(t) \approx \mathbf{r}_o$, and Eq. (31) becomes

$$\mathbf{j}(\mathbf{r},t) = \delta(\mathbf{r} - \mathbf{r}_o) \sum_{\alpha} q_{\alpha} \mathbf{v}_{\alpha}(t) \ . \tag{32}$$

Comparison with Eq. (29) gives

$$\mathbf{j}(\mathbf{r},t) = \delta(\mathbf{r} - \mathbf{r}_o) \frac{d}{dt} \mathbf{d}(\mathrm{t}) \ . \tag{33}$$

Since the current distribution completely determines the electric and magnetic fields, according to Eqs. (25) and (27), we simply define an electric dipole, located at $\mathbf{r}_o$, as a distribution with $\mathbf{j}(\mathbf{r},t)$ given by Eq. (33).

For time harmonic fields, the dipole moment has the form

$$\mathbf{d}(t) = \mathrm{Re}[\mathbf{d}\, e^{-i\omega t}] \tag{34}$$

where **d** is an arbitrary complex-valued vector. The current density follows from Eq. (33), and comparison with Eq. (3) then gives for the time-independent current density

$$\mathbf{j}(\mathbf{r}) = -i\omega\, \delta(\mathbf{r} - \mathbf{r}_o) \mathbf{d} \ . \tag{35}$$

The corresponding charge density follows from Eq. (8):

$$\rho(\mathbf{r}) = -\mathbf{d} \cdot \nabla \delta(\mathbf{r} - \mathbf{r}_o) \tag{36}$$

although we don't need that for the present problem.

Due to the delta function in Eq. (35), the integrals in Eqs. (25) and (27) can be evaluated. For a dipole located at the origin of coordinates we obtain for the fields

$$\mathbf{E}(\mathbf{r}) = \frac{k_o^3}{4\pi\,\varepsilon_o}\overleftrightarrow{\chi}(\mathbf{q})\cdot\mathbf{d} \tag{37}$$

$$\mathbf{B}(\mathbf{r}) = \frac{i}{c}\frac{k_o^3}{4\pi\,\varepsilon_o}\eta(\mathbf{q})\times\mathbf{d} \tag{38}$$

with $\mathbf{q} = k_o\mathbf{r}$. This very elegant result shows that the spatial dependences of the Green's tensor and vector are essentially the spatial distribution of the electric and magnetic field of dipole radiation (apart from the tensor and cross product with **d**).

The composition of the electric field now follows from Eq. (24). The first term on the right-hand side is a delta function, which only exists in the dipole. We call this the self field. The second term has a $1/q^3$ and a $1/q^2$ contribution, which are the near and the middle field, respectively. The last term falls off as $1/q$, and this is the far field. Similarly, for the magnetic field we see from Eq. (28) that this field only has a far and a middle field, but no near or self field.

V. Angular Spectrum Representation of the Scalar Green's Function

As mentioned in the Introduction, for many applications the representation of the Green's tensor and vector as in Eqs. (24) and (28), respectively, is not practical. In this section we shall first consider the scalar Green's function, given by Eq. (10). In order to derive a more useful representation, we first transform to **k**-space. The transformation is

$$G(\mathbf{k}) = \int d^3\mathbf{r}\, \frac{e^{ik_o r}}{r}\, e^{-i\mathbf{k}\cdot\mathbf{r}} \quad . \tag{39}$$

For a given **k**, we use spherical coordinates and such that the *z*-axis is along the **k** vector. First we integrate over the angles. Then the remaining integral over the radial distance does formally not exist, and we have to include a small positive imaginary part $i\varepsilon$ in k_o. The resulting integral can be evaluated with contour integration, and the result is

$$G(\mathbf{k}) = -\frac{4\pi}{k_o^2 - k^2 + i\varepsilon}\,, \quad \varepsilon \downarrow 0 \ . \tag{40}$$

The inverse is then

$$g(\mathbf{r}) = -\frac{1}{2\pi^2}\int d^3\mathbf{k}\, \frac{1}{k_o^2 - k^2 + i\varepsilon}\, e^{i\mathbf{k}\cdot\mathbf{r}}\,, \quad \varepsilon \downarrow 0 \ . \tag{41}$$

This integral can be calculated by using spherical coordinates in **k**-space. The result is again $\exp(ik_o r)/r$, which justifies the construction with the small imaginary part in the wave number.

Instead of using spherical coordinates in **k**-space, we now consider Cartesian coordinates for the integral in Eq. (41). With contour integration we perform the integral over k_z, which yields

$$g(\mathbf{r}) = \frac{i}{2\pi}\int d^2\mathbf{k}_{\|}\, \frac{1}{\beta}\, e^{i\mathbf{K}\cdot\mathbf{r}} \quad . \tag{42}$$

The parameter β is defined in Eq. (2) and the wave vector **K** is given by Eq. (1). The integral runs over the entire $\mathbf{k}_{\|}$ plane, which is the *xy*-plane of **k**-space. Equation (42) is the celebrated angular spectrum representation of the scalar Green's function.

As explained in the Introduction, Eq. (42) is a superposition of traveling and evanescent waves. Inside the circle $k_{\|} = k_o$ in the $\mathbf{k}_{\|}$ plane, the waves $\exp(i\mathbf{K}\cdot\mathbf{r})$ are traveling because β, and thereby K_z, is real, and outside the circle these waves are evanescent since their wave vectors have an imaginary *z*-component. Just on the circle we have $\beta = 0$, and the integrand has a singularity. We shall see below that this singularity is integrable and poses no problems.

VI. Angular Spectrum Representation of the Green's Tensor and Vector

In order to find an angular spectrum representation for the Green's tensor $\overleftrightarrow{\mathrm{g}}(\mathbf{r})$, it would be tempting to take expression (42) for the scalar Green's function, substitute this in the right-hand side of Eq. (22), and then move the operator in large brackets under the $\mathbf{k}_{\|}$ integral. This procedure leads to the wrong result in that it misrepresents the self field (the delta function on the right-hand side of Eq. (22)). The delta function in the Green's tensor came from moving the $\nabla(\nabla\cdot...)$ operator in Eq. (13) under the integral sign in Eq. (9) for $\mathbf{P}(\mathbf{r})$, and this led to Eq. (15). The extra term came from the singularity at $r = 0$ of $g(\mathbf{r}) = \exp(ik_o r)/r$ in $\mathbf{P}(\mathbf{r})$. When we represent $g(\mathbf{r})$ by its angular spectrum, Eq. (42), substitute this in Eq. (9) for $\mathbf{P}(\mathbf{r})$, and change the order of integration, we obtain

$$\mathbf{P}(\mathbf{r}) = -\frac{\omega\mu_o}{8\pi^2}\int d^2\mathbf{k}_{\|}\,\frac{1}{\beta}\int d^3\mathbf{r}'\,\mathbf{j}(\mathbf{r}')e^{i\mathbf{K}(z-z')\cdot(\mathbf{r}-\mathbf{r}')} \quad . \tag{43}$$

Here we have shown explicitly the *z*-dependence of $\mathbf{K}(z)$. If we now consider the operator $\nabla(\nabla\cdot...)$ acting on $\mathbf{P}(\mathbf{r})$, then the singularity at $\mathbf{r}' = \mathbf{r}$ has disappeared.

Therefore, when we change the order of integration, the action of $\nabla(\nabla\cdot ...)$ does not "move the sphere" anymore, and we can freely move this operator under the $\mathbf{r}'$ integral. All following steps are the same, leading to Eq. (22) for $\overleftrightarrow{g}(\mathbf{r})$. Therefore, we can substitute the angular spectrum representation (42) into Eq. (22) and move the derivatives under the integral, but we have to leave out the delta function on the right-hand side of Eq. (22). This then yields

$$\overleftrightarrow{g}(\mathbf{r}) = \frac{i}{2\pi}\int d^2\mathbf{k}_\parallel \frac{1}{\beta}\left(\overleftrightarrow{I} + \frac{1}{k_o^2}\nabla\nabla\right)e^{i\,\mathbf{K}\cdot\mathbf{r}} \quad . \tag{44}$$

The dyadic operator $\nabla\nabla$ now only acts on the exponential $\exp(i\mathbf{K}\cdot\mathbf{r})$, and we can take the derivatives easily. Care should be exercised, however, since **K** depends on z through $\mathrm{sgn}(z)$. With

$$\frac{d}{dz}\mathrm{sgn}(z) = 2\delta(z) \tag{45}$$

we find

$$\nabla\nabla e^{i\mathbf{K}\cdot\mathbf{r}} = [2i\beta\delta(z)\mathbf{e}_z\mathbf{e}_z - \mathbf{K}\mathbf{K}]\, e^{i\mathbf{K}\cdot\mathbf{r}} \quad . \tag{46}$$

Furthermore we use the spectral representation of the two-dimensional delta function

$$\int d^2\mathbf{k}_\parallel\, e^{i\mathbf{k}_\parallel\cdot\mathbf{r}} = 4\pi^2\delta(x)\delta(y) \tag{47}$$

and when we then put everything together we obtain the angular spectrum representation of the dimensionless Green's tensor:

$$\overleftrightarrow{\chi}(\mathbf{q}) = -4\pi\delta(\mathbf{q})\mathbf{e}_z\mathbf{e}_z + \frac{i}{2\pi k_o}\int d^2\mathbf{k}_{\|}\,\frac{1}{\beta}\left(\overleftrightarrow{\mathrm{I}} - \frac{1}{k_o^2}\mathbf{KK}\right)e^{i\mathbf{K}\cdot\mathbf{r}} \quad . \tag{48}$$

It is interesting to notice that a new delta function appears on the right-hand side, which comes from the discontinuous behavior of $\mathbf{K}(z)$ at $z = 0$. When compared to the representation (24) or (22) in **r**-space, we see that here we have a different delta function. Since the previous one represented the self field, the delta function in Eq. (48) must be something different. We will get back to this point in Sec. 8 and Appendix A.

The Green's vector for the magnetic field does not have any of these complications, and from Eq. (26) we immediately obtain

$$\boldsymbol{\eta}(\mathbf{q}) = \frac{1}{2\pi k_o^2}\int d^2\mathbf{k}_{\|}\,\frac{1}{\beta}\,\mathbf{K}\,e^{i\mathbf{K}\cdot\mathbf{r}} \tag{49}$$

since $\nabla\exp(i\mathbf{K}\cdot\mathbf{r}) = i\mathbf{K}\exp(i\mathbf{K}\cdot\mathbf{r})$.

VII. Traveling and Evanescent Waves

The Green's tensor $\overleftrightarrow{\chi}(\mathbf{q})$ in Eq. (48) splits naturally into three parts:

$$\overleftrightarrow{\chi}(\mathbf{q}) = -4\pi\delta(\mathbf{q})\mathbf{e}_z\mathbf{e}_z + \overleftrightarrow{\chi}(\mathbf{q})^{tr} + \overleftrightarrow{\chi}(\mathbf{q})^{ev} \quad . \tag{50}$$

Here, $\overleftrightarrow{\chi}(\mathbf{q})^{tr}$ is the part of $\overleftrightarrow{\chi}(\mathbf{q})$ which only contains the traveling waves, e.g.,

$$\overleftrightarrow{\chi}(\mathbf{q})^{tr} = \frac{i}{2\pi k_o}\int_{k_{\|}<k_o} d^2\mathbf{k}_{\|}\,\frac{1}{\beta}\left(\overleftrightarrow{\mathrm{I}} - \frac{1}{k_o^2}\mathbf{KK}\right)e^{i\mathbf{K}\cdot\mathbf{r}} \tag{51}$$

where the integration only runs over the inside of the circle $k_{||} = k_o$. Similarly, $\overleftrightarrow{\chi}(\mathbf{q})^{ev}$ is the part which only contains the evanescent waves. The Green's vector $\boldsymbol{\eta}(\mathbf{q})$ for the magnetic field has two parts

$$\boldsymbol{\eta}(\mathbf{q}) = \boldsymbol{\eta}(\mathbf{q})^{tr} + \boldsymbol{\eta}(\mathbf{q})^{ev} \tag{52}$$

in obvious notation.

We shall use both spherical coordinates (r,θ,ϕ) and cylinder coordinates (ρ,ϕ,z) for a field point, and most of the time we shall use the dimensionless coordinates $q = k_o r$, $\overline{\rho} = k_o\rho$ and $\overline{z} = k_o z$. The radial unit vector in the *xy*-plane is given by $\mathbf{e}_\rho$ = $\mathbf{e}_x \cos\phi + \mathbf{e}_y \sin\phi$, in terms of which we have $\mathbf{q} = \overline{\rho}\mathbf{e}_\rho + \overline{z}\mathbf{e}_z$, and the tangential unit vector is $\mathbf{e}_\phi = -\mathbf{e}_x \sin\phi + \mathbf{e}_y \cos\phi$. The relation to spherical coordinates is $\overline{\rho} = q\sin\theta$, $\overline{z} = q\cos\theta$, from which $\hat{\mathbf{q}} = \sin\theta\,\mathbf{e}_\rho + \cos\theta\,\mathbf{e}_z$. Let us now consider the integration over the $\mathbf{k}_{||}$-plane. For a given field point **r**, we take the direction of the $\tilde{x}$-axis in the $\mathbf{k}_{||}$-plane along the corresponding $\mathbf{e}_\rho$, and we measure the angle $\tilde{\phi}$ from this axis, as shown in ***Fig. 2***. The dimensionless magnitude of $\mathbf{k}_{||}$ will be denoted by $\alpha = k_{||}/k_o$, which implies that the range $0 \le \alpha < 1$ represents traveling waves and the range $1 < \alpha < \infty$ represents evanescent waves. We further introduce

$$\overline{\beta} = \frac{\beta}{k_o} = \sqrt{1-\alpha^2} \tag{53}$$

with the understanding that $\overline{\beta}$ is positive imaginary for $\alpha > 1$, as in Eq. (2). From Fig. 2 we see that $\mathbf{k}_{||} = \alpha k_o(\mathbf{e}_\rho \cos\tilde{\phi} + \mathbf{e}_\phi \sin\tilde{\phi})$ and therefore

$$\mathbf{K} = \alpha k_o(\mathbf{e}_\rho \cos\tilde{\phi} + \mathbf{e}_\phi \sin\tilde{\phi}) + k_o\overline{\beta}\,\mathrm{sgn}(z)\mathbf{e}_z \tag{54}$$

from which we find $\mathbf{K}\cdot\mathbf{r}=\alpha\overline{\rho}\cos\widetilde{\phi}+\overline{\beta}\,|\,\overline{z}\,|$. Here we used $\mathrm{sgn}(z)z=|\,z\,|$. Combining everything then gives the following translation for an integral over the $\mathbf{k}_{\|}$-plane

$$\int d^2\mathbf{k}_{\|}\,\frac{1}{\beta}\,e^{i\mathbf{K}\cdot\mathbf{r}}(...)=k_o\int_0^\infty d\alpha\,\frac{\alpha}{\overline{\beta}}e^{i\overline{\beta}|\overline{z}|}\int_0^{2\pi}d\widetilde{\phi}\,e^{i\alpha\overline{\rho}\cos\widetilde{\phi}}(...) \tag{55}$$

where the ellipses denote an arbitrary function.

Let us now consider the traveling part of the Green's tensor at the origin of coordinates. We set $\mathbf{r}=0$ in Eq. (51) and use representation (55) for the $\mathbf{k}_{\|}$ integral. The only dependence on $\widetilde{\phi}$ comes in through **KK**, with **K** given by Eq. (54), and the integral over $\widetilde{\phi}$ can be performed directly. For the remaining integral over α we make a change of variables according to $u=(1-\alpha^2)^{1/2}$, after which the integral over u is elementary. Furthermore we recall the resolution of the unit tensor in cylinder coordinates

$$\overleftrightarrow{I}=\mathbf{e}_\rho\mathbf{e}_\rho+\mathbf{e}_\phi\mathbf{e}_\phi+\mathbf{e}_z\mathbf{e}_z \tag{56}$$

which then gives

$$\overleftrightarrow{\chi}(0)^{tr}=\frac{2}{3}i\overleftrightarrow{I}\ . \tag{57}$$

The most important conclusion of this simple result is that the traveling part of the Green's tensor is finite at the origin. Since the Green's tensor itself is highly singular at this point, we conclude that any singularity at $q=0$ must come from the evanescent waves. This also justifies the opinion that near the origin the field of a dipole (or the

Green's tensor) is dominated by the evanescent waves. In the same way we obtain for the Green's vector

$$\boldsymbol{\eta}(0)^{tr} = \frac{1}{2}\mathrm{sgn}(\bar{z})\mathbf{e}_z \tag{58}$$

which is also finite.

VIII. The Auxiliary Functions

In order to study the behavior of the traveling and evanescent waves in detail, we go back to Eq. (48), and we write the $\mathbf{k}_{\|}$ integral as in Eq. (55). Since we now have the exponential of $\mathbf{K}\cdot\mathbf{r} = \alpha\bar{\rho}\cos\tilde{\phi} + \bar{\beta}\,|\,\bar{z}\,|$, the integrals over $\tilde{\phi}$ lead to Bessel functions, as for instance

$$\int_0^{2\pi} d\tilde{\phi}\; e^{i\alpha\bar{\rho}\cos\tilde{\phi}} = 2\pi J_0(\alpha\bar{\rho}) \ . \tag{59}$$

After some rearrangements, the Green's tensor then takes the form

$$\begin{aligned}\overleftrightarrow{\chi}(\mathbf{q}) = &-4\pi\delta(\mathbf{q})\mathbf{e}_z\mathbf{e}_z + \tfrac{1}{2}(\overleftrightarrow{I} + \mathbf{e}_z\mathbf{e}_z)M_a(\mathbf{q}) + \tfrac{1}{2}(\mathbf{e}_\phi\mathbf{e}_\phi - \mathbf{e}_\rho\mathbf{e}_\rho)M_b(\mathbf{q}) \\ &+ \tfrac{1}{2}\mathrm{sgn}(\bar{z})(\mathbf{e}_\rho\mathbf{e}_z + \mathbf{e}_z\mathbf{e}_\rho)M_c(\mathbf{q}) + \tfrac{1}{2}(\overleftrightarrow{I} - 3\mathbf{e}_z\mathbf{e}_z)M_d(\mathbf{q})\end{aligned} \tag{60}$$

where we have introduced four auxiliary functions

$$M_a(\mathbf{q}) = i\int_0^\infty d\alpha \frac{\alpha}{\bar{\beta}} J_0(\alpha\bar{\rho}) e^{i\bar{\beta}|\bar{z}|} \tag{61}$$

$$M_b(\mathbf{q}) = -i\int_0^\infty d\alpha \frac{\alpha^3}{\overline{\beta}} J_2(\alpha\overline{\rho})e^{i\overline{\beta}|\overline{z}|} \tag{62}$$

$$M_c(\mathbf{q}) = 2\int_0^\infty d\alpha\, \alpha^2 J_1(\alpha\overline{\rho})e^{i\overline{\beta}|\overline{z}|} \tag{63}$$

$$M_d(\mathbf{q}) = i\int_0^\infty d\alpha\, \alpha\overline{\beta}\, J_0(\alpha\overline{\rho})e^{i\overline{\beta}|\overline{z}|} \; . \tag{64}$$

These functions are functions of the field point $\mathbf{q}$. They depend on the cylinder coordinates $\overline{\rho}$ and $\overline{z}$ but not on ϕ. With $\overline{\rho} = q\sin\theta$, $\overline{z} = q\cos\theta$, we can also see them as functions of the spherical coordinates q and θ. Furthermore, the $\overline{z}$-dependence only enters as $|\overline{z}|$, and therefore these functions are invariant under reflection in the *xy*-plane. For $\alpha > 1$, $\overline{\beta}$ is positive imaginary, and $\exp(i\overline{\beta}\,|\,\overline{z}\,|)$ decays exponentially with $|\,\overline{z}\,|$, which guarantees the convergence of the integrals. The exception is $\overline{z} = 0$ for which some of the integrals do not exist in the upper limit. We know, however, that the Green's tensor is finite for all points in the *xy*-plane except the origin, so the limit $\overline{z} \to 0$ has to exist. The factors in front of the functions in Eq. (60) show explicitly the tensorial part of the tensor.

In the same way the Green's vector can be written as

$$\boldsymbol{\eta}(\mathbf{q}) = \mathrm{sgn}(\overline{z})\,\mathbf{e}_z\, M_e(\mathbf{q}) + \mathbf{e}_\rho\, M_f(\mathbf{q}) \tag{65}$$

which involves two more auxiliary functions

$$M_e(\mathbf{q}) = \int_0^\infty d\alpha\, \alpha\, J_0(\alpha\overline{\rho})e^{i\overline{\beta}|\overline{z}|} \tag{66}$$

$$M_f(\mathbf{q}) = i\int_0^\infty d\alpha\, \frac{\alpha^2}{\overline{\beta}} J_1(\alpha\overline{\rho})\, e^{i\overline{\beta}|\overline{z}|} \quad . \tag{67}$$

We now have expression (60) for the Green's tensor and expression (24), and these must obviously be the same. We set $\hat{\mathbf{q}} = \sin\theta\,\mathbf{e}_\rho + \cos\theta\,\mathbf{e}_z$ in Eq. (24) and compare to Eq. (60). When equating the corresponding tensorial parts we obtain four equations for the four auxiliary functions. Upon solving this yields the explicit forms

$$M_a(\mathbf{q}) = \frac{e^{iq}}{q} \tag{68}$$

$$M_b(\mathbf{q}) = \sin^2\theta \left[1 + \frac{3}{q}\left(i - \frac{1}{q}\right)\right]\frac{e^{iq}}{q} \tag{69}$$

$$M_c(\mathbf{q}) = -|\sin 2\theta| \left[1 + \frac{3}{q}\left(i - \frac{1}{q}\right)\right]\frac{e^{iq}}{q} \tag{70}$$

$$M_d(\mathbf{q}) = -\frac{8\pi}{3}\delta(\mathbf{q}) - \left(i - \frac{1}{q}\right)\frac{e^{iq}}{q^2} + \cos^2\theta\left[1 + \frac{3}{q}\left(i - \frac{1}{q}\right)\right]\frac{e^{iq}}{q} \quad . \tag{71}$$

We see that $M_a(\mathbf{q})$ is the scalar Green's function from Eq. (10), apart from a factor of k_o, but the other three are more complicated. In particular, $M_d(\mathbf{q})$ has a delta function, which, when added to the delta function in Eq. (60), gives exactly the self field part in Eq. (24). In Appendix A we show that the integral representation (64) contains indeed a delta function, and that it resides entirely in the evanescent part.

Similarly, comparison of Eqs. (28) and (65) gives

$$M_e(\mathbf{q}) = |\cos\theta| \left(\frac{1}{q} - i\right)\frac{e^{iq}}{q} \tag{72}$$

$$M_f(\mathbf{q}) = \sin\theta \left(\frac{1}{q} - i \right) \frac{e^{iq}}{q} \ . \tag{73}$$

IX. Relations Between The Auxiliary Functions

From Eqs. (69) and (70) we observe the relation

$$M_c(\mathbf{q}) = -2\frac{|\,\overline{z}\,|}{\overline{\rho}} M_b(\mathbf{q}) \tag{74}$$

since $|\cos\theta| / \sin\theta = |\,\overline{z}\,| / \overline{\rho}$. Less obvious is:

$$M_d(\mathbf{q}) = M_a(\mathbf{q}) - M_b(\mathbf{q}) - \frac{2}{\overline{\rho}} M_f(\mathbf{q}) \tag{75}$$

as will be shown in Appendix A. Another relation that we notice immediately is

$$M_e(\mathbf{q}) = \frac{|\,\overline{z}\,|}{\overline{\rho}} M_f(\mathbf{q}) \ . \tag{76}$$

Then Eq. (65) becomes

$$\boldsymbol{\eta}(\mathbf{q}) = \frac{1}{\overline{\rho}} \mathbf{q} M_f(\mathbf{q}) \tag{77}$$

as interesting alternative.

When we differentiate the integral representation (61) with respect to $\overline{z}$ and use

$$\frac{d}{d\,\overline{z}} |\,\overline{z}\,| = \mathrm{sgn}(\overline{z}) \tag{78}$$

we obtain the relation

$$\frac{\partial}{\partial \bar{z}} M_a(\mathbf{q}) = -\operatorname{sgn}(\bar{z}) M_e(\mathbf{q}) \tag{79}$$

and similarly

$$\frac{\partial}{\partial \bar{z}} M_e(\mathbf{q}) = \operatorname{sgn}(\bar{z}) M_d(\mathbf{q}) \tag{80}$$

$$\frac{\partial}{\partial \bar{z}} M_f(\mathbf{q}) = -\tfrac{1}{2} \operatorname{sgn}(\bar{z}) M_c(\mathbf{q}) \ . \tag{81}$$

We can also differentiate with respect to $\bar{\rho}$. With $J_0(x)' = -J_1(x)$ we find from Eq. (61)

$$\frac{\partial}{\partial \bar{\rho}} M_a(\mathbf{q}) = -M_f(\mathbf{q}) \tag{82}$$

and similarly

$$\frac{\partial}{\partial \bar{\rho}} M_e(\mathbf{q}) = \operatorname{sgn}(\bar{z}) \frac{\partial}{\partial \bar{z}} M_f(\mathbf{q}) \ . \tag{83}$$

Many other relations can be derived, especially involving higher derivatives.

X. The Evanescent Part

The evanescent part $\overleftrightarrow{\chi}(\mathbf{q})^{ev}$ of the Green's tensor is given by Eq. (51), except that the integration range is $k_{\|} > k_o$. When expressed in auxiliary functions it becomes

$$\overleftrightarrow{\chi}(\mathbf{q})^{ev} = \tfrac{1}{2}(\overleftrightarrow{I} + \mathbf{e}_z\mathbf{e}_z) M_a(\mathbf{q})^{ev} + \tfrac{1}{2}(\mathbf{e}_\phi\mathbf{e}_\phi - \mathbf{e}_\rho\mathbf{e}_\rho) M_b(\mathbf{q})^{ev}$$
$$+ \tfrac{1}{2}\operatorname{sgn}(\bar{z})(\mathbf{e}_\rho\mathbf{e}_z + \mathbf{e}_z\mathbf{e}_\rho) M_c(\mathbf{q})^{ev} + \tfrac{1}{2}(\overleftrightarrow{I} - 3\mathbf{e}_z\mathbf{e}_z) M_d(\mathbf{q})^{ev} \tag{84}$$

and the functions $M_k(\mathbf{q})^{ev}$, $k = a, b, ...$ are the evanescent parts of the functions defined by integral representations in Sec. VIII. This simply means that the lower integration limits become $\alpha = 1$. The evanescent part of the Green's vector $\boldsymbol{\eta}(\mathbf{q})$ is defined similarly.

For $\alpha > 1$ the parameter $\overline{\beta}$ is positive imaginary: $\overline{\beta} = i(\alpha^2 - 1)^{1/2}$. The following theorem for n = 0, 1, ...

$$\int_1^\infty d\alpha \frac{\alpha^{n+1}}{\sqrt{\alpha^2 - 1}} J_n(\alpha\overline{\rho}) e^{-|\overline{z}|\sqrt{\alpha^2-1}} = \frac{1}{|\overline{z}|} J_n(\overline{\rho}) + \frac{\overline{\rho}}{|\overline{z}|} \int_1^\infty d\alpha\, \alpha^n J_{n-1}(\alpha\overline{\rho}) e^{-|\overline{z}|\sqrt{\alpha^2-1}} \tag{85}$$

can be proved as follows. In the integral on the left-hand side, substitute the identity

$$\frac{\alpha}{\sqrt{\alpha^2 - 1}} e^{-|\overline{z}|\sqrt{\alpha^2-1}} = -\frac{1}{|\overline{z}|} \frac{d}{d\alpha} e^{-|\overline{z}|\sqrt{\alpha^2-1}} \tag{86}$$

and integrate by parts. For the derivative in the integrand of the remaining integral use $(x^n J_n(x))' = x^n J_{n-1}(x)$.

For $n = 2$, Eq. (85) can be written as

$$M_c(\mathbf{q})^{ev} = -\frac{2}{\overline{\rho}} \left(J_2(\overline{\rho}) + |\overline{z}|\, M_b(\mathbf{q})^{ev} \right) \tag{87}$$

and for $n = 1$ it becomes

$$M_e(\mathbf{q})^{ev} = -\frac{1}{\overline{\rho}} \left(J_1(\overline{\rho}) - |\overline{z}|\, M_f(\mathbf{q})^{ev} \right). \tag{88}$$

It is interesting to notice the similarity to Eqs. (74) and (76), respectively. Due to the splitting, an additional Bessel function appears on the right-hand side. In Appendix A it is shown that

$$M_d(\mathbf{q})^{ev} = M_a(\mathbf{q})^{ev} - M_b(\mathbf{q})^{ev} - \frac{2}{\overline{\rho}} M_f(\mathbf{q})^{ev} \tag{89}$$

which is identical in form to Eq. (75) for the unsplit functions. Here, no additional term appears. Eqs. (87)-(89) show that if we are able to compute the evanescent parts of $M_a(\mathbf{q})$, $M_b(\mathbf{q})$ and $M_f(\mathbf{q})$ then we also know the evanescent parts of the other three. Since we also know the sum of the traveling and evanescent parts, we will also know the traveling parts of the auxiliary functions. Also the relations involving derivates in Sec. IX carry over to traveling and evanescent waves, since these were derived from the integral representations without using explicitly the limits of integration.

In the integral representations of the evanescent parts of the auxiliary functions we make the change of variables $u = (\alpha^2 - 1)^{1/2}$, which leads to the new representations

$$M_a(\mathbf{q})^{ev} = \int_0^\infty du\, J_0(\overline{\rho}\sqrt{1+u^2})\, e^{-u|\overline{z}|} \tag{90}$$

$$M_b(\mathbf{q})^{ev} = -\int_0^\infty du\, (1+u^2) J_2(\overline{\rho}\sqrt{1+u^2})\, e^{-u|\overline{z}|} \tag{91}$$

$$M_c(\mathbf{q})^{ev} = 2\int_0^\infty du\, u\sqrt{1+u^2} J_1(\overline{\rho}\sqrt{1+u^2})\, e^{-u|\overline{z}|} \tag{92}$$

$$M_d(\mathbf{q})^{ev} = -\int_0^\infty du\, u^2 J_0(\overline{\rho}\sqrt{1+u^2})\, e^{-u|\overline{z}|} \tag{93}$$

$$M_e(\mathbf{q})^{ev} = \int_0^\infty du\ uJ_0(\bar{\rho}\sqrt{1+u^2})e^{-u|\bar{z}|} \tag{94}$$

$$M_f(\mathbf{q})^{ev} = \int_0^\infty du\ \sqrt{1+u^2}J_1(\bar{\rho}\sqrt{1+u^2})e^{-u|\bar{z}|}\ . \tag{95}$$

As a first observation we notice that the singularities (the factors $1/\bar{\beta}$) in the lower limit have disappeared, which proves that these singularities are indeed integrable. A second point to notice is that the evanescent parts are pure real. Conversely, this means that the entire imaginary parts of the Green's tensor and vector consist of traveling waves. Or, only the real parts of the auxiliary functions split

$$\mathrm{Re}\,M_k(\mathbf{q}) = \mathrm{Re}\,M_k(\mathbf{q})^{tr} + M_k(\mathbf{q})^{ev}\ , \quad k = a,b,...f\ . \tag{96}$$

Since we know $M_k(\mathbf{q})$, given by Eqs. (68)-(73), we also know the real parts. Therefore, if we know either the first or the second term on the right-hand side of Eq. (96), we know the other. We shall make use of this frequently.

XI. The Traveling Part

The traveling parts of the auxiliary functions, $M_k(\mathbf{q})^{tr}$, are given by the integral representations of Sec. VIII with the integrations limited to $0 \le \alpha < 1$ and the corresponding Green's tensor then follows from Eq. (84) with the superscripts *ev* replaced by *tr*. As explained in the previous section, the imaginary parts of these functions are

$$\mathrm{Im}\,M_k(\mathbf{q})^{tr} = \mathrm{Im}\,M_k(\mathbf{q})\ , \quad k = a,b,...f \tag{97}$$

and the functions on the right-hand side are the imaginary parts of the right-hand sides of Eqs. (68)-(73). So we shall only be concerned with the real parts of the functions $M_k(\mathbf{q})^{tr}$.

We now make the change of variables $u = (1-\alpha^2)^{1/2}$ in the integral representations, and we take the real parts. This yields the following representations

$$\mathrm{Re}\, M_a(\mathbf{q})^{tr} = -\int_0^1 du\, J_0(\bar{\rho}\sqrt{1-u^2})\sin(u\,|\,\bar{z}\,|) \tag{98}$$

$$\mathrm{Re}\, M_b(\mathbf{q})^{tr} = \int_0^1 du\, (1-u^2) J_2(\bar{\rho}\sqrt{1-u^2})\sin(u\,|\,\bar{z}\,|) \tag{99}$$

$$\mathrm{Re}\, M_c(\mathbf{q})^{tr} = 2\int_0^1 du\, u\sqrt{1-u^2}\, J_1(\bar{\rho}\sqrt{1-u^2})\cos(u\,|\,\bar{z}\,|) \tag{100}$$

$$\mathrm{Re}\, M_d(\mathbf{q})^{tr} = -\int_0^1 du\, u^2 J_0(\bar{\rho}\sqrt{1-u^2})\sin(u\,|\,\bar{z}\,|) \tag{101}$$

$$\mathrm{Re}\, M_e(\mathbf{q})^{tr} = \int_0^1 du\, u J_0(\bar{\rho}\sqrt{1-u^2})\cos(u\,|\,\bar{z}\,|) \tag{102}$$

$$\mathrm{Re}\, M_f(\mathbf{q})^{tr} = -\int_0^1 du\, \sqrt{1-u^2}\, J_1(\bar{\rho}\sqrt{1-u^2})\sin(u\,|\,\bar{z}\,|)\ . \tag{103}$$

We shall use these representations for numerical integration, and in the graphs of the following sections, this will be referred to as the “exact” solutions. By computing these integrals numerically, we also have a reference for the evanescent parts, according to Eq. (96). It should be noted that for large values of $\bar{\rho}$ and/or $|\,\bar{z}\,|$ this becomes very computer time consuming due to the fast oscillations of the integrands.

Equations (74)-(76) show relations between the unsplit functions. If we take the real parts of these equations, they still hold in the same form since all terms are real. The corresponding relations for the traveling parts then follow by taking the difference with Eqs. (87)-(89) for the evanescent parts, according to Eq. (96). We thus find

$$\mathrm{Re}\,M_c(\mathbf{q})^{tr} = \frac{2}{\overline{\rho}}\left(J_2(\overline{\rho}) - |\,\overline{z}\,|\,\mathrm{Re}\,M_b(\mathbf{q})^{tr}\right) \tag{104}$$

$$\mathrm{Re}\,M_e(\mathbf{q})^{tr} = \frac{1}{\overline{\rho}}\left(J_1(\overline{\rho}) + |\,\overline{z}\,|\,\mathrm{Re}\,M_f(\mathbf{q})^{tr}\right) \tag{105}$$

$$\mathrm{Re}\,M_d(\mathbf{q})^{tr} = \mathrm{Re}\,M_a(\mathbf{q})^{tr} - \mathrm{Re}\,M_b(\mathbf{q})^{tr} - \frac{2}{\overline{\rho}}\mathrm{Re}\,M_f(\mathbf{q})^{tr} \ . \tag{106}$$

XII. The *z*-Axis

Let us consider a field point on the *z*-axis ($\overline{z} \neq 0$). We then have $\overline{\rho} = 0$, and with $J_0(0) = 1$ we find from Eq. (90)

$$M_a(\mathbf{q})^{ev} = \frac{1}{|\,\overline{z}\,|} \tag{107}$$

for the scalar Green's function. Similarly, from Eqs. (93) and (94) we obtain

$$M_d(\mathbf{q})^{ev} = -\frac{2}{|\,\overline{z}\,|^3} \tag{108}$$

$$M_e(\mathbf{q})^{ev} = \frac{1}{|\,\overline{z}\,|^2} \ . \tag{109}$$

Since $J_n(0) = 0$ for $n \neq 0$ the remaining functions vanish on the *z*-axis:

$$M_b(\mathbf{q})^{ev} = M_c(\mathbf{q})^{ev} = M_f(\mathbf{q})^{ev} = 0 \ . \tag{110}$$

The evanescent parts of the Green's tensor and vector then become

$$\overleftrightarrow{\chi}(\mathbf{q})^{ev} = \tfrac{1}{2}(\overleftrightarrow{\mathrm{I}} + \mathbf{e}_z\mathbf{e}_z)\frac{1}{|\bar{z}|} - (\overleftrightarrow{\mathrm{I}} - 3\mathbf{e}_z\mathbf{e}_z)\frac{1}{|\bar{z}|^3} \tag{111}$$

$$\boldsymbol{\eta}(\mathbf{q})^{ev} = \mathrm{sgn}(\bar{z})\,\mathbf{e}_z \frac{1}{|\bar{z}|^2} \ . \tag{112}$$

On the z-axis, we have $|\bar{z}| = q$ so the first term on the right-hand side of Eq. (111) is of the far field type, being $\mathcal{O}(1/q)$, or $\mathcal{O}(1/r)$. As mentioned in the Introduction, fields that drop off with distance as $\mathcal{O}(1/r)$ can be detected at a macroscopic distance from the source. It seems counterintuitive that waves which decay exponentially in the z-direction can survive in the far field on this z-axis. We also notice that the Green's vector, representing the magnetic field, is $\mathcal{O}(1/q^2)$. We thus conclude that the electric evanescent waves end up in the far field on the z-axis, but the corresponding magnetic evanescent waves do not.

Some years ago, the subject of evanescent waves in the far field of an electric dipole was vigorously debated in the literature. The origin of the controversy goes back to a series of papers by Xiao (for instance, Xiao, 1996), who also derived Eq. (111) for the Green's tensor on the z-axis. He made the unfortunate mistake to conclude that since the z-axis is an arbitrary axis in space, Eq. (111) should hold for all directions, so $\overleftrightarrow{\chi}(\mathbf{q})^{ev}$ for all $\mathbf{r}$ should follow from Eq. (111) by replacing $|\bar{z}|$ by q and $\mathbf{e}_z$ by $\hat{\mathbf{q}}$ (in our notation). Wolf and Foley (1998) responded by noting that evanescent waves can only contribute to the far field along the z-axis (or the xy-plane), similar to the Stokes phenomenon in asymptotic analysis, and that this whole issue is of no interest and just a mathematical oddity. We shall see below that this conclusion is also incorrect, although closer to the truth. This discussion continued for a while (Xiao, 1999; Carney, *et.al.*, 2000; Lakhtakia and Weiglhofer, 2000; Xiao, 2000) until the correct solution to this problem was presented by Shchegrov and Carney (1999) and Setälä, *et.al.* (1999).

On the z-axis we have $\hat{\mathbf{q}} = \mathrm{sgn}(z)\mathbf{e}_z$, $q = |\bar{z}|$ and the unsplit Green's tensor and vector follow from Eqs. (24) and (28), respectively:

$$\overleftrightarrow{\chi}(\mathbf{q}) = (\overleftrightarrow{\mathrm{I}} - \mathbf{e}_z\mathbf{e}_z)\frac{e^{i|\bar{z}|}}{|\bar{z}|} + (\overleftrightarrow{\mathrm{I}} - 3\mathbf{e}_z\mathbf{e}_z)\left(i - \frac{1}{|\bar{z}|}\right)\frac{e^{i|\bar{z}|}}{|\bar{z}|^2} \tag{113}$$

$$\boldsymbol{\eta}(\mathbf{q}) = \mathrm{sgn}(\bar{z})\mathbf{e}_z\left(\frac{1}{|\bar{z}|} - i\right)\frac{e^{i|\bar{z}|}}{|\bar{z}|} \;. \tag{114}$$

It should be noted that the tensor structure in Eq. (113) is different from the structure in Eq. (111). Another noticeable difference is that the evanescent tensor and vector do not have the factors $\exp(i|\bar{z}|)$, and therefore do not correspond to outgoing spherical waves.

XIII. The *xy*-Plane

Next we consider the situation in the xy-plane. Here we have $\bar{z} = 0$, and the integrals defining the evanescent parts of the auxiliary functions, Eqs. (90)-(95), may not exist. To get around this we first consider the traveling part. From Eqs. (98), (99), (101) and (103) we obtain

$$\mathrm{Re}\,M_a(\mathbf{q})^{tr} = \mathrm{Re}\,M_b(\mathbf{q})^{tr} = \mathrm{Re}\,M_d(\mathbf{q})^{tr} = \mathrm{Re}\,M_f(\mathbf{q})^{tr} = 0 \tag{115}$$

because $\sin(u\,|\,\bar{z}\,|)=0$. The two remaining ones involve integrals over Bessel functions, but with Eqs. (104) and (105) we immediately obtain

$$\mathrm{Re}\,M_c(\mathbf{q})^{tr}=\frac{2}{\bar{\rho}}J_2(\bar{\rho}) \tag{116}$$

$$\mathrm{Re}\,M_e(\mathbf{q})^{tr}=\frac{1}{\bar{\rho}}J_1(\bar{\rho})\ . \tag{117}$$

On the other hand, the real parts of $M_k(\mathbf{q})$ follow by taking the real parts of the right-hand sides of Eqs. (68)-(73), after which the $M_k(\mathbf{q})^{ev}$'s follow by taking the difference with Eqs. (115)-(117), according to Eq. (96). We find

$$M_a(\mathbf{q})^{ev}=\frac{\cos\bar{\rho}}{\bar{\rho}} \tag{118}$$

$$M_b(\mathbf{q})^{ev}=\frac{\cos\bar{\rho}}{\bar{\rho}}-\frac{3}{\bar{\rho}^2}\left(\sin\bar{\rho}+\frac{\cos\bar{\rho}}{\bar{\rho}}\right) \tag{119}$$

$$M_c(\mathbf{q})^{ev}=-\frac{2}{\bar{\rho}}J_2(\bar{\rho}) \tag{120}$$

$$M_d(\mathbf{q})^{ev}=\frac{1}{\bar{\rho}^2}\left(\sin\bar{\rho}+\frac{\cos\bar{\rho}}{\bar{\rho}}\right) \tag{121}$$

$$M_e(\mathbf{q})^{ev}=-\frac{1}{\bar{\rho}}J_1(\bar{\rho}) \tag{122}$$

$$M_f(\mathbf{q})^{ev}=\frac{1}{\bar{\rho}}\left(\sin\bar{\rho}+\frac{\cos\bar{\rho}}{\bar{\rho}}\right)\ . \tag{123}$$

An interesting point to observe is that from Eqs. (70) and (72) we find

$$M_c(\mathbf{q})=M_e(\mathbf{q})=0 \tag{124}$$

since $\theta=\pi/2$ in the *xy*-plane. However, the evanescent parts of these functions are *not* zero, and neither are the traveling parts, Eqs. (116) and (117). So two functions which are identically zero each split in a traveling and evanescent part with opposite sign.

In the *xy*-plane we have in leading order

$$M_a(\mathbf{q})^{ev} = \frac{\cos\bar{\rho}}{\bar{\rho}} \approx M_b(\mathbf{q})^{ev} \tag{125}$$

$$M_f(\mathbf{q})^{ev} \approx \frac{\sin\bar{\rho}}{\bar{\rho}} \tag{126}$$

for $\bar{\rho}$ large (the Bessel functions are $\mathcal{O}(1/\sqrt{\bar{\rho}}\,)$. This shows that the evanescent waves along the *xy*-plane also have an $\mathcal{O}(1/q)$ part which survives in the far field. The evanescent part of the Green's tensor is in leading order for $\bar{\rho}$ large

$$\overleftrightarrow{\chi}(\mathbf{q})^{ev} \approx (\overleftrightarrow{\mathrm{I}} - \mathbf{e}_\rho \mathbf{e}_\rho)\frac{\cos\bar{\rho}}{\bar{\rho}} \tag{127}$$

and the Green's vector is

$$\boldsymbol{\eta}(\mathbf{q})^{ev} \approx \mathbf{e}_\rho \frac{\sin\bar{\rho}}{\bar{\rho}} \quad . \tag{128}$$

It follows from Eqs. (24) and (28) that the unsplit Green's tensor and vector for large q are

$$\overleftrightarrow{\chi}(\mathbf{q}) \approx (\overleftrightarrow{\mathrm{I}} - \hat{\mathbf{q}}\hat{\mathbf{q}})\frac{e^{iq}}{q} \tag{129}$$

$$\boldsymbol{\eta}(\mathbf{q}) \approx -i\hat{\mathbf{q}}\frac{e^{iq}}{q} \quad . \tag{130}$$

In the *xy*-plane we have $q = \bar{\rho}$ and $\hat{\mathbf{q}} = \mathbf{e}_\rho$, so we find

$$\mathrm{Re}\,\overleftrightarrow{\chi}(\mathbf{q}) \approx \overleftrightarrow{\chi}(\mathbf{q})^{ev} \tag{131}$$

$$\mathrm{Re}\,\boldsymbol{\eta}(\mathbf{q}) \approx \boldsymbol{\eta}(\mathbf{q})^{ev} \quad . \tag{132}$$

So, in the *xy*-plane the real parts of the Green's tensor and vector consist purely of evanescent waves in the far field, and the imaginary parts are pure traveling. This shows that in the *xy*-plane the traveling and evanescent waves contribute "equally" to the far field. It should also be noted that the evanescent waves here are of the spherical wave type, unlike on the *z*-axis. ***Figure 3*** shows a polar graph of $M_a(\mathbf{q})^{ev}$ and $\mathrm{Re}\, M_a(\mathbf{q})^{tr}$ for $q = 8\pi$, and we see that near the *xy*-plane the evanescent waves dominate over the real part of the traveling waves. On the *z*-axis we have $\mathrm{Re}\, M_a(\mathbf{q})^{tr} = (\cos|\bar{z}|-1)/|\bar{z}|$, and this is zero for $q = 8\pi$, so also there the evanescent waves dominate for this value of q. For other values of *q*, the traveling and evanescent waves contribute about equally near the *z*-axis, but near the *xy*-plane the evanescent waves dominate over $\mathrm{Re}\, M_a(\mathbf{q})^{tr}$ for all *q*, since $\mathrm{Re}\, M_a(\mathbf{q})^{tr} = 0$ for all *q*.

From

$$\mathrm{Re}\, M_a(\mathbf{q})^{tr} + M_a(\mathbf{q})^{ev} = \mathrm{Re}\, M_a(\mathbf{q}) = \frac{\cos q}{q} \tag{133}$$

we see that this unsplit function is independent of the polar angle θ. The splitting introduces a strong angle dependence of both the evanescent part and the real part of the traveling part, as can be seen in Fig. 3. This angle dependence of the split auxiliary functions will be studied in detail in the next sections.

XIV. Relation to Lommel Functions

The traveling part of $M_a(\mathbf{q})$ is given by the integral representation (61) with the upper limit replaced by $\alpha = 1$. Explicitly

$$M_a(\mathbf{q})^{tr} = i\int_0^1 d\alpha \, \frac{\alpha}{\sqrt{1-\alpha^2}} J_0(\alpha\overline{\rho}) e^{i|\overline{z}|\sqrt{1-\alpha^2}} \quad . \tag{134}$$

It turns out that this integral is tabulated (Prudnikov, *et.al.*, 1986b), although the formula contains a misprint. The factor [exp(*ia*...)...] should read [-*i*exp(*ia*...)...]. The result is expressed in terms of a Lommel function (Watson, 1922; page 487 of Born and Wolf, 1980), which is a function of two variables, defined as a series with each term containing a Bessel function. This result has been applied by Bertilone (1991a, 1991b) for the study of scalar diffraction problems. Since $M_a(\mathbf{q}) = \exp(iq)/q$ we can obtain the evanescent part by taking the difference. The result is

$$M_a(\mathbf{q})^{ev} = \frac{1}{q}\left[J_0(\overline{\rho}) + 2\sum_{m=1}^{\infty}\left(-\tan^2 \tfrac{1}{2}\theta\right)^m J_{2m}(\overline{\rho}) \right] \tag{135}$$

for $|\overline{z}| > 0$. For $|\overline{z}| < 0$ we then use the fact that $M_a(\mathbf{q})^{ev}$ is invariant under reflection in the *xy*-plane. By taking derivatives as in Sec. IX and with the various relations between the evanescent parts, given in Sec. X, we can find the other auxiliary functions in a similar form (Arnoldus and Foley, 2002a). We see from Eq. (135) that $M_a(\mathbf{q})^{ev}$ is expressed in the coordinates $\overline{\rho}$ and θ, which is a mix of cylinder and spherical coordinates. For $\theta = 0$ the entire series disappears, and with $\overline{\rho} = 0$ for $\theta = 0$ we also have $J_0(0)=1$, so that $M_a(\mathbf{q})^{ev}=1/q$, as in Eq. (107). For larger values of θ all terms contribute, but the series remains convergent for all θ and $\overline{\rho}$. Result (135) is interesting in its own right, and provides an alternative to numerical integration. However, it does not shed much light on the behavior of the evanescent waves in the near- and the far field. Also, the expressions for the other auxiliary functions are not as elegant as Eq. (135), it seems. In the next section we shall derive our own series expansions, also in terms of Bessel functions, and the result will be applied to obtain the expansions of $M_k(\mathbf{q})^{ev}$ in series with q as the variable, and in the neighborhood of the origin, e.g., the near field. The result will exhibit precisely how the evanescent waves determine the near field, and in particular how the singular behavior at the origin arises.

XV. Expansion in Series with Bessel Functions

In order to arrive at a useful expansion of the evanescent parts of the Green's tensor and vector near the origin, we start with the real parts of the traveling parts of the auxiliary functions. Their integral representations are given in Eqs. (98)-(103). We shall illustrate the method with $\mathrm{Re}\,M_a(\mathbf{q})^{tr}$ and then give the results for the other functions. First we replace the Bessel function by its series expansion:

$$J_n(x)=\sum_{k=0}^{\infty}\frac{(-1)^k}{k!(k+n)!}\left(\frac{x}{2}\right)^{2k+n} \tag{136}$$

with $n=0$ and $x=\overline{\rho}(1-u^2)^{1/2}$, and we replace $\sin(u\,|\,\overline{z}\,|)$ by its expansion for small argument. We then obtain the double series

$$\mathrm{Re}\, M_a(\mathbf{q})^{tr} = \sum_{k=0}^{\infty} \sum_{\ell=0}^{\infty} \frac{(-1)^{k+\ell+1}}{(k!)^2 (2\ell+1)!} \left(\frac{\overline{\rho}}{2} \right)^{2k} |\,\overline{z}\,|^{2\ell+1} \times \int_0^1 du\, (1-u^2)^k u^{2\ell+1} \ . \tag{137}$$

The integral on the right-hand side can be evaluated, with result $\frac{1}{2} k!\ell!/(k+\ell+1)!$. When we substitute this into Eq. (137) and compare to Eq. (136) then we recognize the summation over k as the series representation of a Bessel function of order $\ell+1$. In this fashion we find the following series representation:

$$\mathrm{Re}\, M_a(\mathbf{q})^{tr} = -\frac{|\,\overline{z}\,|}{\overline{\rho}} \sum_{\ell=0}^{\infty} \frac{\ell!}{(2\ell+1)!} \left(-\frac{2\overline{z}^2}{\overline{\rho}} \right)^{\ell} J_{\ell+1}(\overline{\rho}) \ . \tag{138}$$

With $|\,J_{\ell+1}(\overline{\rho})\,| \leq 1$ and for $\overline{\rho} \neq 0$, it follows from the ratio test that this series converges. For $\overline{\rho} \to 0$ we have to take into account the behavior of the Bessel functions near $\overline{\rho} = 0$, given by the first term of the series in Eq. (136). When substituted into the right-hand side of Eq. (138) it follows again by the ratio test that the series also converges for $\overline{\rho} = 0$.

The series expansions for the other auxiliary functions follow in the same way, with result:

$$\mathrm{Re}\, M_b(\mathbf{q})^{tr} = \frac{|\,\overline{z}\,|}{\overline{\rho}} \sum_{\ell=0}^{\infty} \frac{\ell!}{(2\ell+1)!} \left(-\frac{2\overline{z}^2}{\overline{\rho}} \right)^{\ell} J_{\ell+3}(\overline{\rho}) \tag{139}$$

$$\mathrm{Re}\, M_c(\mathbf{q})^{tr} = \frac{2}{\overline{\rho}} \sum_{\ell=0}^{\infty} \frac{\ell!}{(2\ell)!} \left(-\frac{2\overline{z}^2}{\overline{\rho}} \right)^{\ell} J_{\ell+2}(\overline{\rho}) \tag{140}$$

$$\mathrm{Re}\, M_d(\mathbf{q})^{tr} = -\frac{2|\bar{z}|}{\bar{\rho}^2}\sum_{\ell=0}^{\infty}\frac{(\ell+1)!}{(2\ell+1)!}\left(-\frac{2\bar{z}^2}{\bar{\rho}}\right)^{\ell} J_{\ell+2}(\bar{\rho}) \tag{141}$$

$$\mathrm{Re}\, M_e(\mathbf{q})^{tr} = \frac{1}{\bar{\rho}}\sum_{\ell=0}^{\infty}\frac{\ell!}{(2\ell)!}\left(-\frac{2\bar{z}^2}{\bar{\rho}}\right)^{\ell} J_{\ell+1}(\bar{\rho}) \tag{142}$$

$$\mathrm{Re}\, M_f(\mathbf{q})^{tr} = -\frac{|\bar{z}|}{\bar{\rho}}\sum_{\ell=0}^{\infty}\frac{\ell!}{(2\ell+1)!}\left(-\frac{2\bar{z}^2}{\bar{\rho}}\right)^{\ell} J_{\ell+2}(\bar{\rho})\,. \tag{143}$$

The most interesting way to look at this is by considering this as Taylor series expansions in $|\bar{z}|$ around $|\bar{z}|=0$ for $\bar{\rho}$ fixed. For $|\bar{z}|=0$ only the first term, $\ell=0$, contributes, and we get exactly the result from Sec. XIII, Eqs. (115)-(117). For $|\bar{z}|\neq 0$ we need to keep more terms. Then, if we calculate $\mathrm{Re}\, M_k(\mathbf{q})^{tr}$ with the series expansions above, we can also find the evanescent parts near the *xy*-plane with Eq. (96), where $\mathrm{Re}\, M_k(\mathbf{q})$ are the real parts of the right-hand sides of Eqs. (68)-(73). For instance

$$M_a(\mathbf{q})^{ev} = \frac{\cos q}{q} + \frac{|\bar{z}|}{\bar{\rho}} J_1(\bar{\rho}) - \frac{1}{3}\frac{|\bar{z}|^3}{\bar{\rho}^2} J_2(\bar{\rho}) + \dots\,. \tag{144}$$

Figure 4 shows $M_a(\mathbf{q})^{ev}$ for $\bar{\rho}=5$, computed this way, and with the series summed up to $\ell=20$. It is seen that the series expansion perfectly reproduces the exact result, obtained with numerical integration, up to about $|\bar{z}|=12$. If more terms are included, the range gets larger, but also the computation has to be done in double precision.

The series solution (144) can be seen as an expansion near the *xy*-plane. On the other hand, the solution with Lommel functions, Eq. (135), could be considered an expansion near the *z*-axis, since for a field point on the *z*-axis we only need to keep one term. In this sense, both result are complementary. In the next section we shall derive an expansion which is truly complementary to the above. We shall consider again $\bar{\rho}$ fixed and $|\bar{z}|$ as the variable, but now with $|\bar{z}|$ large, leading to an asymptotic series in $|\bar{z}|$.

XVI. Asymptotic Series

In order to derive an asymptotic expansion for large $|\bar{z}|$ we start from the integral representations for $M_k(\mathbf{q})^{ev}$, Eqs. (90)-(95). We notice that these integrals have the form of Laplace transforms with $|\bar{z}|$ as the Laplace parameter. The standard procedure for obtaining an asymptotic expansion for integrals of this type is repeated integration by parts. In this way we get one term at a time, and every next term becomes more difficult to obtain. In this section we take a different approach, which leads to the entire asymptotic series.

As in the previous section, we expand the Bessel function in Eq. (90) in its power series, Eq. (136), but now we do not expand the exponential. This gives

$$M_a(\mathbf{q})^{ev} = \sum_{k=0}^{\infty} \frac{(-1)^k}{(k!)^2} \left(\frac{\bar{\rho}}{2}\right)^{2k} \int_0^{\infty} du\, (1+u^2)^k e^{-u|\bar{z}|} \tag{145}$$

in analogy to Eq. (137). We expand $(1+u^2)^k$ with Newton's binomium and then we integrate each term. This yields

$$M_a(\mathbf{q})^{ev} = \sum_{k=0}^{\infty} \sum_{\ell=0}^{k} \frac{(-1)^k (2\ell)!}{k!\ell!(k-\ell)!} \left(\frac{\bar{\rho}}{2}\right)^{2k} \frac{1}{|\bar{z}|^{2\ell+1}} \ . \tag{146}$$

Then we change the order of summation and set $n = k - \ell$ in the summation over k:

$$M_a(\mathbf{q})^{ev} = \sum_{\ell=0}^{\infty} \sum_{n=0}^{\infty} \frac{(-1)^{n+\ell}(2\ell)!}{n!\ell!(n+\ell)!} \left(\frac{\overline{\rho}}{2}\right)^{2n+2\ell} \frac{1}{|\overline{z}|^{2\ell+1}} \ . \tag{147}$$

Here we recognize the summation over n as the series expansion for the Bessel function $J_\ell(\overline{\rho})$, which then gives

$$M_a(\mathbf{q})^{ev} = \frac{1}{|\overline{z}|} \sum_{\ell=0}^{\infty} \frac{(2\ell)!}{\ell!} \left(-\frac{\overline{\rho}}{2\overline{z}^2}\right)^{\ell} J_\ell(\overline{\rho}) \tag{148}$$

in striking resemblance with Eq. (138). For the other auxiliary functions we obtain along the same lines

$$M_b(\mathbf{q})^{ev} = -\frac{1}{|\overline{z}|} \sum_{\ell=0}^{\infty} \frac{(2\ell)!}{\ell!} \left(-\frac{\overline{\rho}}{2\overline{z}^2}\right)^{\ell} J_{\ell-2}(\overline{\rho}) \tag{149}$$

$$M_c(\mathbf{q})^{ev} = -\frac{2}{|\overline{z}|^2} \sum_{\ell=0}^{\infty} \frac{(2\ell+1)!}{\ell!} \left(-\frac{\overline{\rho}}{2\overline{z}^2}\right)^{\ell} J_{\ell-1}(\overline{\rho}) \tag{150}$$

$$M_d(\mathbf{q})^{ev} = -\frac{1}{|\overline{z}|^3} \sum_{\ell=0}^{\infty} \frac{(2\ell+2)!}{\ell!} \left(-\frac{\overline{\rho}}{2\overline{z}^2}\right)^{\ell} J_\ell(\overline{\rho}) \tag{151}$$

$$M_e(\mathbf{q})^{ev} = \frac{1}{|\overline{z}|^2} \sum_{\ell=0}^{\infty} \frac{(2\ell+1)!}{\ell!} \left(-\frac{\overline{\rho}}{2\overline{z}^2}\right)^{\ell} J_\ell(\overline{\rho}) \tag{152}$$

$$M_f(\mathbf{q})^{ev} = -\frac{1}{|\overline{z}|} \sum_{\ell=0}^{\infty} \frac{(2\ell)!}{\ell!} \left(-\frac{\overline{\rho}}{2\overline{z}^2}\right)^{\ell} J_{\ell-1}(\overline{\rho}) \ . \tag{153}$$

For Bessel functions with negative order we have $J_{-n}(\overline{\rho}) = (-1)^n J_n(\overline{\rho})$.

For $\overline{\rho} = 0$ the only possibly surviving terms are the $k = 0$ terms, but since $J_n(0) = 0$ for $n \neq 0$, we will only have a non-zero term left if the $k = 0$ term has the Bessel function $J_0(\overline{\rho})$. This happens for $M_a(\mathbf{q})^{ev}$, $M_d(\mathbf{q})^{ev}$ and $M_e(\mathbf{q})^{ev}$, and the single terms are exactly Eqs. (107)-(109). All others are zero for $\overline{\rho} = 0$, e.g., on the z-axis, in agreement with Eq. (110). For $\overline{\rho} \neq 0$ the series diverge and they have to be considered asymptotic series for $|\overline{z}|$ large, given $\overline{\rho}$.

XVII. Evanescent Waves in the Far Field

In the far field, q is large and θ is arbitrary. The standard method to obtain an asymptotic solution for q large from an angular spectrum representation is by the method of stationary phase. It is shown in Appendix B that it seems to follow from this method that only traveling waves contribute to the far field, and it is also shown that this might not necessarily be true. In any case, we shall consider the contribution of the evanescent waves to the far field by means of our asymptotic expansion from the previous section. This asymptotic solution is in terms of the cylinder coordinates $\overline{\rho}$ and $\overline{z}$, so we shall consider $|\overline{z}|$ large and $\overline{\rho}$ arbitrary. Since $\overline{z} = q\cos\theta$, the factors in front of the series are already $\mathcal{O}(1/q)$ or of higher order. For $|\overline{z}|$ sufficiently large, compared to $\overline{\rho}$, at most the $\ell = 0$ term will contribute to the far field. We then find

$$M_a(\mathbf{q})^{ev} \approx \frac{1}{|\overline{z}|} J_0(\overline{\rho}) \tag{154}$$

$$M_b(\mathbf{q})^{ev} \approx -\frac{1}{|\overline{z}|} J_2(\overline{\rho}) \tag{155}$$

$$M_f(\mathbf{q})^{ev} \approx \frac{1}{|\overline{z}|} J_1(\overline{\rho}) \tag{156}$$

and the others are of higher order and therefore give no possible contribution to the far field.

First we notice that on the z-axis we have $J_0(0)=1$, $J_1(0)=J_2(0)=0$, and Eqs. (154)-(156) simplify further to

$$M_a(\mathbf{q})^{ev} \approx \frac{1}{|\bar{z}|} \tag{157}$$

with all others of higher order. The corresponding evanescent parts of the Green's tensor and vector are therefore

$$\overleftrightarrow{\chi}(\mathbf{q})^{ev} \approx \tfrac{1}{2}(\overleftrightarrow{I} + \mathbf{e}_z\mathbf{e}_z)\frac{1}{q} \tag{158}$$

$$\boldsymbol{\eta}(\mathbf{q})^{ev} \approx 0 \tag{159}$$

since $|\bar{z}| = q$, which is in agreement with Eqs. (111) and (112) up to leading order. Therefore, the electric field is $\mathcal{O}(1/q)$, and the magnetic field does not survive on the z-axis in the far field. Let us now consider $\bar{\rho}$ large. We can then use the asymptotic form of the Bessel functions

$$J_n(\bar{\rho}) \approx \sqrt{\frac{2}{\pi\bar{\rho}}}\cos(\bar{\rho} - \tfrac{1}{2}n\pi - \tfrac{1}{4}\pi) \ . \tag{160}$$

With $\bar{\rho} = q\sin\theta$ we see that the Bessel functions are $\mathcal{O}(1/q^{1/2})$, and the three functions in Eqs. (154)-(156) become $\mathcal{O}(1/q^{3/2})$. This shows that $M_a(\mathbf{q})^{ev}$ varies from $\mathcal{O}(1/q)$ on the z-axis to $\mathcal{O}(1/q^{3/2})$ off the z-axis, and the transition goes smoothly as given by Eq. (154). The other two functions are zero on the z-axis and they go over in $\mathcal{O}(1/q^{3/2})$ off the z-axis. All other functions remain of higher order. This shows that to leading order off the z-axis the evanescent waves are $\mathcal{O}(1/q^{3/2})$, which drops off faster than $\mathcal{O}(1/q)$, and therefore they do not contribute to the far field. They could be considered to be just in between the far field and the middle field. The transition between $\mathcal{O}(1/q)$ and $\mathcal{O}(1/q^{3/2})$ occurs where the asymptotic approximation (160) sets in, which is at about $\overline{\rho} = 1$. Therefore we conclude that there is a cylindrical region around the *z*-axis with a diameter of about a wavelength, and inside this cylinder the evanescent waves of the electric field survive in the far field, whereas outside this cylinder they do not. Since the diameter of this cylinder is finite, its angular measure $\Delta\theta$ is zero for q large. So, seen as a function of θ, the evanescent waves only survive for $\theta = 0$ and π, giving the impression of a point singularity of no significance, but it should be clear now that such an interpretation is a consequence of using the wrong coordinates (spherical rather than cylinder coordinates).

For $\overline{\rho}$ large it follows from Eq. (160) that $J_2(\overline{\rho}) \approx -J_0(\overline{\rho})$, so that $M_b(\mathbf{q})^{ev} \approx M_a(\mathbf{q})^{ev}$. We then find for the Green's tensor and vector

$$\overleftrightarrow{\chi}(\mathbf{q})^{ev} \approx \frac{1}{q^{3/2}} \frac{1}{|\cos\theta|} \sqrt{\frac{2}{\pi \sin\theta}} \cos(q \sin\theta - \pi/4)\,(\overleftrightarrow{\mathrm{I}} - \mathbf{e}_\rho \mathbf{e}_\rho) \tag{161}$$

$$\vec{\eta}(\mathbf{q})^{ev} \approx \frac{1}{q^{3/2}} \frac{1}{|\cos\theta|} \sqrt{\frac{2}{\pi \sin\theta}} \sin(q \sin\theta - \pi/4)\,\mathbf{e}_\rho \tag{162}$$

expressed in spherical coordinates. It is interesting to see that also the tensor structure of $\overleftrightarrow{\chi}(\mathbf{q})^{ev}$ off the *z*-axis is different from the tensor structure on the *z*-axis, as shown in Eq. (158).

Finally, the asymptotic approximations for the Green's tensor and vector that hold both on and off the *z*-axis, including the smooth transition, are given by

$$\overleftrightarrow{\chi}(\mathbf{q})^{ev} \approx \tfrac{1}{2}(\overleftrightarrow{\mathrm{I}} + \mathbf{e}_z \mathbf{e}_z) M_a(\mathbf{q})^{ev} + \tfrac{1}{2}(\mathbf{e}_\phi \mathbf{e}_\phi - \mathbf{e}_\rho \mathbf{e}_\rho) M_b(\mathbf{q})^{ev} \tag{163}$$

$$\boldsymbol{\eta}(\mathbf{q}) \approx \mathbf{e}_\rho M_f(\mathbf{q}) \tag{164}$$

with the auxiliary functions given by (154)-(156). Obviously, the approximation discussed in this section does not hold near the *xy*-plane, since we used the asymptotic expansion for $|\bar{z}|$ large. However, it is interesting to notice that for a field point in the *xy*-plane with $\bar{\rho}$ large, the same three auxiliary functions have an $\mathcal{O}(1/q)$ part, according to Eqs. (125) and (126). Therefore, the Green's tensor and vector are identical in form to Eqs. (163) and (164), but the expressions for the auxiliary functions must be different. The question now arises whether it would be possible to find expressions for the three auxiliary functions such that Eqs. (163) and (164) would give the asymptotic (q large, any θ) approximation for the Green's tensor and vector everywhere. This is the topic of the next section.

XVIII. Uniform Asymptotic Approximation

The behavior of the evanescent waves near the *xy*-plane follows from Sec. XV, and the result takes the form as in Eq. (144). The leading term is the total, unsplit, $\mathrm{Re}\, M_k(\mathbf{q})$, and the series is a Taylor series in $|\bar{z}|$ for a fixed $\bar{\rho}$. Although this is perfect for numerical computation, it does not indicate how the solution in the *xy*-plane goes over in the typical $\mathcal{O}(1/q^{3/2})$ behavior off the *xy*-plane. In this section we shall derive an asymptotic approximation which connects the solution in the *xy*-plane in a smooth way to the solution off the *xy*-plane. The method described below was introduced by Berry (2001) in this problem, who considered the evanescent part of the scalar Green's function, and this approach was extended by us (Arnoldus and Foley, 2002b) to include all auxiliary functions of the Green's tensor. We also improved Berry's result in that our solution covers the entire range of angles from the *xy*-plane up to the *z*-axis with a single asymptotic approximation.

A. Derivation

The starting point is the integral representations (90)-(95) for the evanescent parts. It appears that all six integrals can be covered with one formalism. To this end we write the integrals in the generic form

$$M(\mathbf{q})^{ev} = \int_0^\infty du\; f(u) J_n(\bar{\rho}\sqrt{1+u^2})e^{-u|\bar{z}|} \tag{165}$$

and they differ from each other in the function $f(u)$ and the order n of the Bessel function. ***Table 1*** lists $f(u)$ and n for each of the integrals. Initially, we will be looking for an asymptotic approximation for $M(\mathbf{q})^{ev}$ in the neighborhood of the *xy*-plane. This implies $\bar{\rho}$ large, and therefore we can approximate the Bessel function by its asymptotic approximation, Eq. (160), which we shall now write as

$$J_n(x) \approx \sqrt{\frac{2}{\pi x}}\,\mathrm{Re}(-i)^n e^{i(x-\pi/4)} \;. \tag{166}$$

We substitute this into Eq. (165) with $x = \bar{\rho}(1+u^2)^{1/2}$, and then write the result as

$$M(\mathbf{q})^{ev} \approx \sqrt{\frac{2}{\pi\bar{\rho}}}\,\mathrm{Re}(-i)^n e^{-i\pi/4} m(\mathbf{q}) \tag{167}$$

in terms of the new functions $m(\mathbf{q})$, defined as

$$m(\mathbf{q}) = \int_0^\infty du \, \frac{f(u)}{(1+u^2)^{1/4}} e^{qw(u)} \quad . \tag{168}$$

The complex function $w(u)$ is

$$w(u) = -u\,|\cos\theta| + i\sin\theta\sqrt{1+u^2} \quad . \tag{169}$$

Equation (168) shows the appearance of the large parameter q in the exponent. We now wish to make an asymptotic approximation of $m(\mathbf{q})$ for q large, and a given θ. One critical point of the integrand is the lower limit of integration, $u = 0$, and the second one is the saddle point u_o of $w(u)$, defined by

$$w'(u_o) = 0 \quad . \tag{170}$$

With Eq. (169) we find that this saddle point is located at

$$u_o = -i\,|\cos\theta| \tag{171}$$

in the complex u-plane. At the saddle point we have $w(u_o) = i$. For $\theta \to \pi/2$, this saddle point approaches the lower integration limit, which is also a critical point. We get the situation that two critical points can be close together. Approximations to this type of integrals can be made with what is called Bleistein's method (Olver, 1974; Bleistein and Handelsman, 1986; Wong, 1989). With Bleistein's method, we first make a change of integration variable $u \to t$ according to

$$w(u) = -u\,|\cos\theta| + i\sin\theta\sqrt{1+u^2} = -\tfrac{1}{2}t^2 + at + b \equiv w(t) \tag{172}$$

with a and b to be determined. The function $w(u)$ now goes over in the quadratic form on the right-hand side. The change of variables also brings the integration curve into the complex t-plane. We now require that the new curve starts at $t=0$, and that this corresponds to the beginning of the old curve, $u=0$. We then see immediately that b must be

$$b = i\sin\theta \quad . \tag{173}$$

The right-hand side of Eq. (172) now has a saddle point t_o in the t-plane, which is the solution of $w'(t_o)=0$. We see that $t_o = a$, and we now require that under the transformation the new saddle point is the image of the old saddle point. Since at the saddle point we have $w(u_o)=i$, this leads to $i = -\frac{1}{2}t_o^2 + at_o + \beta$, and with $t_o = a$ we then obtain

$$a = -(1+i)\sqrt{1-\sin\theta} \quad . \tag{174}$$

This saddle point approaches the origin of the t-plane for $\theta \to \pi/2$, so we have again two critical points that approach each other for $\theta \to \pi/2$. The contour in the t-plane follows from the transformation (172), which can be solved for t as a function of u:

$$t(u) = -(1+i)\sqrt{1-\sin\theta} + \sqrt{2u\,|\cos\theta| + 2i(1-\sin\theta\sqrt{1+u^2})} \quad . \tag{175}$$

For $0 \le u < \infty$ this then gives the parametrization of the new contour C, which is shown in Fig. 5 for $\theta = \pi/6$. The integral then becomes

$$m(\mathbf{q}) = \int_C dt \, \frac{du}{dt} \frac{f(u)}{(1+u^2)^{1/4}} e^{qw(t)} \tag{176}$$

with $u = u(t)$.

We now approximate the integrand, apart from the exponential, by a linear form

$$\frac{du}{dt} \frac{f(u)}{(1+u^2)^{1/4}} \approx c_1 + c_2 t \tag{177}$$

and we choose the constants c_1 and c_2 such that the approximation is exact in the critical points $t = 0$ and $t = a$. From the transformation (172) we find

$$\frac{du}{dt} = -\frac{t-a}{w'(u)} \tag{178}$$

with

$$w'(u) = -|\cos\theta| + i\sin\theta \frac{u}{\sqrt{1+u^2}} \quad . \tag{179}$$

Let us first consider the critical point $t = 0$, for which $u = 0$. Then $w'(0) = -|\cos\theta|$, and with Eq. (177) with $t = 0$ we then find $c_1 = -f(0)a/|\cos\theta|$. Substituting a from Eq. (174) then gives, after some rearrangements

$$c_1 = \frac{(1+i)f(0)}{\sqrt{1+\sin\theta}} \tag{180}$$

and the values of $f(0)$ for the various functions are given in Table 1. For the second critical point $t = a$, $u = u_o$, we have $w'(u_o) = 0$ and the right-hand side of Eq. (178) becomes undetermined. From Eq. (175) we have

$$t-a=\sqrt{2u\,|\cos\theta|+2i(1-\sin\theta\sqrt{1+u^2})} \tag{181}$$

and here the right-hand side has a branch point at $u=u_o=-i\,|\cos\theta|$. We expand the argument of the large square root in a Taylor series around u_o, which yields

$$t-a=\frac{u-u_o}{\sin\theta}\sqrt{-i+...} \tag{182}$$

and the Taylor expansion of $w'(u)$ is

$$w'(u)=(u-u_o)\frac{i}{\sin^2\theta}+...\ . \tag{183}$$

We so obtain

$$\left.\frac{du}{dt}\right|_{t=a}=\sqrt{i}\sin\theta\ . \tag{184}$$

Then we set $t=a$ in Eq. (177) and solve for c_2, which gives

$$c_2=\frac{1}{|\cos\theta|}\left[f(0)-f(u_o)b(\theta)\right] \tag{185}$$

in terms of

$$b(\theta)=\sqrt{\tfrac{1}{2}\sin\theta(1+\sin\theta)}\ . \tag{186}$$

The values of $f(u_o)$ are listed in Table 1.

There appears to be a complication with $\theta\to\pi/2$, since $|\cos\theta|\to 0$ in the denominator on the right-hand side of Eq. (185). But for $\theta\to\pi/2$ we also have $u_o\to 0$ and $b(\theta)\to 1$, leaving d undetermined. It appears necessary to consider this case as a limit. To this end, we first expand $f(u_o)$ in a Taylor series around $u=0$, as $f(u_o)=f(0)+u_o f'(0)+...$, and then substitute this into Eq. (185), giving

$$c_2 = f(0)\frac{1-b(\theta)}{|\cos\theta|} + if'(0) + ... \tag{187}$$

where we used $u_o = -i|\cos\theta|$. The factor $(1-b(\theta))/|\cos\theta|$ is still undetermined for $\theta \to \pi/2$. In order to find this limit we expand the numerator and the denominator in a Taylor series around $\pi/2$, from which we find

$$\lim_{\theta\to\pi/2} \frac{1-b(\theta)}{|\cos\theta|} = 0 \tag{188}$$

which finally gives

$$\lim_{\theta\to\pi/2} c_2 = if'(0) \ . \tag{189}$$

The values of $f'(0)$ are listed in Table 1.

The integrand of the integral in Eq. (176) is analytic for all *t*, so we can bring the contour back to the real axis. We then find

$$m(\mathbf{q}) \approx e^{i\bar{\rho}} \int_0^\infty dt\, (c_1 + c_2 t) e^{-\frac{1}{2}qt^2 + aqt} \tag{190}$$

since $qb = i\bar{\rho}$. This integral can be calculated in closed form. We make the change of variables $\xi = (t-a)\sqrt{q/2}$, which turns the exponent into a perfect square. It also brings the lower integration limit to $\xi = -a\sqrt{q/2}$ in the complex ξ-plane. The result can be expressed in terms of the complementary error function, defined as

$$\operatorname{erfc}(z) = \frac{2}{\sqrt{\pi}} \int_z^\infty d\xi \, e^{-\xi^2} \tag{191}$$

for z complex. The path of integration runs from z to infinity on the positive real axis. We then obtain

$$m(\mathbf{q}) \approx \frac{c_2}{q} e^{i\bar{\rho}} + (c_1 + a\,c_2) \sqrt{\frac{\pi}{2q}} \, e^{i\bar{\rho} + \frac{1}{2} q a^2} \operatorname{erfc}(-a\sqrt{\frac{q}{2}}) \tag{192}$$

With the expressions for c_1, c_2 and a this can be simplified further and expressed in terms of the coordinates as

$$m(\mathbf{q}) \approx f(u_o) \sqrt{\frac{\pi \sin\theta}{2q}} \, e^{i(q+\pi/4)} \operatorname{erfc}(\sqrt{i(q-\bar{\rho}})$$

$$+ \frac{1}{q} \frac{f(0) - f(u_o) b(\theta)}{|\cos\theta|} e^{i\bar{\rho}} \; . \tag{193}$$

For later reference we note that the case $\theta \to \pi/2$ still has to be done with a limit. With $\bar{\rho} = q$, $\operatorname{erfc}(0) = 1$ and Eqs. (185) and (189) we obtain

$$m(\mathbf{q})_{\theta=\pi/2} \approx f(u_o) \sqrt{\frac{\pi}{2q}} \, e^{i(q+\pi/4)} + \frac{i}{q} f'(0) e^{iq} \; . \tag{194}$$

We now substitute the result (193) into Eq. (167) for $M(\mathbf{q})^{ev}$. After some rearrangements this yields

$$M(\mathbf{q})^{ev} \approx \frac{f(0)}{|\bar{z}|} \sqrt{\frac{2}{\pi \bar{\rho}}} \operatorname{Re}(-i)^n e^{i(\bar{\rho} - \pi/4)}$$

$$+ \frac{1}{q} \operatorname{Re}(-i)^n f(u_o) \left[e^{iq} \operatorname{erfc}(\sqrt{i(q-\bar{\rho})}) - \frac{e^{i\bar{\rho}}}{\sqrt{i\pi(q-\bar{\rho})}} \right] . \tag{195}$$

In the first term on the right-hand side we recognize the asymptotic approximation for $J_n(\bar{\rho})$ from Eq. (166). For reasons explained below we now put this back in. Then we introduce the function

$$N(\mathbf{q}) = |\cos\theta| \left[e^{i\bar{\rho}} \frac{1}{\sqrt{i\pi(q-\bar{\rho})}} - e^{iq} \mathrm{erfc}(\sqrt{i(q-\bar{\rho})}) \right] \tag{196}$$

in terms of which the asymptotic approximation becomes

$$M(\mathbf{q})^{ev} \approx \frac{f(0)}{|\bar{z}|} J_n(\bar{\rho}) - \frac{1}{|\bar{z}|} \mathrm{Re}(-i)^n f(u_o) N(\mathbf{q}) \tag{197}$$

and this is the final form. In the definition of $N(\mathbf{q})$ we have included a factor $|\cos\theta|$ which cancels against the same factor in $|\bar{z}| = q|\cos\theta|$ in the denominator. The reason is that in this way the function $N(\mathbf{q})$ remains finite in the limit $\theta \to \pi/2$. To see this we write $N(\mathbf{q})$ in the alternative form

$$N(\mathbf{q}) = \sqrt{\frac{1+\sin\theta}{\pi q}}\, e^{i(\bar{\rho}-\pi/4)} - |\cos\theta|\, e^{iq} \mathrm{erfc}(\sqrt{i(q-\bar{\rho})}) \tag{198}$$

from which we have

$$N(\mathbf{q})_{\theta=\pi/2} = \sqrt{\frac{2}{\pi q}}\, e^{i(q-\pi/4)} \tag{199}$$

which is finite.

B. Results

The asymptotic approximation of the evanescent parts of the auxiliary functions $M(\mathbf{q})^{ev}$ is given by Eq. (197), which involves the universal function $N(\mathbf{q})$. Let us temporarily set

$$\xi = \sqrt{i(q-\overline{\rho})} = (1+i)\sqrt{\tfrac{1}{2}q(1-\sin\theta)} \ . \tag{200}$$

Then $N(\mathbf{q})$ can be written as

$$N(\mathbf{q}) = -|\cos\theta|\, e^{iq}\left[\operatorname{erfc}(\xi) - \frac{1}{\xi\sqrt{\pi}}e^{-\xi^2}\right] . \tag{201}$$

For a field point in the *xy*-plane we have $\overline{\rho} = q$, $\operatorname{erfc}(0) = 1$, and $N(\mathbf{q})$ is given by Eq. (199). In particular we see that $N(\mathbf{q}) = \mathcal{O}(1/q^{1/2})$. On the other hand, off the *xy*-plane we have with $q-\overline{\rho} = q(1-\sin\theta)$ that $q-\overline{\rho}$ becomes large with q for θ fixed. In that case, ξ is large and we use the asymptotic approximation for the complementary error function (Abramowitz and Stegun, 1972)

$$\operatorname{erfc}(\xi) = \frac{1}{\xi\sqrt{\pi}}e^{-\xi^2}\left[1+\sum_{n=1}^{\infty}(-1)^n\frac{1\cdot 3\cdot \ldots \cdot (2n-1)}{(2\xi^2)^n}\right] . \tag{202}$$

We see that the first term is just the second term in square brackets in Eq. (201). Since $\xi^2 = i(q-\overline{\rho})$ the factor $\exp(-\xi^2)$ does not influence the order, and we find that $N(\mathbf{q})$ = $\mathcal{O}(1/\xi^3)$, which is $N(\mathbf{q}) = \mathcal{O}(1/q^{3/2})$. ***Figure 6*** shows $N(\mathbf{q})$ as a function of θ and for $q = 10\pi$. We see indeed that near $\theta = 90^{\circ}$ the real and imaginary parts of $N(\mathbf{q})$ have a strong peak.

To see the structure of result (197) we go back to Eqs. (193) and (194). The second term on the right-hand sides of both is $\mathcal{O}(1/q)$. The first term on the right-hand side of Eq. (194) is $\mathcal{O}(1/q^{1/2})$. Off the *xy*-plane, we consider Eq. (193) in which $\operatorname{erfc}(\xi) = \mathcal{O}(1/q^{1/2})$, making both terms on the right-hand side $\mathcal{O}(1/q)$. It is inherent in Bleistein's method that these are the orders that are resolved properly. The next leading order, which is not resolved, is $\mathcal{O}(1/q^{3/2})$ (p. 383 of Bleistein and Handelsman, 1986). To obtain $M(\mathbf{q})^{ev}$ from $m(\mathbf{q})$, Eq. (167), an additional $\mathcal{O}(1/q^{1/2})$ appears due to the $1/\sqrt{\overline{\rho}}$. So we see that the leading order of $\mathcal{O}(1/q)$ for $M(\mathbf{q})^{ev}$ in the *xy*-plane comes from the term with the complementary error function $\operatorname{erfc}(\xi)$ with $\xi = 0$ in Eq. (193). Off the *xy*-plane both terms become of the same order and both contribute an $\mathcal{O}(1/q^{3/2})$ to $M(\mathbf{q})^{ev}$, which is the typical result for the evanescent waves (Sec. XVII).

When the result is written as in Eq. (197), we have to look at this in a different way because both terms are mixed differently. First of all, due to the $1/|\overline{z}|$ in both terms on the right-hand side, the case of the *xy*-plane still has to be considered with a limit. This factor $1/|\overline{z}|$ is $\mathcal{O}(1/q)$, and for $\overline{\rho}$ large the Bessel function is $\mathcal{O}(1/q^{1/2})$, making the first term the typical $\mathcal{O}(1/q^{3/2})$. Off the *xy*-plane, the function $N(\mathbf{q})$ is $\mathcal{O}(1/q^{3/2})$, and this makes the second term $\mathcal{O}(1/q^{5/2})$, and as indicated in the previous paragraph, this order is not properly resolved. The fact that this $\mathcal{O}(1/q^{5/2})$ appears as leading term is a result of the regrouping of terms in such a way that the second term in brackets in Eq. (201) is just the leading term of the asymptotic series. Then we might as well drop $N(\mathbf{q})$, and set

$$M(\mathbf{q})^{ev} \approx \frac{f(0)}{|\overline{z}|} J_n(\overline{\rho}) \ . \tag{203}$$

Now we compare this to Eqs. (154)-(156) and we see with the values of $f(0)$ and n from Table 1, that the approximation (203) is the same as the approximation that connected the value on the z-axis to the field part off the z-axis. In this sense we have made a *uniform* asymptotic expansion, which holds for all angles, and reaches the z-axis in the correct way. This was the reason for putting the Bessel function back in in Eq. (197). When we now approach the xy-plane, the error function approaches $\mathrm{erfc}(0)=1$ and $N(\mathbf{q})$ becomes $\mathcal{O}(1/q^{1/2})$. But then it is not clear anymore from Eq. (197) what happens to $M(\mathbf{q})^{ev}$, since this has to be considered with a limit. We go back to Eq. (194) and substitute this into Eq. (167), which gives for the limit of the xy-plane

$$M(\mathbf{q})^{ev} \approx \frac{1}{q}\mathrm{Re}(-i)^n e^{iq}\left[f(0) + f'(0)e^{i\pi/4}\sqrt{\frac{2}{\pi q}}\right] \tag{204}$$

and this is $\mathcal{O}(1/q)$, provided, of course, that $f(0)\neq 0$.

From the discussion above we see that this $\mathcal{O}(1/q)$ behavior in the xy-plane comes from $\mathrm{erfc}(\xi)\approx 1$ for $\xi\approx 0$. When the argument ξ of the complementary error function becomes large, so that the asymptotic approximation of $\mathrm{erfc}(\xi)$ sets in, the behavior goes over in $\mathcal{O}(1/q^{3/2})$. This happens for $|\xi|\approx 1$, and with Eq. (200) this gives $q\approx 1+\overline{\rho}$. With $q=(\overline{\rho}^2+\overline{z}^2)^{1/2}$ and $|\overline{z}| << \overline{\rho}$ we find by Taylor expansion that this is equivalent to $|\overline{z}|^2\approx 2\overline{\rho}$. So, given $\overline{\rho}$, there is a layer of thickness $|\overline{z}|\sim\sqrt{\overline{\rho}}$, and within this layer the evanescent waves are $\mathcal{O}(1/q)$, and end up in the far field. The angular width of this layer is $\Delta\theta \sim |\overline{z}|/\overline{\rho}\sim 1/\sqrt{\overline{\rho}}$ and this goes to zero for $\overline{\rho}\to\infty$, even though the thickness of the layer grows indefinitely with $\overline{\rho}$.

With the parameters from Table 1 we find with Eq. (197) the uniform asymptotic expansions of the auxiliary functions, three of which are

$$M_a(\mathbf{q})^{ev} \approx \frac{1}{|\bar{z}|}\left[J_0(\bar{\rho}) - \operatorname{Re} N(\mathbf{q})\right] \tag{205}$$

$$M_b(\mathbf{q})^{ev} \approx -\frac{1}{|\bar{z}|}\left[J_2(\bar{\rho}) + \sin^2\theta \operatorname{Re} N(\mathbf{q})\right] \tag{206}$$

$$M_f(\mathbf{q})^{ev} \approx \frac{1}{|\bar{z}|}\left[J_1(\bar{\rho}) - \sin\theta \operatorname{Im} N(\mathbf{q})\right] . \tag{207}$$

These are the generalizations of Eqs. (154)-(156). Off the *xy*-plane the terms with $N(\mathbf{q})$ are $\mathcal{O}(1/q^{5/2})$ and are therefore negligible. Then Eqs. (205)-(207) are asymptotically identical to Eqs. (154)-(156). Near the *xy*-plane we have to consider this as a limit, which will be discussed in more detail below. ***Figures 7 and 8*** show the exact $M_a(\mathbf{q})^{ev}$ and its asymptotic approximation (205). We see from Fig. 7 that already for $q = 2\pi$ the approximation is excellent, except near the *xy*-plane. For $q = 15\pi$, as shown in Fig. 8, the approximation near the *xy*-plane has improved considerably as compared to Fig. 7. For ***Fig. 9*** we took $q = 100\pi$ and the exact and approximate solutions are indistinguishable. This graph also shows that $M_a(\mathbf{q})^{ev}$ is much larger near the *z*-axis and the *xy*-plane than in between. This reflects the $\mathcal{O}(1/q)$ and $\mathcal{O}(1/q^{3/2})$ dependence, respectively.

The approximations to the other three functions are

$$M_c(\mathbf{q})^{ev} \approx \frac{2\sin\theta}{q} \operatorname{Re} N(\mathbf{q}) \tag{208}$$

$$M_d(\mathbf{q})^{ev} \approx -\frac{|\cos\theta|}{q} \operatorname{Re} N(\mathbf{q}) \tag{209}$$

$$M_e(\mathbf{q})^{ev} \approx -\frac{1}{q} \operatorname{Im} N(\mathbf{q}) . \tag{210}$$

These functions are $\mathcal{O}(1/q^{5/2})$ off the *xy*-plane, and are therefore negligible. Near the *xy*-plane these functions are $\mathcal{O}(1/q^{3/2})$, so they do not contribute to the far field along the *xy*-plane. Furthermore we see that $M_d(\mathbf{q})^{ev}$ is proportional to $|\cos\theta|$, which is zero in the *xy*-plane, and therefore we can effectively set

$$M_d(\mathbf{q})^{ev} \approx 0 \tag{211}$$

everywhere.

Let us now consider the limit $\theta \to \pi/2$, for which we use the asymptotic approximation given by Eq. (204). With the values listed in Table 1 we find for three of the functions

$$M_a(\mathbf{q})^{ev} \approx M_b(\mathbf{q})^{ev} \approx \frac{\cos q}{q} \tag{212}$$

$$M_f(\mathbf{q})^{ev} \approx \frac{\sin q}{q} \quad . \tag{213}$$

The exact values in the *xy*-plane are given in Sec. XIII. With $\overline{\rho} = q$ we see from Eq. (118) that the approximation to $M_a(\mathbf{q})^{ev}$ gives the exact value. This seems to be in contradiction with Figs. 7 and 8 where the exact and asymptotic values near $\theta = 90^{\mathrm{o}}$ are not the same. The reason is that the limit for the *xy*-plane was derived from Eq. (194), before we replaced the first term on the right-hand side of Eq. (195) with a Bessel function. ***Figure 10*** shows the asymptotic approximation for $M_a(\mathbf{q})^{ev}$ but with $J_0(\overline{\rho})$ again replaced with its asymptotic from, Eq. (166). Now we see that that the result near the *xy*-plane is indeed exact, but now the approximation diverges near the *z*-axis. It seems to be a coincidence that without introducing the Bessel function in Eq. (197) the result near the *xy*-plane is better since we already approximated the Bessel function in Eq.

(165). Apparently for this case the approximated Bessel function gives a better result than the exact function.

From Eqs. (119) and (123) we observe that the asymptotic results for $M_b(\mathbf{q})^{ev}$ and $M_f(\mathbf{q})^{ev}$ agree to leading order. For $M_d(\mathbf{q})^{ev}$ we find the approximate solution $M_d(\mathbf{q})^{ev} \approx 0$ in the *xy*-plane, which agrees with Eq. (121) in leading order. For the remaining two functions we find

$$M_c(\mathbf{q})^{ev} \approx \frac{2}{q}\sqrt{\frac{2}{\pi q}}\sin(q+\pi/4) \tag{214}$$

$$M_e(\mathbf{q})^{ev} \approx \frac{1}{q}\sqrt{\frac{2}{\pi q}}\cos(q+\pi/4) \tag{215}$$

and with Eq. (166) we verify that these solutions are asymptotically equivalent to the exact results from Eqs. (120) and (122).

To conclude this section, let us summarize. As far as the evanescent waves in the far field, $\mathcal{O}(1/q)$, are concerned, the Green's tensor and vector are given by Eqs. (163) and (164), and with the three auxiliary functions given by Eqs. (205)-(207). This accounts for a far field contribution near the *z*-axis and near the *xy*-plane. In between these functions are $\mathcal{O}(1/q^{3/2})$, which is also properly resolved. Here, the terms with $N(\mathbf{q})$ in Eqs. (205)-(207) are negligible since these are $\mathcal{O}(1/q^{5/2})$. Then, if one wishes to resolve the evanescent waves up to $\mathcal{O}(1/q^{3/2})$ uniformly everywhere, then the terms with $M_c(\mathbf{q})^{ev}$ and $M_e(\mathbf{q})^{ev}$ should be added to the Green's tensor and vector, respectively, since these functions are $\mathcal{O}(1/q^{3/2})$ near the *xy*-plane (and negligible elsewhere). The function $M_d(\mathbf{q})^{ev}$ never contributes.

XIX. Traveling Waves in the Near Field

Let us now turn our attention to the near field. We already found in Sec. VII that the traveling waves are finite at the origin, and therefore all singular behavior near the origin must come from the evanescent waves. It turns out to be easier to consider the traveling waves first. In Sec. XV we obtained series expansions for the functions $\mathrm{Re}\, M_k(\mathbf{q})^{tr}$. These series are Taylor series in $|\bar{z}|$ for a given $\bar{\rho}$, and the Taylor coefficients became functions of $\bar{\rho}$, involving Bessel functions. We will now be seeking series expansions in q, around $q = 0$, for a given θ. In this way, the Taylor coefficients become functions of θ.

To this end, we start from the result from Sec. XV, Eqs. (138)-(143). For the Bessel functions we substitute their series expansion as given by Eq. (136). For $\mathrm{Re}\, M_a(\mathbf{q})^{tr}$ we then find

$$\mathrm{Re}\, M_a(\mathbf{q})^{tr} = -\frac{|\bar{z}|}{\bar{\rho}} \sum_{\ell=0}^{\infty} \sum_{k=0}^{\infty} (-1)^{\ell+k} \frac{\ell!}{(2\ell+1)!k!(k+\ell+1)!} \bar{z}^{2\ell} \left(\frac{\bar{\rho}}{2}\right)^{2k+1} . \quad (216)$$

This double series can be written as a single series, similar to the Cauchy product, which yields

$$\mathrm{Re}\, M_a(\mathbf{q})^{tr} = -\tfrac{1}{2} \sum_{n=0}^{\infty} \sum_{\ell=0}^{n} (-1)^n \frac{\ell!}{(2\ell+1)!(n-\ell)!(n+1)!} |\bar{z}|^{2\ell+1} \left(\frac{\bar{\rho}}{2}\right)^{2n-2\ell} . \quad (217)$$

Then we change variables with $\bar{\rho} = q\sin\theta$, $\bar{z} = q\cos\theta$, and collect the powers of q. We then obtain the series expansion in q:

$$\mathrm{Re}\, M_a(\mathbf{q})^{tr} = -\tfrac{1}{2} q\,|\cos\theta| \sum_{n=0}^{\infty} P_n(\theta) \frac{(-\frac{1}{4}q^2)^n}{n!(n+1)!} \ , \tag{218}$$

with the coefficient functions $P_n(\theta)$ functions of θ. We have split off an overall $|\cos\theta|$ for later convenience, and also the factors $1/(n!(n+1)!)$ and $1/4^n$. These overall factors are taken out in order to keep the coefficient functions $P_n(\theta)$ reasonable, meaning that they have a very weak *n* dependence, as will be shown below. If we don't take out just the right factors, then the coefficient functions will either increase or decrease very rapidly with *n*, leading to numerical problems. The functions $P_n(\theta)$ are explicitly

$$P_n(\theta) = n! \sum_{k=0}^{n} \frac{k!}{(n-k)!(2k+1)!} (\sin^2\theta)^{n-k} (4\cos^2\theta)^k \ . \tag{219}$$

We notice an overall factor *n*!, which of course cancels against the $1/n!$ in Eq. (218), but in this way the function $P_n(\theta)$ becomes well-behaved.

For $\mathrm{Re}\, M_b(\mathbf{q})^{tr}$ we find in the same way

$$\mathrm{Re}\, M_b(\mathbf{q})^{tr} = \tfrac{1}{8} q^3 \sin^2\theta\,|\cos\theta| \sum_{n=0}^{\infty} P_n(\theta) \frac{(-\frac{1}{4}q^2)^n}{n!(n+3)!} \ , \tag{220}$$

and this series involves the same coefficient function $P_n(\theta)$. The remaining auxiliary functions have the series representations

$$\mathrm{Re}\, M_c(\mathbf{q})^{tr} = \tfrac{1}{2} q \sin\theta \sum_{n=0}^{\infty} Q_n(\theta) \frac{(-\frac{1}{4}q^2)^n}{n!(n+2)!} \tag{221}$$

$$\mathrm{Re}\, M_d(\mathbf{q})^{tr} = -\tfrac{1}{4} q\,|\cos\theta| \sum_{n=0}^{\infty} [P_n(\theta) + Q_n(\theta)] \frac{(-\frac{1}{4}q^2)^n}{n!(n+2)!} \tag{222}$$

$$\mathrm{Re}\, M_e(\mathbf{q})^{tr} = \tfrac{1}{2}\sum_{n=0}^{\infty} Q_n(\theta)\frac{(-\frac{1}{4}q^2)^n}{n!(n+1)!} \tag{223}$$

$$\mathrm{Re}\, M_f(\mathbf{q})^{tr} = -\tfrac{1}{4}q^2 \sin\theta\,|\cos\theta|\sum_{n=0}^{\infty} P_n(\theta)\frac{(-\frac{1}{4}q^2)^n}{n!(n+2)!} \tag{224}$$

and these involve only one more coefficient function, defined by

$$Q_n(\theta) = n!\sum_{k=0}^{n}\frac{k!}{(n-k)!(2k)!}(\sin^2\theta)^{n-k}(4\cos^2\theta)^k \ . \tag{225}$$

With $Q_0(\theta) = 1$ we see that for $q = 0$ we have $\mathrm{Re}\, M_e(0)^{tr} = 1/2$, and this gives Eq. (58) for the traveling part of the Green's vector at the origin. All other functions vanish at the origin, and the Green's tensor at the origin only involves the imaginary parts of the auxiliary functions, and these are pure traveling, giving Eq. (57).

XX. The Coefficient Functions

In order to study the coefficient functions in some detail we introduce the generating functions

$$g_P(\theta;t) = \sum_{n=0}^{\infty} P_n(\theta)\frac{t^n}{n!} \tag{226}$$

$$g_Q(\theta;t) = \sum_{n=0}^{\infty} Q_n(\theta)\frac{t^n}{n!} \ . \tag{227}$$

When we substitute $P_n(\theta)$ from Eq. (219) into the right-hand side of Eq. (226), the result has the appearance of a Cauchy product of a double series. We then use the Cauchy product backwards, and express this result in a double series, giving

$$g_P(\theta;t) = \sum_{k=0}^{\infty} \sum_{\ell=0}^{\infty} \frac{k!}{\ell!(2k+1)!} (t \sin^2 \theta)^{\ell} (4t \cos^2 \theta)^k \, . \tag{228}$$

Here the summation over ℓ gives an exponential, so that

$$g_P(\theta;t) = e^{t \sin^2 \theta} \sum_{k=0}^{\infty} \frac{k!}{(2k+1)!} (4t \cos^2 \theta)^k \quad . \tag{229}$$

The series on the right-hand side can be found in a table (Prudnikov, *et.al.*, 1986a), and we obtain

$$g_P(\theta;t) = \frac{1}{2\cos\theta} \sqrt{\frac{\pi}{t}} \, e^t \, \mathrm{erf}(\sqrt{t} \cos\theta) \tag{230}$$

in terms of the error function. Similarly, the generating function for $Q_n(\theta)$ is found to be

$$g_Q(\theta;t) = e^{t \sin^2 \theta} + \cos\theta \sqrt{\pi t} \, e^t \, \mathrm{erf}(\sqrt{t} \cos\theta) \quad . \tag{231}$$

The coefficient functions $P_n(\theta)$ can be recovered from the generating function by differentiation:

$$P_n(\theta) = \left. \frac{d^n g_P(\theta;t)}{dt^n} \right|_{t=0} \tag{232}$$

and similarly for $Q_n(\theta)$. To this end, we first expand the error function in its known series (p. 297 of Abramowitz and Stegun, 1972) and then write the generating function as

$$g_P(\theta;t) = \sum_{k=0}^{\infty} \frac{(-\cos^2\theta)^k}{k!(2k+1)} (t^k e^t) \ . \tag{233}$$

Then we differentiate this n times and set $t = 0$. This gives

$$P_n(\theta) = \sum_{k=0}^{n} \binom{n}{k} \frac{(-\cos^2\theta)^k}{2k+1} \tag{234}$$

as an alternative to the form in Eq. (219). With the same procedure for $Q_n(\theta)$ the same sum appears, but with $n-1$, and due to the term $\exp(t\sin^2\theta)$ on the right-hand side of Eq. (231) an extra term $(\sin\theta)^{2n}$ appears. We then find the relation

$$Q_n(\theta) = (\sin\theta)^{2n} + 2n\cos^2\theta\, P_{n-1}(\theta) \ , \quad n = 1,2,... \ . \tag{235}$$

Then we set $\sin^2\theta = 1 - \cos^2\theta$ and use Newton's binomium to represent the n^{th} power, and we combine the two terms, which gives

$$Q_n(\theta) = -\sum_{k=0}^{n} \binom{n}{k} \frac{(-\cos^2\theta)^k}{2k-1} \ . \tag{236}$$

When we set $\theta = 0$ (or π) in Eq. (219) only the term $k = n$ contributes and we find

$$P_n(0) = \frac{4^n (n!)^2}{(2n+1)!} \tag{237}$$

and similarly from Eq. (225)

$$Q_n(0) = \frac{4^n (n!)^2}{(2n)!} \quad . \tag{238}$$

For $\theta = \pi / 2$ we look at Eqs. (234) and (236) and we see that only the $k = 0$ contributes, so that for points in the *xy*-plane we have

$$P_n(\pi / 2) = Q_n(\pi / 2) = 1 \quad . \tag{239}$$

To see the behavior of $P_n(0)$ and $Q_n(0)$ for *n* large, we use Stirling's formula (Arfken and Weber, 1995) to approximate the factorials. We then find

$$P_n(0) \approx \frac{1}{2}\sqrt{\frac{\pi}{n}} \tag{240}$$

$$Q_n(0) \approx \sqrt{\pi\, n} \tag{241}$$

for *n* large. This shows that $P_n(0)$ and $Q_n(0)$ have a very mild *n* dependence. It can be shown (proof omitted here) that $P_n(\theta)$ and $Q_n(\theta)$ are bounded by

$$0 < P_n(\theta) \le 1 \tag{242}$$

$$1 \le Q_n(\theta) \le 1 + 2n \quad . \tag{243}$$

Figure 11 shows the coefficient functions for $n = 3$.

For the summation of the series for $\mathrm{Re}\, M_k(\mathbf{q})^{tr}$ we need a large number of coefficient functions, and using Eqs. (234) and (236) repeatedly is not convenient. We shall now derive recursion relations for the coefficient functions, which will provide a very efficient method for obtaining these functions. In view of Eq. (234) we temporarily set

$$Y_n(x) = \sum_{k=0}^{n} \binom{n}{k} \frac{(-1)^k}{2k+1} x^{2k+1} \quad , \quad n = 0,1,... \tag{244}$$

so that $Y_n(\cos\theta) = \cos\theta\, P_n(\theta)$. Differentiating gives

$$\frac{dY_n}{dx} = (1-x^2)^n \quad . \tag{245}$$

From Eq. (244) we see that $Y_n(0) = 0$, and therefore

$$Y_n(x) = \int_0^x dt\, (1-t^2)^n \quad . \tag{246}$$

Then we write $(1-t^2)^n = (1-t^2)(1-t^2)^{n-1}$, which gives

$$Y_n(x) = Y_{n-1}(x) - \int_0^x dt\, t^2 (1-t^2)^{n-1} \, . \tag{247}$$

In this integral we set $u(t) = (1-t^2)^n$, from which $(1-t^2)^{n-1} = (-2nt)^{-1} du/dt$. Integration by parts then gives a relation between $Y_n(x)$ and $Y_{n-1}(x)$, and when we substitute $x = \cos\theta$ we obtain the recursion relation for the coefficient functions

$$(2n+1)P_n(\theta) = 2nP_{n-1}(\theta) + (\sin^2\theta)^n \quad , \quad n = 1,2,... \quad . \tag{248}$$

This recursion allows us to generate these functions very efficiently from the initial value of $P_0(\theta) = 1$. Then Eq. (235) shows that the $Q_n(\theta)$'s are related to the $P_n(\theta)$'s, and therefore Eq. (248) implies a recursion relation for the $Q_n(\theta)$'s. We find this relation to be

$$(2n-1)Q_n(\theta) = 2nQ_{n-1}(\theta) - (\sin^2\theta)^n \quad , \quad n = 1,2,... \tag{249}$$

and the initial value is $Q_0(\theta) = 1$. ***Figure 12*** shows the result of a series summation.

XXI. Integral Representations

From Eq. (246), with $x = \cos\theta$ and $Y_n(\cos\theta) = \cos\theta\, P_n(\theta)$ we find the representation

$$P_n(\theta) = \frac{1}{\cos\theta} \int_0^{\cos\theta} dt\, (1-t^2)^n \ . \tag{250}$$

In this section we shall restrict our attention to $z \geq 0$ in order to simplify some of the notation. We already know that $P_n(\theta)$ and $Q_n(\theta)$ are invariant under reflection in the *xy*-plane (they only depend on θ through $\cos^2\theta$, Eqs. (234) and (236)), so this is no limitation. We make the substitution $t = \cos\alpha$ in the integrand of Eq. (250), which yields the alternative representation

$$P_n(\theta) = \frac{1}{\cos\theta} \int_\theta^{\pi/2} d\alpha\, (\sin\alpha)^{2n+1} \ . \tag{251}$$

We now substitute this representation in the series expansion (218). It then appears that the summation over *n* can be written as a Bessel function, according to Eq. (136). We thus obtain the remarkable result (Arnoldus and Foley, 2003c)

$$\mathrm{Re}\, M_a(\mathbf{q})^{tr} = -\int_\theta^{\pi/2} d\alpha\, J_1(q\sin\alpha) \ . \tag{252}$$

The original representation, Eq. (98), is considerably more complicated in appearance. We also note that both representations involve a Bessel function of different order. In the same way we find new representations for the other two auxiliary functions which were expressed in $P_n(\theta)$

$$\mathrm{Re}\, M_b(\mathbf{q})^{tr} = \sin^2\theta \int_\theta^{\pi/2} d\alpha\, \frac{1}{\sin^2\alpha} J_3(q\sin\alpha) \tag{253}$$

$$\mathrm{Re}\, M_f(\mathbf{q})^{tr} = -\sin\theta \int_\theta^{\pi/2} d\alpha\, \frac{1}{\sin\alpha} J_2(q\sin\alpha)\ . \tag{254}$$

The remaining three functions involve the coefficient functions $Q_n(\theta)$. In order to obtain interesting integral representations for these functions, we introduce temporarily the function

$$Z_n(x) = \sum_{k=1}^{n} \binom{n}{k} \frac{(-1)^k}{2k-1} x^{2k-1} \tag{255}$$

in analogy to the function $Y_n(x)$ in Eq. (244). It then follows from Eq. (236) that $Q_n(\theta) = 1 - \cos\theta\, Z_n(\cos\theta)$. Upon differentiating we find that $Z_n(x)$ satisfies the differential equation

$$\frac{d\,Z_n}{dx} = \frac{1}{x^2}\left[(1-x^2)^n - 1\right]. \tag{256}$$

With $Z_n(0) = 0$ we can integrate this again, as in Eq. (246), and then we set $x = \cos\theta$ which yields

$$Q_n(\theta) = 1 + \cos\theta \int_0^{\cos\theta} dt \frac{1}{t^2}\left[1 - (1 - t^2)^n\right]. \tag{257}$$

It should be noted that this integral can not be split in two integrals, since both would not exist in the lower limit. Now we set again $t = \cos\alpha$, which gives

$$Q_n(\theta) = 1 + \cos\theta \int_\theta^{\pi/2} d\alpha \frac{\sin\alpha}{\cos^2\alpha}\left[1 - (\sin\alpha)^{2n}\right] \tag{258}$$

in analogy to Eq. (251) for $P_n(\theta)$.

We substitute this representation for $Q_n(\theta)$ into Eq. (221). The summation over n leads again to Bessel functions and we find

$$\begin{aligned}\operatorname{Re} M_c(\mathbf{q})^{tr} &= \frac{2}{q}\sin\theta\, J_2(q) \\ &\quad - \frac{1}{q}\sin 2\theta \int_\theta^{\pi/2} d\alpha\, \frac{1}{\cos^2\alpha\sin\alpha}\left[J_2(q\sin\alpha) - \sin^2\alpha\;\; J_2(q)\right].\end{aligned} \tag{259}$$

In the same way we find from Eq. (223)

$$\begin{aligned}\operatorname{Re} M_e(\mathbf{q})^{tr} &= \frac{1}{q} J_1(q) \\ &\quad - \frac{1}{q}\cos\theta \int_\theta^{\pi/2} d\alpha\, \frac{1}{\cos^2\alpha}\left[J_1(q\sin\alpha) - \sin\alpha\, J_1(q)\right].\end{aligned} \tag{260}$$

Finally, for $\operatorname{Re} M_d(\mathbf{q})^{tr}$, Eq. (222), we need the integral representations for both $P_n(\theta)$ and $Q_n(\theta)$, and we obtain

$$\operatorname{Re} M_d(\mathbf{q})^{tr} = -\frac{1}{q}\cos\theta\, J_2(q)$$

$$-\frac{1}{q}\int_{\theta}^{\pi/2} d\alpha\,\frac{1}{\sin\alpha}\left[J_2(q\sin\alpha)+\frac{\cos^2\theta}{\cos^2\alpha}\left(\sin^2\alpha J_2(q)-J_2(q\sin\alpha)\right)\right]. \quad (261)$$

We have verified by numerical integration that these new representations do indeed give the same results as the old ones.

XXII. Evanescent Waves in the Near Field

Now that we have the real part of the traveling part, we can obtain the evanescent part from

$$M_k(\mathbf{q})^{ev} = \mathrm{Re}\,M_k(\mathbf{q}) - \mathrm{Re}\,M_k(\mathbf{q})^{tr} \ . \quad (262)$$

The functions $M_k(\mathbf{q})$ are given by Eqs. (68)-(73), from which we take the real parts. These are all standard functions, and we expand these in series around $q = 0$. For instance,

$$\mathrm{Re}\,M_a(\mathbf{q}) = \frac{\cos q}{q} = \frac{1}{q} + \sum_{n=0}^{\infty}\frac{(-1)^{n+1}q^{2n+1}}{(2n+2)!} \quad (263)$$

with the remaining ones similar, but more complicated. We split off the singular terms, as the $1/q$ in Eq. (263), and we combine the remaining Taylor series with the series of Sec. XIX. For instance, we subtract the right-hand side of Eq. (218) from the right-hand side of Eq. (263). After some serious regrouping, terms with factorials appear, which have exactly the form of either Eq. (237) or Eq. (238) for $P_n(0)$ and $Q_n(0)$, respectively. For $M_a(\mathbf{q})^{ev}$ we find

$$M_a(\mathbf{q})^{ev} = \frac{1}{q} - \tfrac{1}{2} q \sum_{n=0}^{\infty} p_n(\theta) \frac{(-\tfrac{1}{4} q^2)^n}{n!(n+1)!} \tag{264}$$

which involves a new coefficient function $p_n(\theta)$, defined in terms of $P_n(\theta)$ as

$$p_n(\theta) = P_n(0) - |\cos\theta| P_n(\theta) \ . \tag{265}$$

The other functions follow in the same way, for which we need one more coefficient function

$$q_n(\theta) = |\cos\theta| Q_n(0) - Q_n(\theta) \ . \tag{266}$$

The result is

$$M_b(\mathbf{q})^{ev} = -\sin^2\theta \left(\frac{3}{q^3} + \frac{1}{2q} + \frac{q}{8} \right) + \tfrac{1}{8} q^3 \sin^2\theta \sum_{n=0}^{\infty} p_n(\theta) \frac{(-\tfrac{1}{4} q^2)^n}{n!(n+3)!} \tag{267}$$

$$M_c(\mathbf{q})^{ev} = |\sin 2\theta| \left(\frac{3}{q^3} + \frac{1}{2q} \right) + \tfrac{1}{2} q \sin\theta \sum_{n=0}^{\infty} q_n(\theta) \frac{(-\tfrac{1}{4} q^2)^n}{n!(n+2)!} \tag{268}$$

$$\begin{aligned} M_d(\mathbf{q})^{ev} = {} & \frac{1}{q^3}(1 - 3\cos^2\theta) + \frac{1}{2q}\sin^2\theta \\ & - \tfrac{1}{4} q \sum_{n=0}^{\infty} [p_n(\theta) + |\cos\theta| q_n(\theta)] \frac{(-\tfrac{1}{4} q^2)^n}{n!(n+2)!} \end{aligned} \tag{269}$$

$$M_e(\mathbf{q})^{ev} = \frac{1}{q^2} |\cos\theta| + \tfrac{1}{2} \sum_{n=0}^{\infty} q_n(\theta) \frac{(-\tfrac{1}{4} q^2)^n}{n!(n+1)!} \tag{270}$$

$$M_f(\mathbf{q})^{ev} = \sin\theta \left(\frac{1}{q^2} + \frac{1}{2} \right) - \tfrac{1}{4} q^2 \sin\theta \sum_{n=0}^{\infty} p_n(\theta) \frac{(-\tfrac{1}{4} q^2)^n}{n!(n+2)!} \ . \tag{271}$$

This solution for the evanescent waves in the near field has the remarkable feature that each "series part" is identical in form, including the overall factor, to the corresponding solution for $\mathrm{Re}\, M_k(\mathbf{q})^{tr}$ from Sec. XIX, under the substitutions

$$|\cos\theta|\, P_n(\theta) \;\to\; p_n(\theta) \tag{272}$$

$$Q_n(\theta) \;\to\; q_n(\theta) \ . \tag{273}$$

Furthermore, all singular behavior of the evanescent waves appears as additional terms on the right-hand sides of the equations above. This shows clearly how all singular behavior of the near field is accounted for by the evanescent waves.

Since $p_n(\theta)$ and $q_n(\theta)$ are defined in terms of $P_n(\theta)$ and $Q_n(\theta)$, the recursion relations (248) and (249) imply recursion relations for $p_n(\theta)$ and $q_n(\theta)$. We find

$$(2n+1)\, p_n(\theta) = 2n\, p_{n-1}(\theta) - |\cos\theta|\, (\sin^2\theta)^n \tag{274}$$

$$(2n-1) q_n(\theta) = 2n\, q_{n-1}(\theta) + (\sin^2\theta)^n \tag{275}$$

and the initial values are $p_0(\theta) = 1 - |\cos\theta|$ and $q_0(\theta) = |\cos\theta| - 1$. The values at $\theta = 0$ (or π) are

$$p_n(0) = q_n(0) = 0 \tag{276}$$

and for a field point in the *xy*-plane we obtain

$$p_n(\pi/2) = P_n(0) = \frac{4^n (n!)^2}{(2n+1)!} \tag{277}$$

$$q_n(\pi/2) = -1 \ . \tag{278}$$

Figure 13 shows these new coefficient functions for $n = 3$ as a function of θ. The accuracy of the series expansion is illustrated in ***Fig. 14***, where as an example $M_b(\mathbf{q})^{ev}$ is shown as a function of the radial distance q for $\theta = 30^{\mathrm{o}}$.

XXIII. Integral Representations for the Evanescent Waves

In order to obtain new integral representations for the evanescent parts, we need suitable representations for the functions $p_n(\theta)$ and $q_n(\theta)$. We shall assume again that $0 \le \theta \le \pi/2$. To this end, we notice that Eq. (245) can also be integrated as

$$Y_n(x) = Y_n(1) + \int_1^x dt\,(1-t^2)^n \quad . \tag{279}$$

Since $Y_n(1) = P_n(0)$ and $Y_n(\cos\theta) = \cos\theta\, P_n(\theta)$ this can be written as

$$P_n(\theta) = \frac{1}{\cos\theta}\left[P_n(0) - \int_{\cos\theta}^{1} dt\,(1-t^2)^n \right] . \tag{280}$$

When we compare this to definition (265) of $p_n(\theta)$ we find that this is just

$$p_n(\theta) = \int_{\cos\theta}^{1} dt\,(1-t^2)^n \quad . \tag{281}$$

Similarly, Eq. (256) can be integrated as

$$Z_n(x) = Z_n(1) + \int_1^x dt\,\frac{1}{t^2}\left[(1-t^2)^n - 1\right] . \tag{282}$$

With $Q_n(\theta) = 1 - \cos\theta\, Z_n(\cos\theta)$ we see that $Z_n(1) = 1 - Q_n(0)$. We now split off the "-1 part" in the integrand, which then gives the representation

$$Q_n(\theta) = \cos\theta\left[Q_n(0) + \int_{\cos\theta}^{1} dt\, \frac{1}{t^2}(1-t^2)^n \right] . \tag{283}$$

Comparison with the definition (266) of $q_n(\theta)$ then yields

$$q_n(\theta) = -\cos\theta \int_{\cos\theta}^{1} dt\, \frac{1}{t^2}(1-t^2)^n \; . \tag{284}$$

For the situation $\theta \to \pi/2$ we have $\cos\theta \to 0$, and the integral does not exist in the lower limit. However, we can prove the following limit

$$\lim_{x\to 0} x\int_{x}^{1} dt\, \frac{1}{t^2}(1-t^2)^n = 1 \tag{285}$$

which gives $q_n(\pi/2) = -1$, in agreement with Eq. (278).

With the substitution $t = \cos\alpha$ in the integrand of Eq. (281) we get

$$p_n(\theta) = \int_0^{\theta} d\alpha\, (\sin\alpha)^{2n+1} \tag{286}$$

and then we insert this into Eqs. (264), (267) and (271). This yields the new representations

$$M_a(\mathbf{q})^{ev} = \frac{1}{q} - \int_0^{\theta} d\alpha\; J_1(q\sin\alpha) \tag{287}$$

$$M_b(\mathbf{q})^{ev} = -\sin^2\theta\left(\frac{3}{q^3}+\frac{1}{2q}+\frac{q}{8}\right)+\sin^2\theta\int_0^\theta d\alpha\,\frac{1}{\sin^2\alpha}\,J_3(q\sin\alpha) \tag{288}$$

$$M_f(\mathbf{q})^{ev} = \sin\theta\left(\frac{1}{q^2}+\frac{1}{2}\right)-\sin\theta\int_0^\theta d\alpha\,\frac{1}{\sin\alpha}\,J_2(q\sin\alpha)\ . \tag{289}$$

This result has a striking resemblance with Eqs. (252)-(254) for $\mathrm{Re}\,M_k(\mathbf{q})^{tr}$. The integrals appearing there are the same as here, except that the integration limits are $\alpha=\theta$ and $\alpha=\pi/2$. When we add for instance Eqs. (252) and (287) we get $\mathrm{Re}\,M_a(\mathbf{q})$ for which we find

$$\mathrm{Re}\,M_a(\mathbf{q}) = \frac{1}{q} - \int_0^{\pi/2} d\alpha\; J_1(q\sin\alpha) \tag{290}$$

and we know that this is $\cos q/q$. In this form the singular part $1/q$ is split off, and this part is entirely evanescent. The remaining integral is zero at the origin. The remarkable feature here is that if we split the integration range exactly at the polar angle θ of the field point **q**, then the integral over $0\le\alpha\le\theta$ represents the remaining evanescent waves in $\mathrm{Re}\,M_a(\mathbf{q})$, and the integral over $\theta\le\alpha\le\pi/2$ accounts for the traveling waves. The same conclusion holds for $\mathrm{Re}\,M_b(\mathbf{q})$ and $\mathrm{Re}\,M_f(\mathbf{q})$, although for these the parts that are split off contain a non-singular contribution, equal to $-(q/8)\sin^2\theta$ and $(\sin\theta)/2$, respectively.

For the series involving $q_n(\theta)$ we set $t=\cos\alpha$ in the integrand of Eq. (284), giving

$$q_n(\theta) = -\cos\theta\int_0^\theta d\alpha\,\frac{1}{\cos^2\alpha}\,(\sin\alpha)^{2n+1} \tag{291}$$

and along similar lines as above we obtain from Eq. (268)

$$M_c(\mathbf{q})^{ev} = \sin 2\theta \left(\frac{3}{q^3} + \frac{1}{2q} \right) - \frac{1}{q} \sin 2\theta \int_0^\theta d\alpha \, \frac{1}{\cos^2 \alpha \sin \alpha} J_2(q \sin \alpha) \; . \tag{292}$$

When we compare this to Eq. (259) for $\mathrm{Re}\, M_c(\mathbf{q})^{tr}$ we notice that both integrals do not have the same integrands. With some manipulations, however, we can make them the same. This gives

$$M_c(\mathbf{q})^{ev} = -\frac{2}{q} \sin\theta \, J_2(q) + \sin 2\theta \left(\frac{3}{q^3} + \frac{1}{2q} + \frac{1}{q} J_2(q) \right) - \frac{1}{q} \sin 2\theta \int_0^\theta d\alpha \, \frac{1}{\cos^2 \alpha \sin \alpha} \left[J_2(q \sin \alpha) - \sin^2\alpha J_2(q) \right] . \tag{293}$$

Here we notice the appearance of $-(2/q)\sin\theta \, J_2(q)$ on the right-hand side. This same term, but without the minus sign, appeared in Eq. (259) for $\mathrm{Re}\, M_c(\mathbf{q})^{tr}$. When added, these terms cancel, so we are led to the conclusion that these terms appear due to the splitting in traveling and evanescent, since in the sum they are absent. This peculiarity was already observed in Sec. XIII for a field point in the *xy*-plane, and is now found to hold more generally. In the form of Eq. (293), also an additional term $(\sin 2\theta) J_2(q)/q$ appears on the right-hand side.

In the same way we find

$$M_e(\mathbf{q})^{ev} = \frac{1}{q^2}\cos\theta - \frac{1}{q}\cos\theta \int_0^\theta d\alpha \, \frac{1}{\cos^2\alpha} J_1(q\sin\alpha) \tag{294}$$

and in order to make this comparable to Eq. (260) we rearrange this as

$$\begin{aligned} M_e(\mathbf{q})^{ev} &= \frac{1}{q^2}\cos\theta + \frac{1}{q} J_1(q)(\cos\theta - 1) \\ &\quad - \frac{1}{q}\cos\theta \int_0^\theta d\alpha \, \frac{1}{\cos^2\alpha}\left[J_1(q\sin\alpha) - \sin\alpha \, J_1(q)\right] . \end{aligned} \tag{295}$$

Here we notice the same phenomenon that a term $J_1(q)/q$ appears in $\mathrm{Re}\, M_e(\mathbf{q})^{tr}$ and the same term appears with a minus sign in $M_e(\mathbf{q})^{ev}$. Finally for $M_d(\mathbf{q})^{ev}$ we find

$$\begin{aligned} M_d(\mathbf{q})^{ev} &= \frac{1}{q}\cos\theta \, J_2(q) + \frac{1}{q^3}(1 - 3\cos^2\theta) + \frac{1}{q}\left(\tfrac{1}{2}\sin^2\theta - \cos^2\theta \, J_2(q)\right) \\ &\quad - \frac{1}{q}\int_0^\theta d\alpha \, \frac{1}{\sin\alpha}\left[J_2(q\sin\alpha) + \frac{\cos^2\theta}{\cos^2\alpha}\left(\sin^2\alpha \, J_2(q) - J_2(q\sin\alpha)\right)\right] \end{aligned} \tag{296}$$

and here we have canceling terms of $\pm\cos\theta \, J_2(q)/q$ in the traveling and evanescent parts.

XXIV. Conclusions

Evanescent waves play an important role in near field optics where spatial resolution of a radiation field on the order of a wavelength is essential. In an angular spectrum representation, these waves have wave vectors with a parallel component, with respect to the *xy*-plane, corresponding to wavelengths that are smaller than the optical wavelength of the radiation, and as such they serve to resolve details of a radiating source on a scale smaller than a wavelength. In addition, at distances from the source comparable to a wavelength or smaller, the evanescent waves dominate over the traveling waves in amplitude. In fact, all singular behavior of a radiation field at short distances is due to the evanescent waves. We have studied in detail the nature of the evanescent waves at short distances by means of a series expansion with the radial distance to the (localized) source as variable. This was accomplished by considering the Green's tensor of the electric field and the Green's vector of the magnetic field, rather than the fields itself. In this fashion, the spatial structure of the radiation could be studied independent of the details of the radiating source. A prime example of a localized source is the electric dipole for which the fields and the Green's tensor and vector are essentially identical.

It appears also possible that evanescent waves end up in the far field, together with the traveling waves, and they contribute to the emitted power. For the electric field, this happens in a cylindrical region around the z-axis, where the diameter of the cylinder is about an optical wavelength. The evanescent waves also contribute to the far field near the xy-plane. One envisions a "sheet" with a thickness that grows with distance to the source, as the square root of the distance, and within this circular sheet the evanescent waves in the electric field survive in the far field and contribute to the observable power. As for the evanescent waves in the magnetic field, they do contribute to the far field along the xy-plane, but they do not survive along the z-axis.

References

Abramowitz, M., and Stegun, I. A. (1972). *Handbook of Mathematical Functions.* New York: Dover, p. 298.

Arfken, G. B., and Weber, H. J. (1995). *Mathematical Methods for Scientists and Engineers.* 4th edition. San Diego, CA: Academic Press, p. 612.

Arnoldus, H. F., and George, T. F. (1991). Phase-conjugated fluorescence. *Phys. Rev. A* **43,** 3675-3689.

Arnoldus, H. F. (2001). Representation of the near-field, middle-field, and far-field electromagnetic Green's functions in reciprocal space. *J. Opt. Soc. Am. B* **18,** 547-555.

Arnoldus, H. F., and Foley, J. T. (2002a). Traveling and evanescent parts of the electromagnetic Green's tensor. *J. Opt. Soc. Am. A* **19,** 1701-1711.

Arnoldus, H. F., and Foley, J. T. (2002b). Uniform asymptotic approximation of the evanescent part of the Green's tensor. *Opt. Commun.* **207,** 7-15.

Arnoldus, H. F. (2003a). Transverse and longitudinal components of the optical self-, near-, middle- and far-field. *J. Mod. Opt.* **50,** 755-770.

Arnoldus, H. F., and Foley, J. T. (2003b). Spatial separation of the traveling and evanescent parts of dipole radiation. *Opt. Lett.* **28,** 1299-1301.

Arnoldus, H. F., and Foley, J. T. (2003c). Traveling and evanescent parts of the optical near field. *J. Mod. Opt.* **50,** 1883-1901.

Arnoldus, H. F., and Foley, J. T. (2003d). Transmission of dipole radiation through interfaces and the phenomenon of anti-critical angles. *J. Opt. Soc. Am. A*, submitted.

Berry, M. V. (2001). Asymptotics of evanescence. *J. Mod. Opt.* **48,** 1535-1541.

Bertilone, D. C. (1991a). The contributions of homogeneous and evanescent plane waves to the scalar optical field: exact diffraction formulae. *J. Mod. Opt.* **38,** 865-875.

Bertilone, D. C. (1991b). Wave theory for a converging spherical incident wave in an infinite-aperture system. *J. Mod. Opt.* **38,** 1531-1536.

Bleistein, N., and Handelsman, R. A. (1986). *Asymptotic Expansions of Integrals.* New York: Dover, p. 380.

Born, M., and Wolf, E. (1980). *Principles of Optics*, 6th edition. Oxford: Pergamon, Appendix 5.

Carney, P. S., Fischer, D. G., Foley, J. T., Friberg, A. T., Shchegrov, A. V., Visser, T. D., and Wolf, E. (2000). Evanescent waves do contribute to the far field. *J. Mod. Opt.* **47,** 757-758.

Cohen-Tannoudji, C., Dupont-Roc, J., and Grynberg, G. (1989). *Photons & Atoms*. New York: Wiley, p. 7.

Courjon, D., and Bainier, C. (1994). Near field microscopy and near field optics. *Rep. Prog. Phys.* **57,** 989-1028.

Courjon, D. (2003). *Near Field Microscopy and Near Field Optics*. Singapore: World Scientific.

de Fornel, F. (2001). *Evanescent Waves. From Newtonian Optics to Atomic Optics*. Berlin: Springer-Verlag.

Ford, G. W., and Weber, W. H. (1981). Electromagnetic effects on a molecule at a metal surface. *Surf. Sci.* **109,** 451-481.

Ford, G. W., and Weber, W. H. (1984). Electromagnetic interactions of molecules with metal surfaces. *Phys. Rep.* **113,** 195-287.

Grattan, K. T. V., and Meggitt, B. T. (2000). *Optical Fiber Sensor Technology, Fundamentals*. Dordrecht, The Netherlands: Kluwer.

Jackson, J. D. (1975). *Classical Electrodynamics*, 2nd edition. New York: Wiley, p. 141.

Keller, O. (1996). Local fields in the electrodynamics of mesoscopic media. *Phys. Rep.* **268,** 85-262.

Keller, O. (1999a). Electromagnetic propagators in micro- and mesoscopic optics, in *Computational Studies of New Materials*, edited by D. A. Jelski and T. F. George. Singapore: World Scientific, pp. 375-439.

Keller, O. (1999b). Attached and radiated electromagnetic fields of an electric point dipole. *J. Opt. Soc. Am. B* **16,** 835-847.

Lakhtakia, A., and Weiglhofer, W. S. (2000). Evanescent plane waves and the far field: resolution of a controversy. *J. Mod. Opt.* **47,** 759-763.

Lukosz, W., and Kunz, R. E. (1977a). Light emission by magnetic and electric dipoles close to a plane interface. I. Total radiated power. *J. Opt. Soc. Am.* **67,** 1607-1615.

Lukosz, W., and Kunz, R. E. (1977b). Light emission by magnetic and electric dipoles close to a plane interface. II. Radiation patterns of perpendicular oriented dipoles. *J. Opt. Soc. Am.* **67,** 1615-1619.

Ohtsu, M., editor. (1998). *Near-Field Nano/Atom Optics and Technology*. New York: Springer-Verlag.

Olver, F. W. J. (1974). *Asymptotics and Special Functions.* New York: Academic Press, p. 344.

Paesler, M. A., and Moyer, P. J. (1996). *Near Field Optics, Theory, Instrumentation, and Applications*. New York: Wiley.

Pohl, D. W. (1991). Scanning near-field optical microscopy (SNOM), in *Advances in Optical and Electron Microscopy*, Vol. 12, edited by T. Mulvey and C. J. R. Sheppard. San Diego, CA: Academic Press, pp. 243-312.

Pohl, D. W., and Courjon, D., editors. (1993). *Near Field Optics, Proceedings of the NATO Advanced Research Workshop on Near Field Optics*, NATO Advanced Study Institute Series, Vol. 242. Dordrecht, The Netherlands: Kluwer.

Prudnikov, A. P., Brychkov, Yu. A., and Marichev, O. I. (1986a). *Integrals and Series*, Vol. 1, Elementary Functions. New York: Gordon and Breach, p. 710, formula 5.2.11.7.

Prudnikov, A. P., Brychkov, Yu. A., and Marichev, O. I. (1986b). *Integrals and Series*, Vol. 2, Special Functions. New York: Gordon and Breach, p. 188, formula 2.12.10.3.

Setala, T., and Kaivola, M. (1999). Decomposition of the point-dipole field into homogeneous and evanescent parts. *Phys. Rev. E* **59,** 1200-1206.

Shchegrov, A. V., and Carney, P. S. (1999). Far-field contribution to the electromagnetic Green's tensor from evanescent modes. *J. Opt. Soc. Am. A* **16,** 2583-2584.

Sherman, G. C., Stamnes, J. J., and Lalor, É. (1976). Asymptotic approximations to angular-spectrum representations. *J. Math. Phys.* **17,** 760-776.

Sipe, J. E. (1981). The dipole antenna problem in surface physics: a new approach. *Surf. Sci.* **105,** 489-504.

Sipe, J. E. (1987). New Green function formalism for surface optics. *J. Opt. Soc. Am. B* **4,** 481-489.

Tai, C. T. (1971). *Dyadic Green's Functions in Electromagnetic Theory*. Scranton: Intext.

van Kranendonk, J., and Sipe, J. E. (1977). Foundations of the macroscopic electromagnetic theory of dielectric media, in *Progress in Optics* **15**, edited by E. Wolf. Amsterdam: North-Holland, pp. 246-350.

Watson, G. N. (1922). *A Treatise on the Theory of Bessel Functions*. Cambridge, UK: Cambridge U. Press, p. 537.

Wolf, E., and Foley, J. T. (1998). Do evanescent waves contribute to the far field?. *Opt. Lett.* **23,** 16-18.

Wong, R. (1989). *Asymptotic Approximations of Integrals.* Boston, MA: Academic Press, p. 410.

Xiao, M. (1996). A study of resolution limit in optical microscopy: near and far field. *Opt. Commun.* **132,** 403-409.

Xiao, M. (1999). Evanescent fields do contribute to the far field. *J. Mod. Opt.* **46,** 729-733.

Xiao, M. (2000). On the evanescent field of dipole. *J. Mod. Opt.* **47,** 765-768.

Appendix A

The Green's tensor $\overleftrightarrow{\chi}(\mathbf{q})$ has a delta function which represents the self field, and according to Eq. (24) this is

$$\overleftrightarrow{\chi}(\mathbf{q}) = -\frac{4\pi}{3}\delta(\mathbf{q})\overleftrightarrow{\mathrm{I}} + \ldots \ . \tag{A1}$$

On the other hand, in the angular spectrum representation, Eq. (48), a different delta function appears, e.g., $\overleftrightarrow{\chi}(\mathbf{q}) = -4\pi\,\delta(\mathbf{q})\mathbf{e}_z\mathbf{e}_z + \ldots$. This one has a different numerical factor and a different tensor structure. Since both Green's tensors are the same, there must be a hidden delta function in the angular spectrum integral on the right-hand side of Eq. (48). When written in terms of the auxiliary functions as in Eq. (60), this hidden delta function must be accounted for by the auxiliary functions. In Sec. VIII it was shown that by simply comparing Eqs. (24) and (60) that this delta function must be in $M_d(\mathbf{q})$, as given by Eq. (71). In this Appendix we shall show that the integral representation (64) for $M_d(\mathbf{q})$ does indeed contain this delta function.

To this end, we start with the spectral representation of the delta function:

$$\delta(\mathbf{r}) = \frac{1}{(2\pi)^3}\int d^3\mathbf{k}\ e^{i\mathbf{k}\cdot\mathbf{r}} \ . \tag{A2}$$

The we use cylinder coordinates $(k_{||},\tilde{\phi},k_z)$ in $\mathbf{k}$ space, and integrate over $k_{||}$ and $\tilde{\phi}$. This yields

$$\delta(\mathbf{r}) = \frac{1}{2\pi}\delta(z)\int_0^\infty dk_{||}k_{||}J_0(k_{||}\rho) \tag{A3}$$

and then we change to dimensionless variables as in Sec. VII, which gives

$$\delta(\mathbf{q}) = \frac{1}{2\pi}\delta(\bar{z})\int_0^A d\alpha\,\alpha\,J_0(\alpha\,\bar{\rho}) \ . \tag{A4}$$

Here we have kept the upper limit finite, otherwise the integral does not exist, and it is understood that "in the end" we take $A \to \infty$. With the relation $x\,J_0(x) = (x\,J_1(x))'$ the integral can be evaluated, and we arrive at the representation

$$\delta(\mathbf{q}) = \frac{1}{2\pi}\delta(\bar{z})\frac{A}{\bar{\rho}}J_1(A\bar{\rho}) \, , \qquad A \to \infty \ . \tag{A5}$$

We now consider the evanescent part $M_d(\mathbf{q})^{ev}$ of the integral representation in Eq. (64), which means that we replace the lower limit $\alpha = 0$ by $\alpha = 1$. First we use $x\,J_0(x) = (x\,J_1(x))'$ and integrate by parts. For the integrated part we keep the upper limit finite as in Eq. (A4). We then obtain

$$M_d(\mathbf{q})^{ev} = -\frac{A}{\bar{\rho}}J_1(A\bar{\rho})\sqrt{A^2-1}\,e^{-|\bar{z}|\sqrt{A^2-1}}$$

$$+\frac{1}{\bar{\rho}}\int_1^\infty d\alpha\;\alpha\;J_1(\alpha\bar{\rho})\frac{d}{d\alpha}\left(\sqrt{\alpha^2-1}\;e^{-|\bar{z}|\sqrt{\alpha^2-1}}\right) \ . \tag{A6}$$

With the representation

$$\delta(\bar{z}) = \tfrac{1}{2}\sqrt{A^2-1}\,e^{-|\bar{z}|\sqrt{A^2-1}} \ , \quad A \to \infty \tag{A7}$$

and Eq. (A5), the first term on the right-hand side of Eq. (A6) becomes $-4\pi\,\delta(\mathbf{q})$. Then we work out the derivative under the integral, after which it appears that this integral can be expressed as a combination of the evanescent parts of two other integrals. We find

$$M_d(\mathbf{q})^{ev} = -4\pi\delta(\mathbf{q}) + \frac{1}{\overline{\rho}} M_f(\mathbf{q})^{ev} - \frac{|\,\overline{z}\,|}{2\overline{\rho}} M_c(\mathbf{q})^{ev} \ . \tag{A8}$$

As the next step we consider the representation (62) for $M_b(\mathbf{q})$. We eliminate $J_2(\alpha\overline{\rho})$ in favor of $J_1(\alpha\overline{\rho})$ and $J_0(\alpha\overline{\rho})$ with $J_2(x) = -J_0(x) + 2J_1(x)/x$, and we use

$$\frac{\alpha^2}{\overline{\beta}} = \frac{1}{\overline{\beta}} - \overline{\beta} \ . \tag{A9}$$

This gives the relation

$$M_b(\mathbf{q}) = M_a(\mathbf{q}) - M_d(\mathbf{q}) - \frac{2}{\overline{\rho}} M_f(\mathbf{q}) \tag{A10}$$

which is Eq. (75). In this derivation we did not use the limits of integration, so this holds for the separate traveling and evanescent parts as well. Finally, we eliminate $M_f(\mathbf{q})$ between Eqs. (A8) and (A10), which yields

$$M_d(\mathbf{q})^{ev} = -\frac{8\pi}{3}\delta(\mathbf{q}) - \frac{1}{3}\left(M_b(\mathbf{q})^{ev} - M_a(\mathbf{q})^{ev} + \frac{|\,\overline{z}\,|}{\overline{\rho}} M_c(\mathbf{q})^{ev} \right) . \tag{A11}$$

This result has the desired delta function on the right-hand side.

If we would have considered $M_d(\mathbf{q})^{tr}$, with the integration range being $0 \le \alpha < 1$, then the first term on the right-hand side of Eq. (A6) would have been zero. Equation (A8) would then become

$$M_d(\mathbf{q})^{tr} = \frac{1}{\bar{\rho}} M_f(\mathbf{q})^{tr} - \frac{|\bar{z}|}{2\bar{\rho}} M_c(\mathbf{q})^{tr} \tag{A12}$$

and since Eq. (A10) also holds for the traveling part, the equivalent of Eq. (A11) is

$$M_d(\mathbf{q})^{tr} = -\frac{1}{3}\left(M_b(\mathbf{q})^{tr} - M_a(\mathbf{q})^{tr} + \frac{|\bar{z}|}{\bar{\rho}} M_c(\mathbf{q})^{tr} \right). \tag{A13}$$

Appendix B

It was shown in Sec. VI that the Green's tensor and vector have an angular spectrum representation, given by Eqs. (48) and (49), respectively. These representations were obtained from the angular spectrum representation, Eq. (42), of the scalar Green's function. These representations define a function of $\mathbf{r}$, and we shall use spherical coordinates (r,θ,ϕ). The goal of the method of stationary phase (Appendix III of Born and Wolf, 1980) is to obtain an expression for r large, with θ and ϕ fixed. The phase in these representations is $\mathbf{K}\cdot\mathbf{r} = \mathbf{k}_{||}\cdot\mathbf{r} + i\beta\,|\,z\,|$, with β defined by Eq. (2). The method of stationary phase asserts that the main contribution to an angular spectrum integral comes from a point in the $\mathbf{k}_{||}$-plane where the phase is stationary (e.g., it has a zero gradient). Let this point be $\mathbf{k}_{||,o}$. The idea is that away from this point, the waves are more or less random, leading to destructive interference, whereas near $\mathbf{k}_{||,o}$ the waves are in phase, leading to constructive interference. The remainder of the integrand is a function of $\mathbf{k}_{||}$, and this function is approximated by its value at $\mathbf{k}_{||,o}$. The phase is then approximated by Taylor expansion around the stationary point, leading to a Gaussian form. This phase is then integrated in closed form over the entire $\mathbf{k}_{\|}$-plane. The stationary point of $\mathbf{K}\cdot\mathbf{r}$ is

$$\mathbf{k}_{\|,o} = k_o \sin\theta\, \mathbf{e}_\rho \tag{B1}$$

with $\mathbf{e}_\rho$ the radial unit vector in the *xy*-plane corresponding to an observation direction (θ,ϕ). The approximation is then

$$\frac{i}{2\pi}\int d^2\mathbf{k}_{\|}\frac{1}{\beta}W(\mathbf{k}_{\|})e^{i\mathbf{K}\cdot\mathbf{r}} \approx W(\mathbf{k}_{\|,o})\frac{e^{ik_o r}}{r}\ . \tag{B2}$$

The result is an outgoing spherical wave of the far-field type, since it is $\mathcal{O}(1/r)$. For a given field point $\mathbf{r}$, we have $\hat{\mathbf{r}} = \mathbf{r}/r$ as the unit vector representing the observation direction. The projection of $\hat{\mathbf{r}}$ onto the *xy*-plane is $\sin\theta\,\mathbf{e}_\rho$, and when multiplied by k_o this gives the stationary point $\mathbf{k}_{\|,o}$. This shows that $\mathbf{k}_{\|,o}$ is inside the circle $k_{\|} = k_o$ in the $\mathbf{k}_{\|}$-plane, and therefore corresponds to a traveling wave $\exp(i\mathbf{K}\cdot\mathbf{r})$ of the angular spectrum. Since the entire contribution seems to come from the stationary point, one might conclude that the far field only contains traveling waves of the angular spectrum. It should also be noted that by considering all observation directions $\hat{\mathbf{r}}$, we cover the entire inside of the circle $k_{\|} = k_o$, so *all* traveling waves contribute to the far field.

In general, this conclusion is justified and very useful for interpretation. A detected wave in the far field, although a spherical wave, has its origin in a single plane wave coming out of the source, when the field is represented by an angular spectrum (Arnoldus and Foley, 2003b, 2003d). Now let us consider a field point in the *xy*-plane. Then $\theta = \pi/2$, and $\mathbf{k}_{\|,o} = k_o\mathbf{e}_\rho$. This stationary point is exactly on the circle $k_{\|} = k_o$. In the method of stationary phase, we expand the phase around this point and then integrate over $\mathbf{k}_{\|}$. Since the point $\mathbf{k}_{\|,o}$ is on the circle, half of its neighboring wave vectors that contribute are in the evanescent region. One would therefore expect that in the *xy*-plane half of the far field comes from evanescent waves. This is indeed the case, as shown in Sec. XIII. A more subtle complication arises when the field point is on the *z*-axis. Then the stationary point is $\mathbf{k}_{\|,o} = 0$. It turns out that also in this case the integral over $\mathbf{k}_{\|}$ picks up a contribution from the evanescent range in the $\mathbf{k}_{\|}$-plane, so that some evanescent waves end up in the far field on the *z*-axis, consistent with the results of Sec. XII. For more details on this we refer to Sherman, *et.al.* (1976).

For the angular spectrum of the scalar Green's function, Eq. (42), we have $W(\mathbf{k}_{\|}) = 1$ and with Eq. (B2) this gives for the asymptotic approximation

$$g(\mathbf{r}) \approx \frac{e^{ik_o r}}{r} \tag{B3}$$

and this is the exact result for all $\mathbf{r}$ (Eq. (10)). For the Green's tensor from Eq. (48), the function $W(\mathbf{k}_{\|})$ involves $\mathbf{K}$ at the stationary point, for which we need first β at the stationary point, which is

$$\beta_o = k_o \,\mathrm{sgn}(z) \cos\theta \ . \tag{B4}$$

From this we find

$$\mathbf{K}_o = k_o \hat{\mathbf{r}} \tag{B5}$$

which yields for the asymptotic approximation of the Green's tensor

$$\overleftrightarrow{\chi}(\mathbf{q}) \approx (\overleftrightarrow{I} - \hat{\mathbf{q}}\hat{\mathbf{q}}) \frac{e^{iq}}{q} \ . \tag{B6}$$

This is indeed the $\mathcal{O}(1/q)$ part of the Green's tensor, as seen from Eq. (24). For the Green's vector we obtain

$$\boldsymbol{\eta}(\mathbf{q}) \approx -i\hat{\mathbf{q}}\frac{e^{iq}}{q} \tag{B7}$$

in agreement with Eq. (28).

Table 1. Table of the various parameters that determine the uniform asymptotic approximations of the evanescent parts of the auxiliary functions.

	$M_a(\boldsymbol{q})^{ev}$	$M_b(\boldsymbol{q})^{ev}$	$M_c(\boldsymbol{q})^{ev}$	$M_d(\boldsymbol{q})^{ev}$	$M_e(\boldsymbol{q})^{ev}$	$M_f(\boldsymbol{q})^{ev}$
$f(u)$	1	$-(1+u^2)$	$2u\sqrt{1+u^2}$	$-u^2$	u	$\sqrt{1+u^2}$
n	0	2	1	0	0	1
$f(0)$	1	-1	0	0	0	1
$f(u_o)$	1	$-\sin^2\theta$	$-i\,\lvert\sin 2\theta\rvert$	$\cos^2\theta$	$-i\,\lvert\cos\theta\rvert$	$\sin\theta$
$f'(0)$	0	0	2	0	1	0

Figure Captions

Figure 1. Schematic illustration of the traveling and evanescent waves in an angular spectrum. Each wave has a wave vector with a real-valued $\mathbf{k}_{||}$. If the *z*-component of the wave vector is also real, then the wave is traveling, as indicated by the wave vectors **K** on the left. At opposite sides of the *xy*-plane, the *z*-components of the wave vector differs by a minus sign, and therefore the propagation direction of the wave is as shown in the diagram. The wave vector **K** has a discontinuity at the *xy*-plane. When the *z*-component of the wave vector is imaginary, the wave decays in the directions away from the *xy*-plane, as shown on the right, and they travel along the *xy*-plane with wave vector $\mathbf{k}_{||}$.

Figure 2. Point P is the projection of the field point **r** on the *xy*-plane. We take this point as the origin of the $\mathbf{k}_{||}$-plane, and we take the new *x*- and *y*-axes as shown.

Figure 3. Polar diagram of $M_a(\mathbf{q})^{ev}$ and $\mathrm{Re}\, M_a(\mathbf{q})^{tr}$ for $q = 8\pi$. The sum of these functions is $(\cos q)/q$, which is independent of the polar angle. The semi-circle is the reference zero. We see clearly that near the *z*-axis and the *xy*-plane the evanescent part is significant whereas in between the traveling waves dominate.

Figure 4. Graph of $M_a(\mathbf{q})^{ev}$ for $\overline{\rho} = 5$ and as a function of $\overline{z}$. The thick line is the exact result and the thin line is the approximation with a series of Bessel functions, Eq. (144), with 22 terms.

Figure 5. Contour in the complex *t*-plane for the integral in Eq. (176) for $\theta = \pi/6$. Point P is the saddle point $t = a$, and the curve approaches a line through the saddle point and under $\theta/2$ with the real axis. For $\theta > \pi/2$ this angle is $(\pi - \theta)/2$.

Figure 6. Curves a and b are the real and imaginary parts of function $N(\mathbf{q})$, shown as a function of θ for $q = 10\pi$.

Figure 7. Function $M_a(\mathbf{q})^{ev}$ as a function of θ for $q = 2\pi$. The thick line is the exact solution and the thin line is the uniform asymptotic approximation.

Figure 8. Function $M_a(\mathbf{q})^{ev}$ as a function of θ for $q = 15\pi$. The thick line is the exact solution and the thin line is the uniform asymptotic approximation. The only difference between the two is the small deviation near 90°, highlighted with the circle.

Figure 9. Function $M_a(\mathbf{q})^{ev}$ as a function of θ for $q = 100\pi$. The difference between the exact solution and the uniform asymptotic approximation can not be seen anymore. Here we see that $M_a(\mathbf{q})^{ev}$ is much more pronounced near $\theta = 0^{\mathrm{o}}$ and $\theta = 90^{\mathrm{o}}$, which reflects the fact that in these regions the evanescent waves end up in the far field.

Figure 10. Same as Fig. 7, but with the Bessel function in the asymptotic approximation replaced by its asymptotic value. The result at $\theta = 90^{\mathrm{o}}$ is now exact but the approximation diverges at $\theta = 0^{\mathrm{o}}$.

Figure 11. This graph illustrates the typical behavior of the coefficient functions $P_n(\theta)$ and $Q_n(\theta)$ as a function of the polar angle θ.

Figure 12. The thick line is $\mathrm{Re}\, M_a(\mathbf{q})^{tr}$ as a function of q for $\theta = 30^{\mathrm{o}}$, and the thin line is the approximation by the series from Eq. (218) summed up to $n = 20$.

Figure 13. Illustration of the functions $p_n(\theta)$ and $q_n(\theta)$.

Figure 14. This graph shows the evanescent part of $M_b(\mathbf{q})$ for $\theta = 30^{\mathrm{o}}$. The thick line is the exact value, obtained by numerical integration, and the thin line is the approximation by series expansion, Eq. (267), up to $n = 20$.

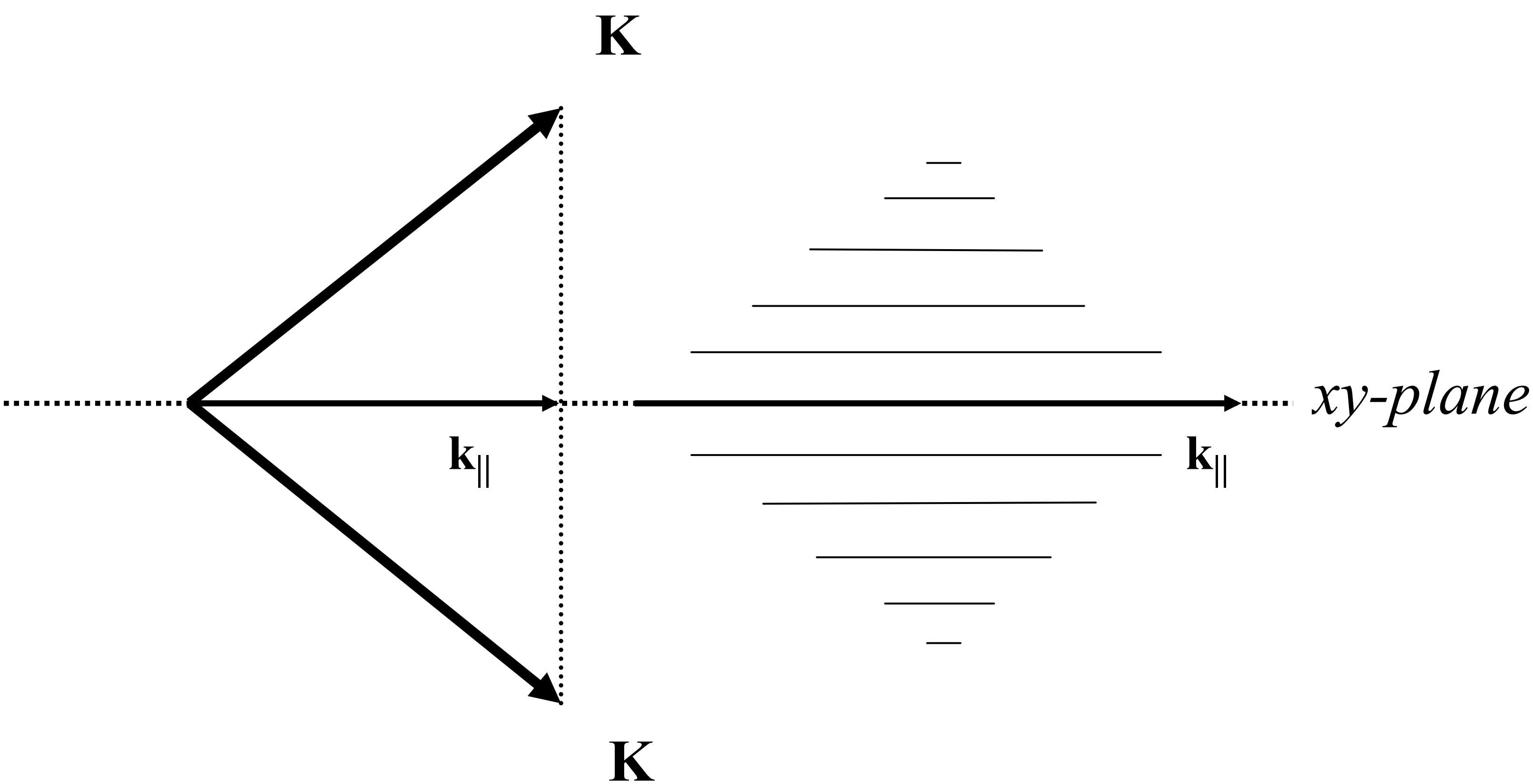

Figure 1

Figure 2

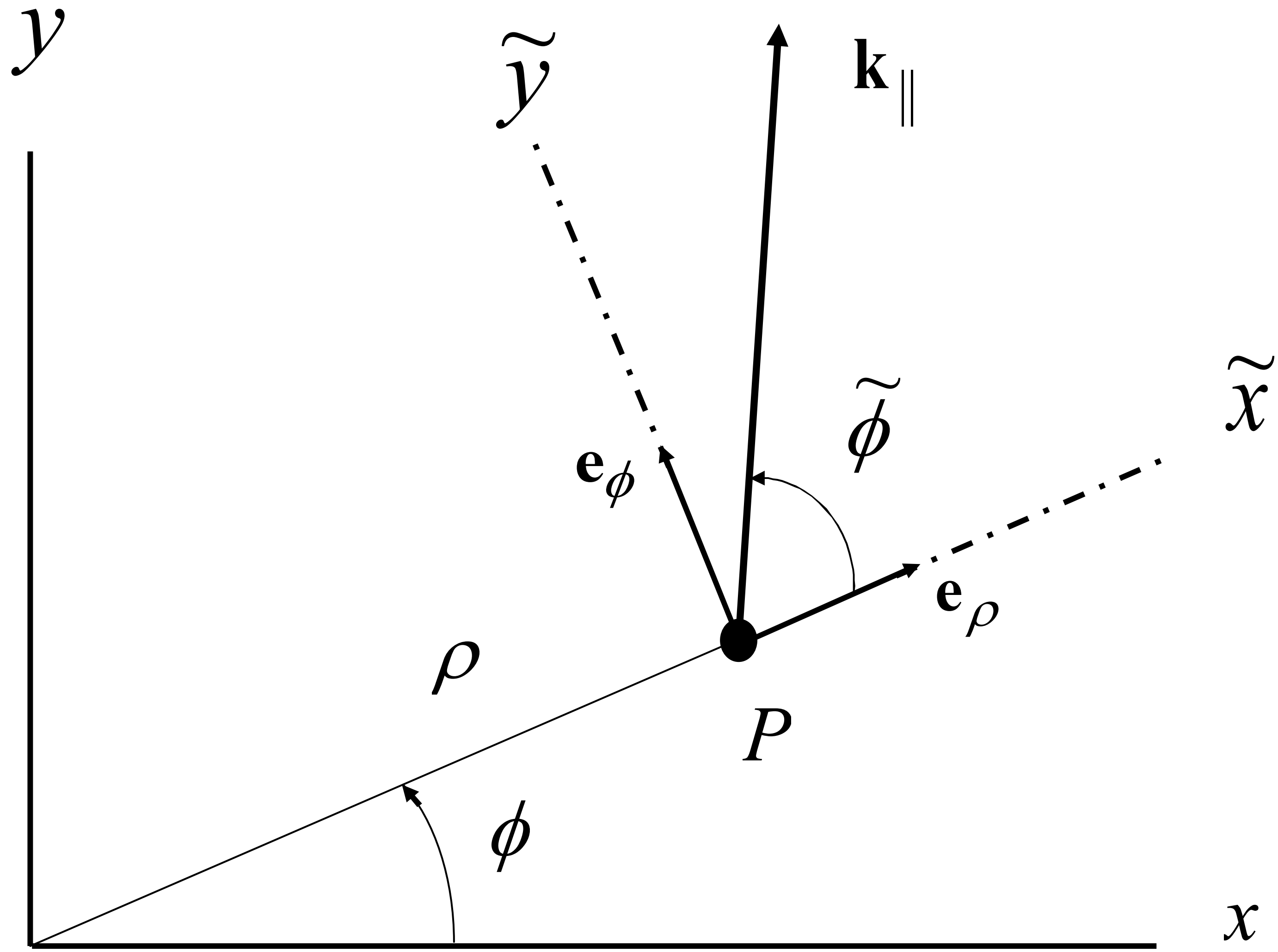

y
$\tilde{y}$
$\mathbf{k}_{\parallel}$
$\tilde{\phi}$
$\tilde{x}$
$\mathbf{e}_{\phi}$
$\mathbf{e}_{\rho}$
ρ
P
ϕ
x

Figure 3

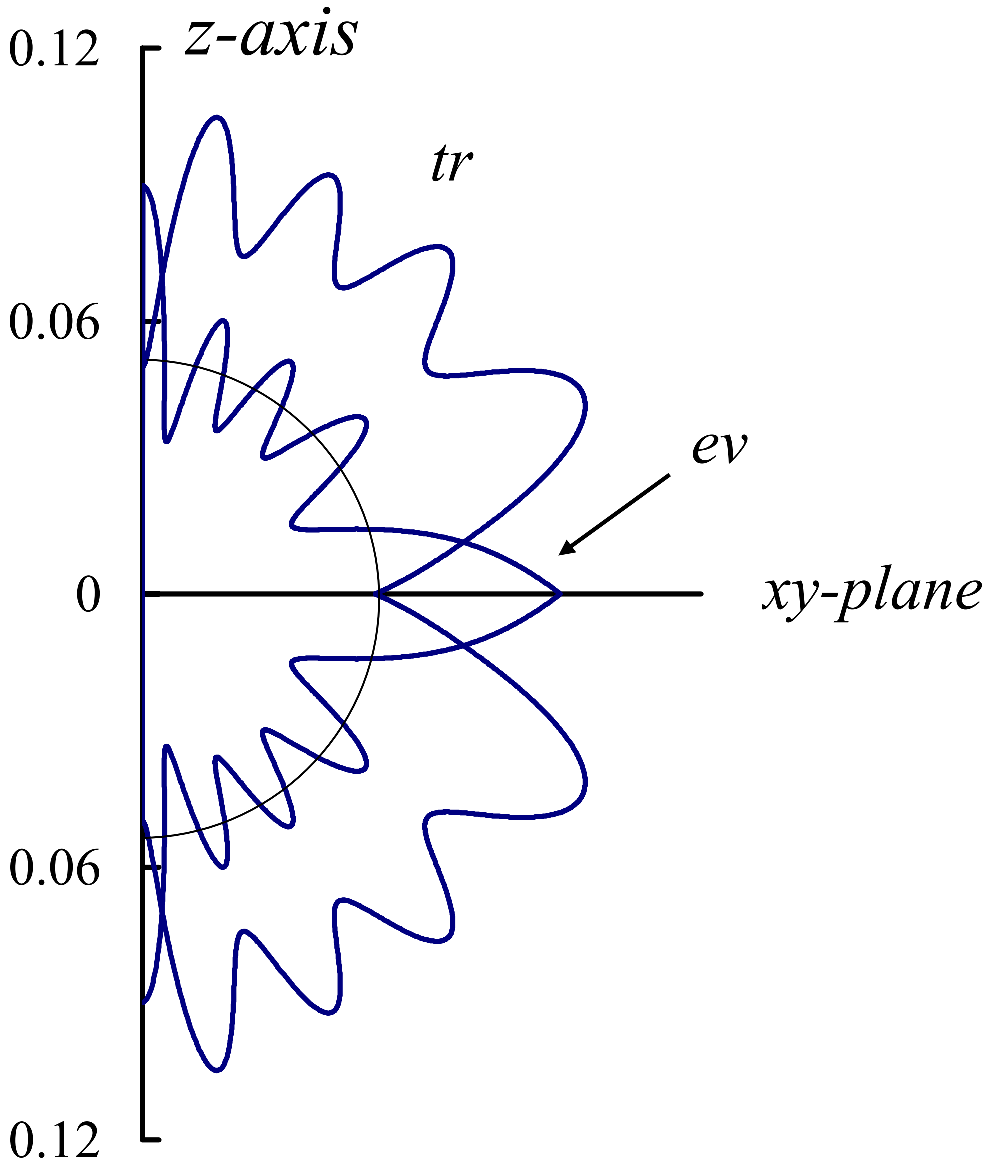

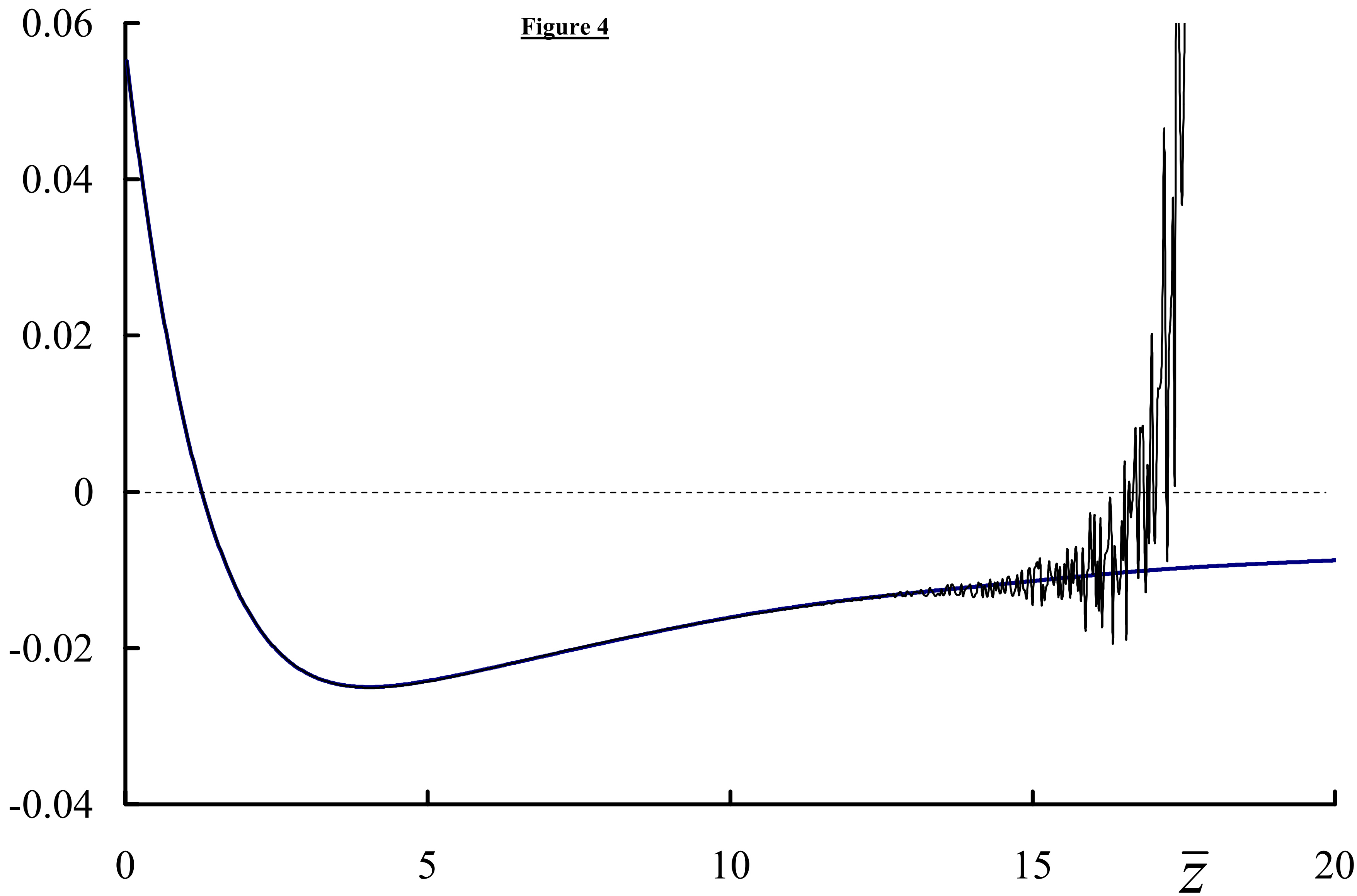
Figure 4
0.06
0.04
0.02
0
-0.02
-0.04
0
5
10
15
$\overline{z}$
20

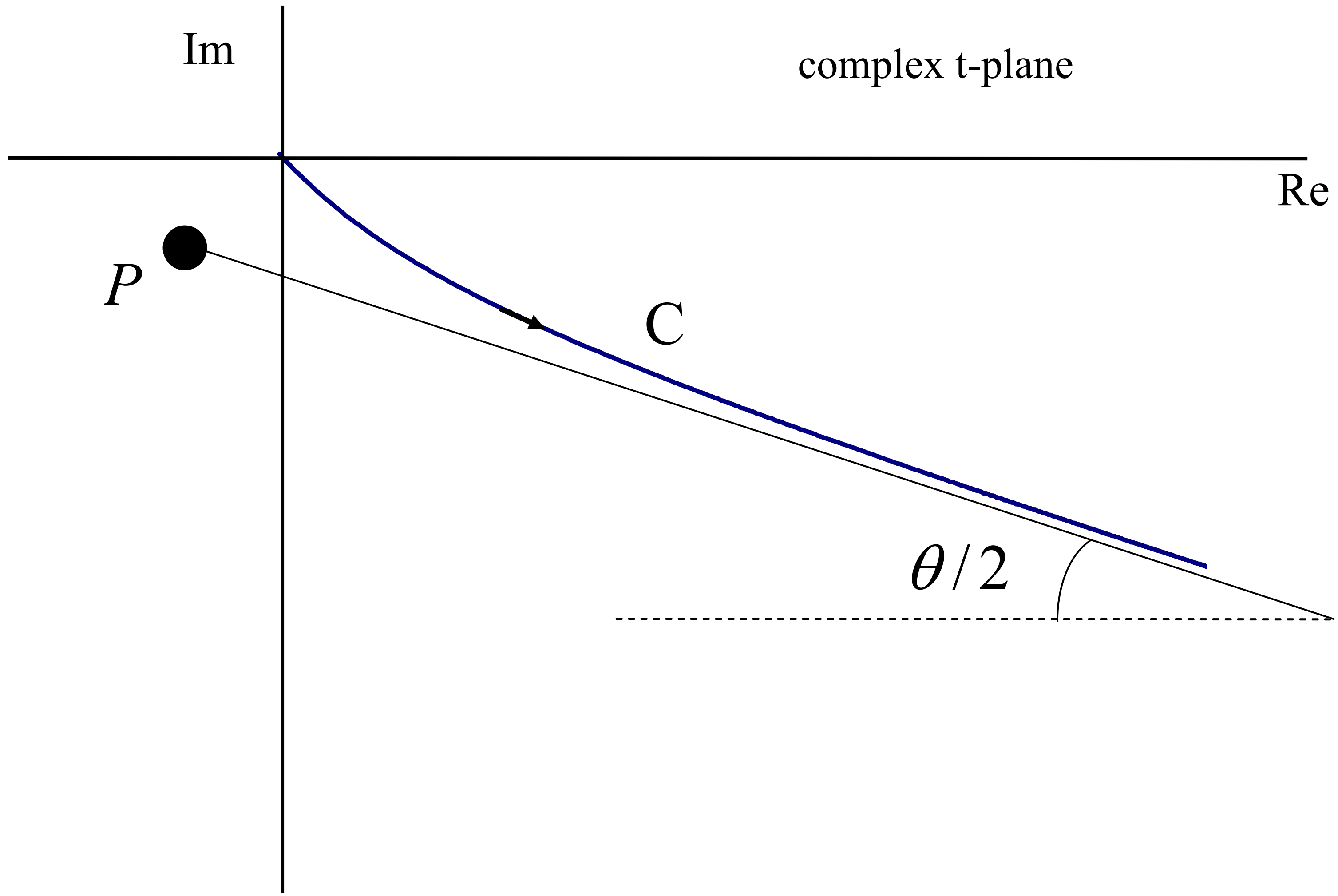

Figure 5

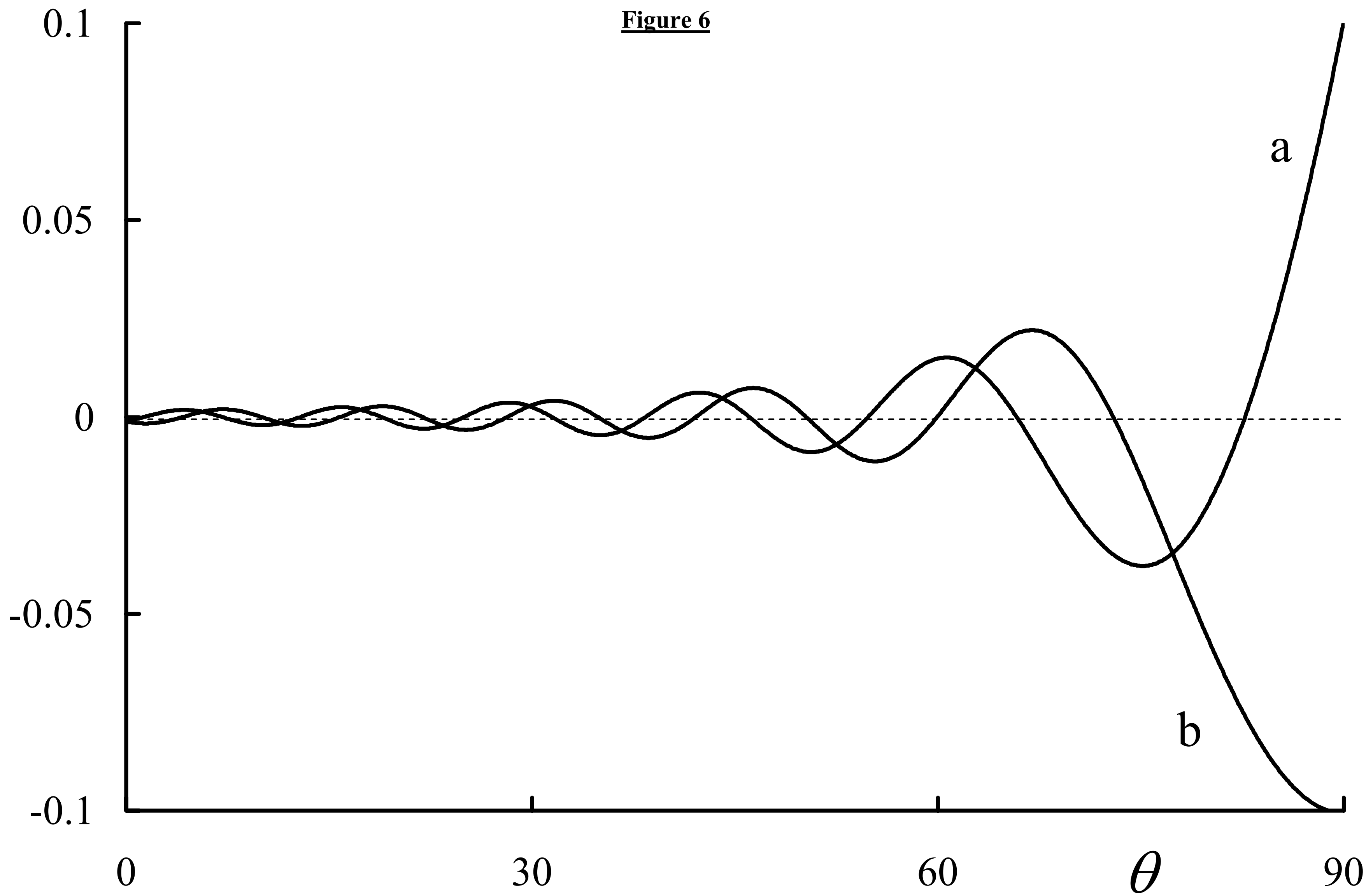
Figure 6
0.1
0.05
0
-0.05
-0.1
0
30
60
θ
90
a
b

Figure 7

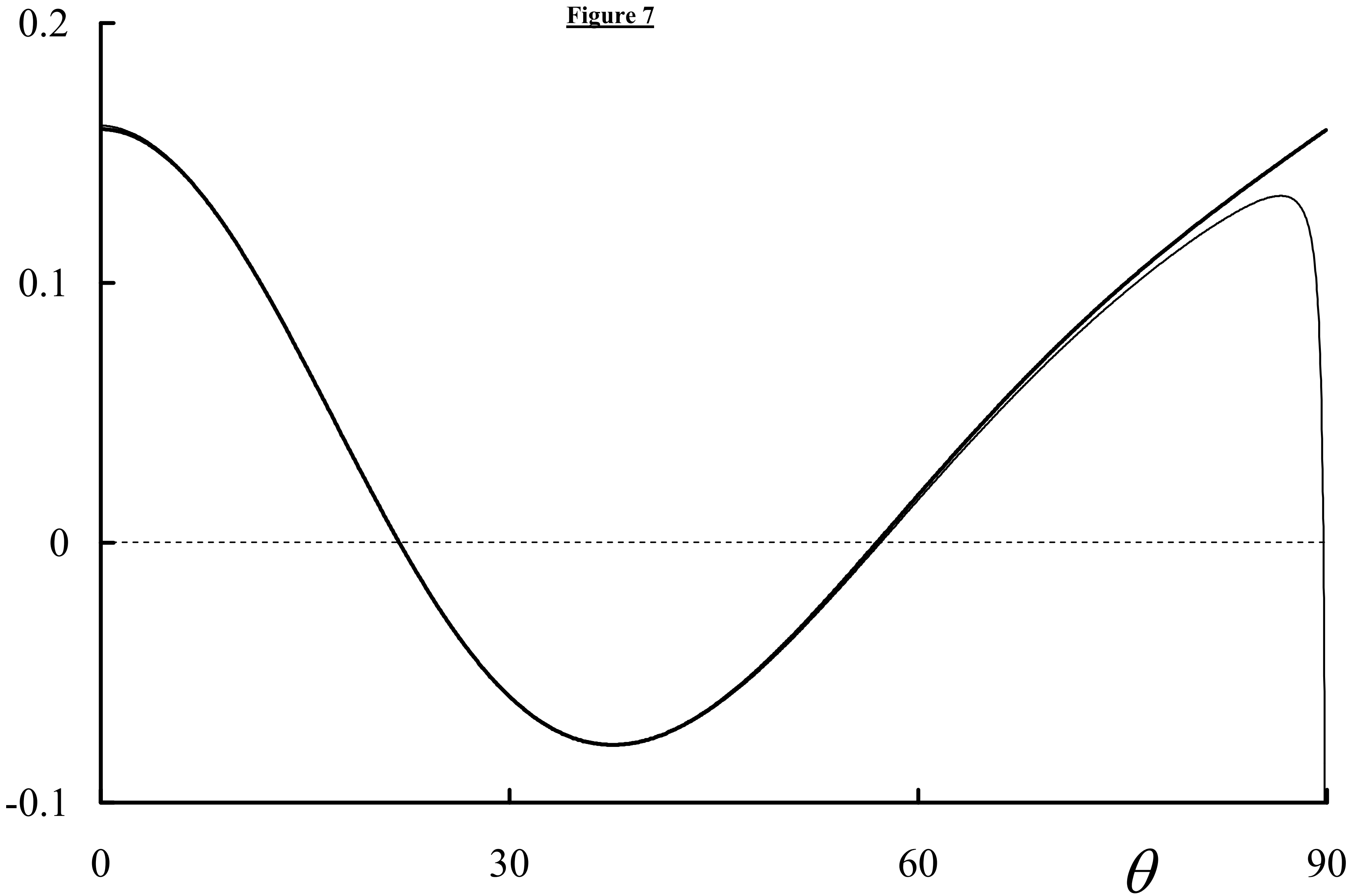

Figure 8

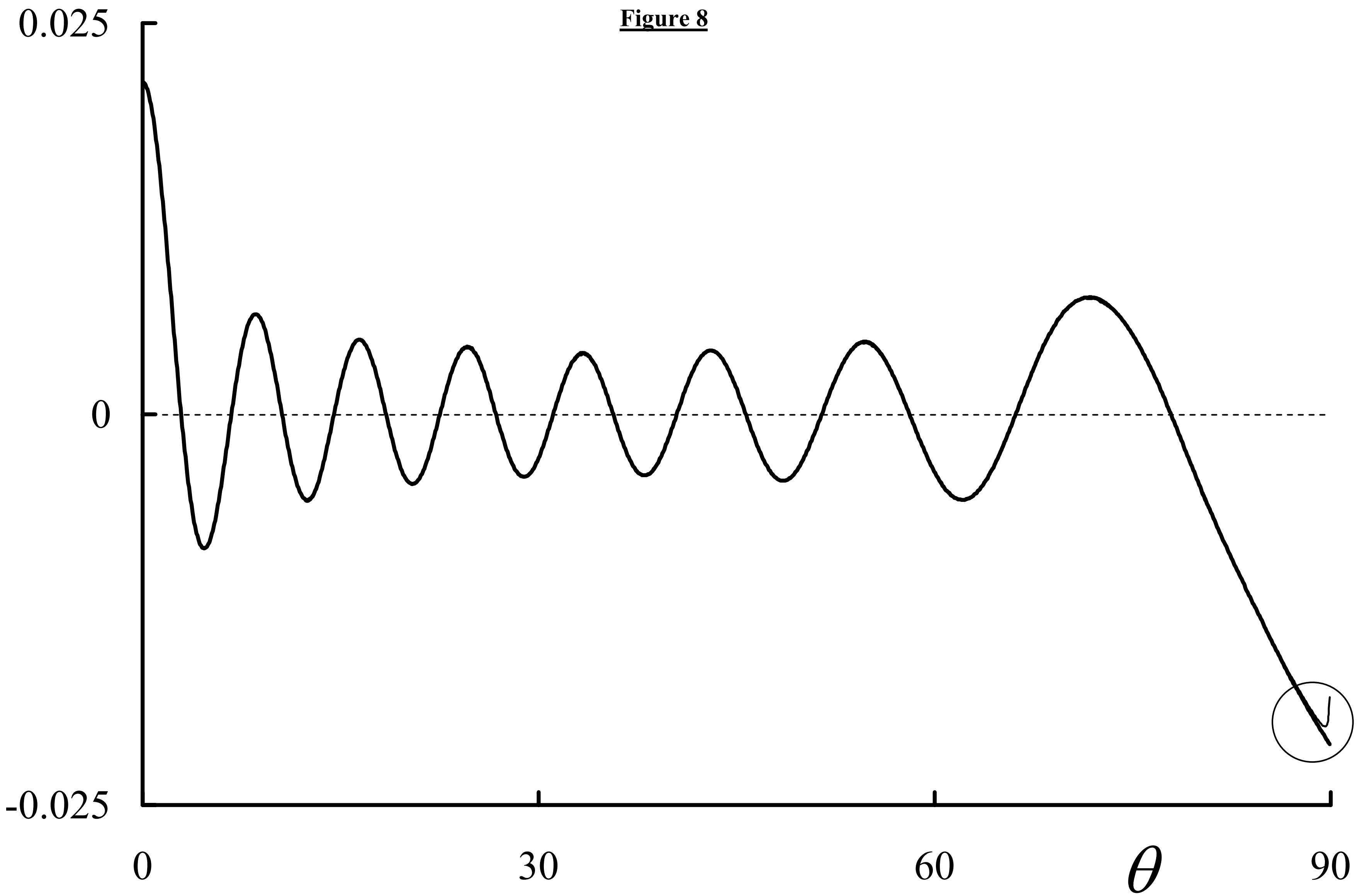

Figure 9

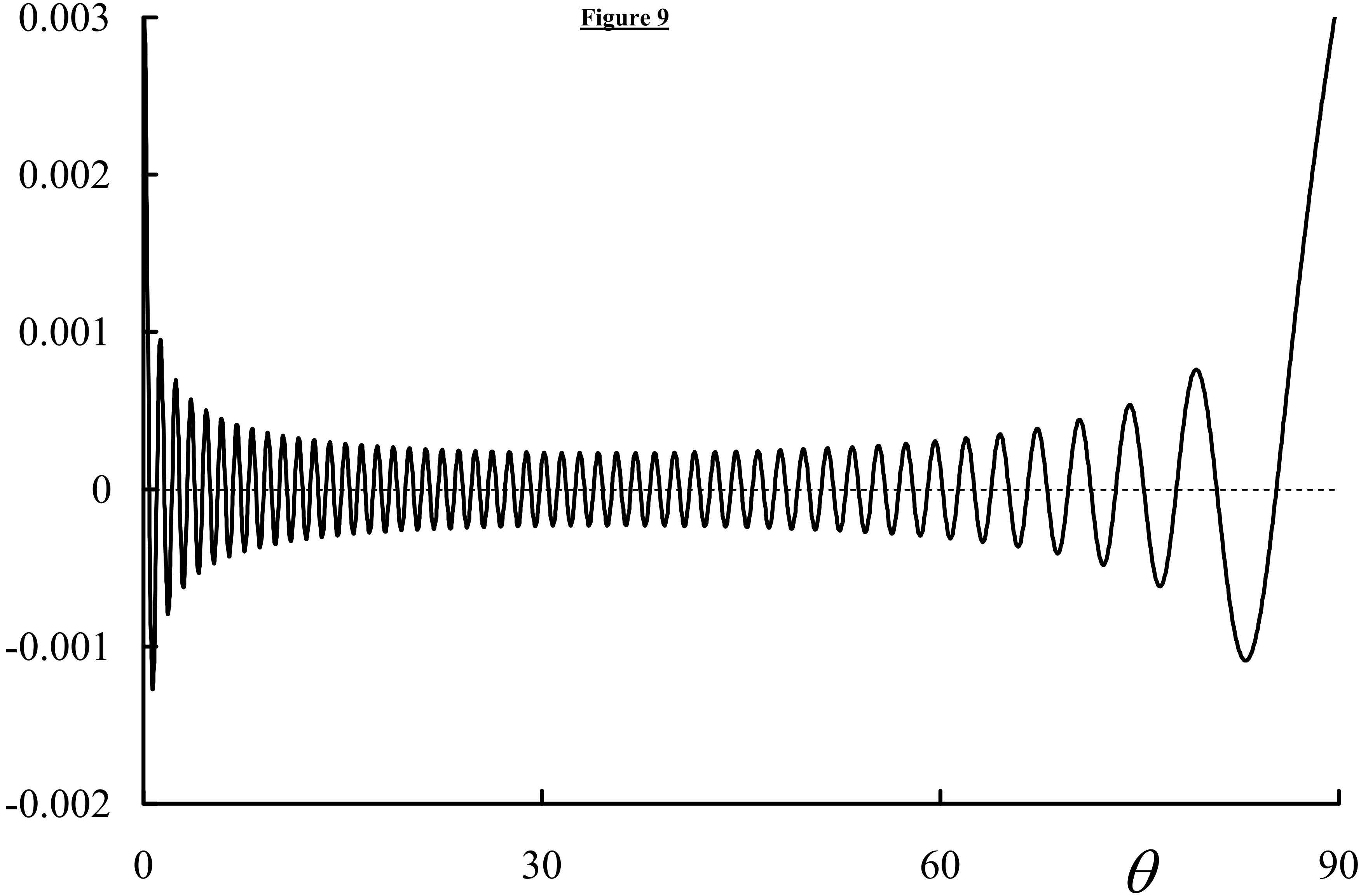

Figure 10

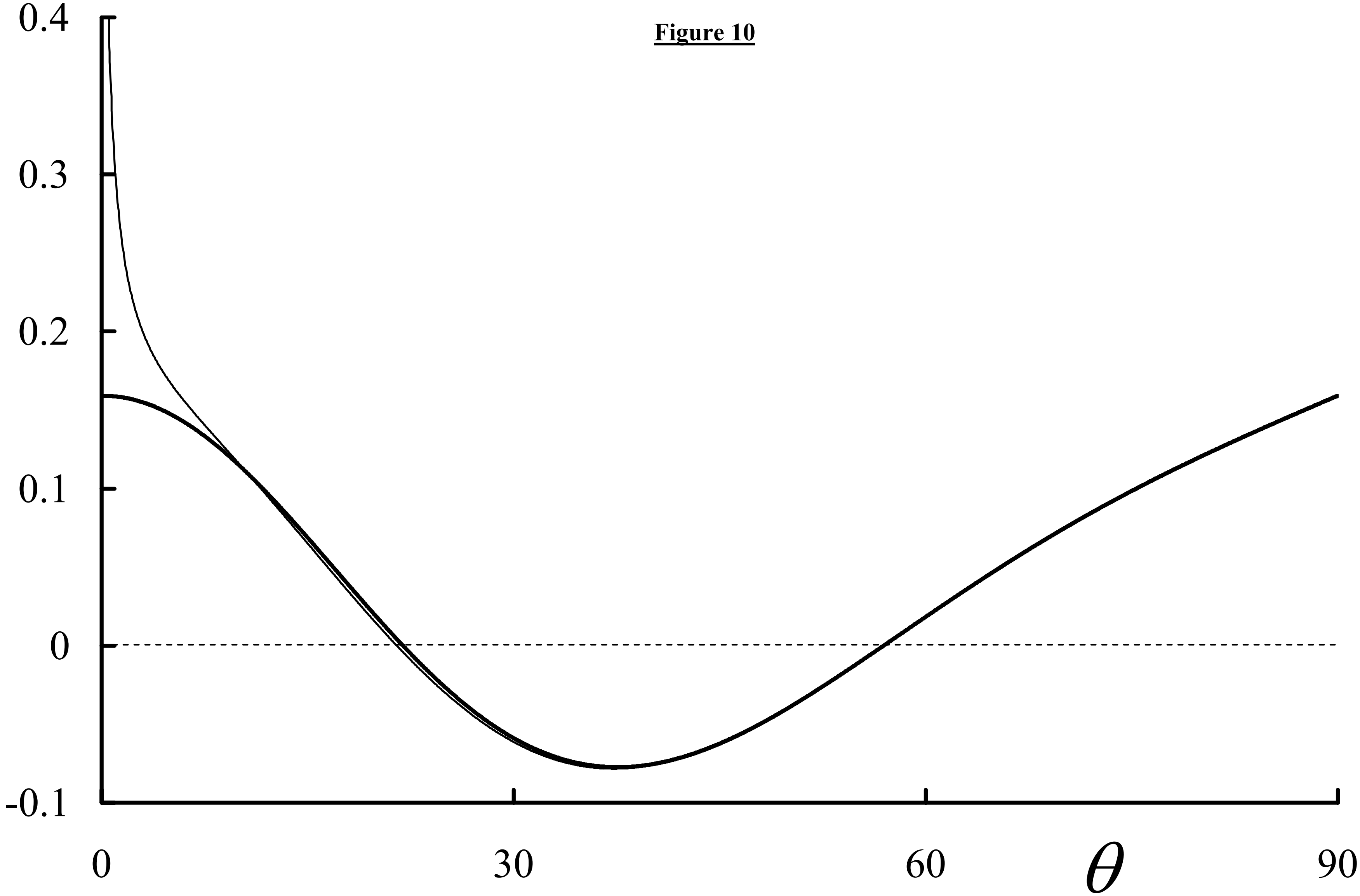

Figure 11

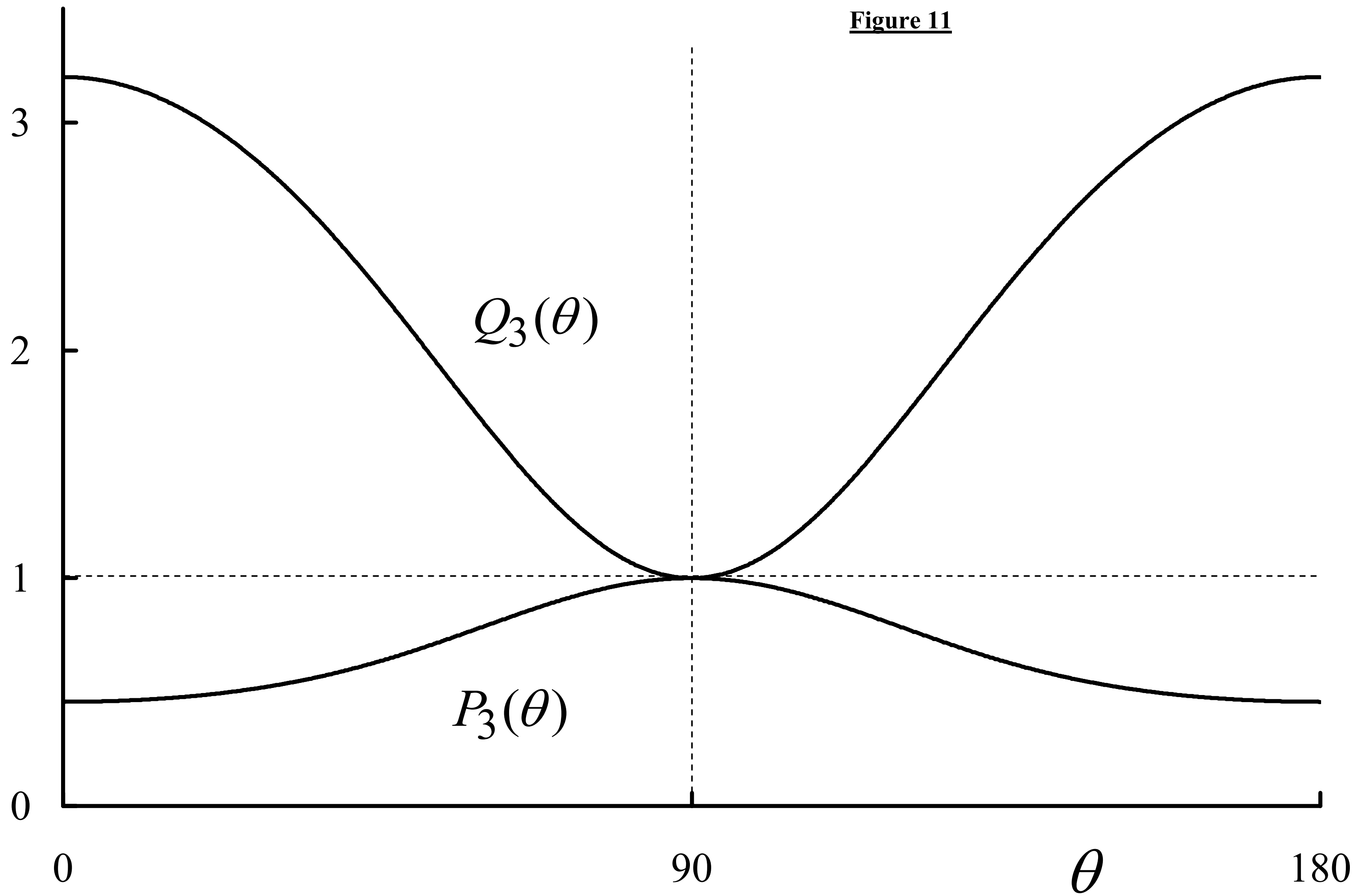

Figure 12

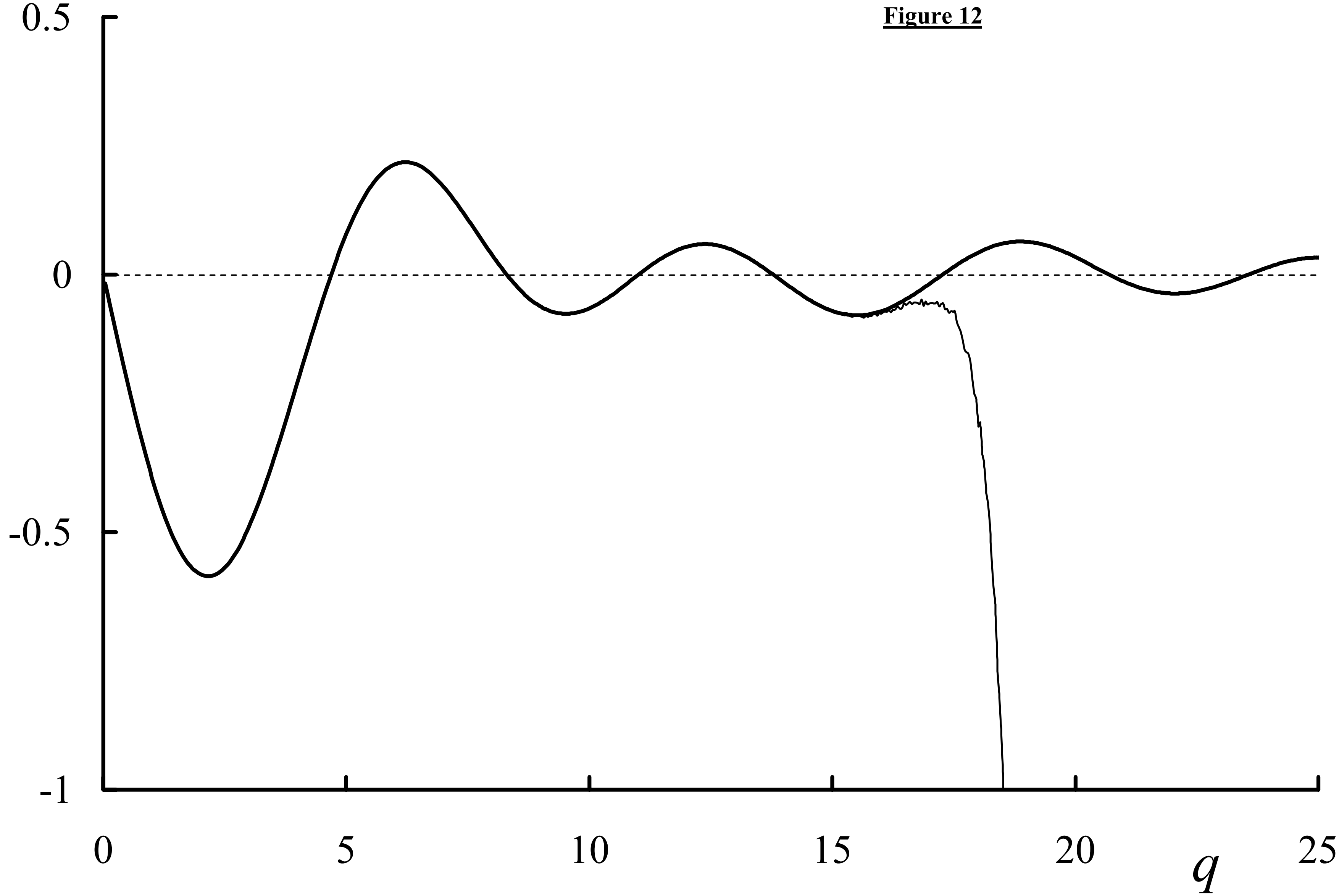

Figure 13

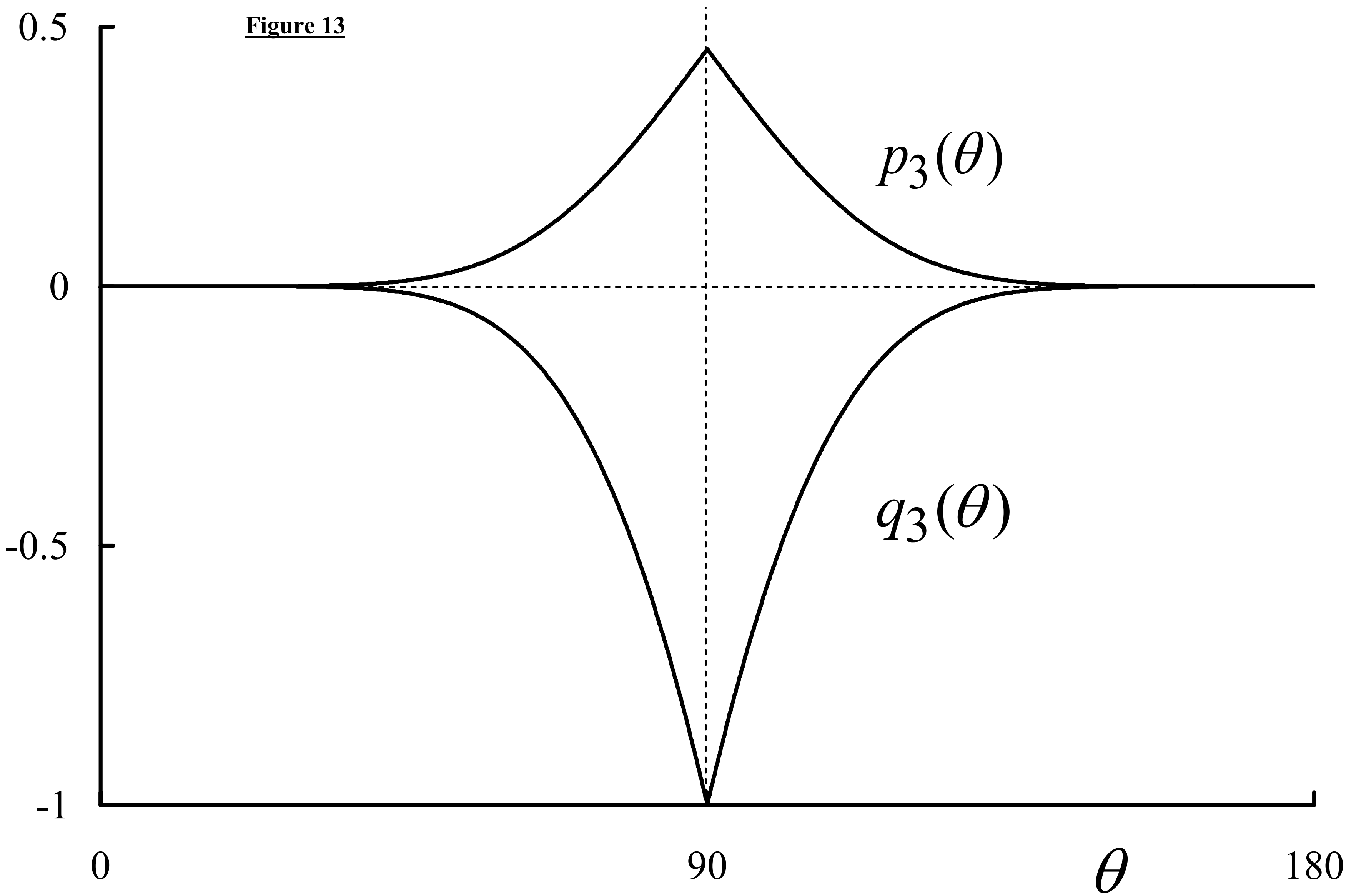

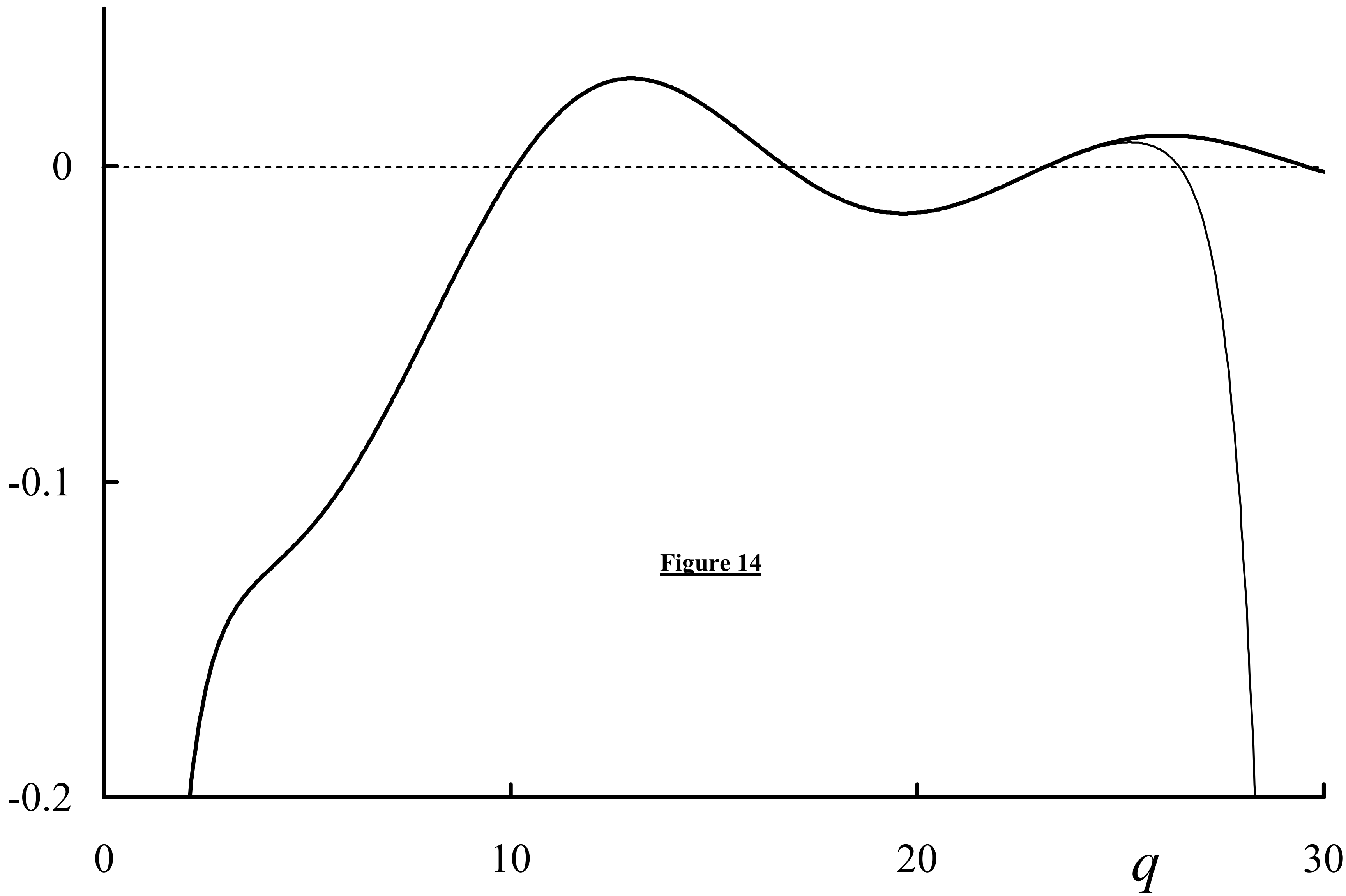

Figure 14